CHARLES PANKOW
FOUNDATION
Building Innovation through Research

Defining Structurally Acceptable Properties of High-Strength Steel Bars through Material and Column Testing

PART I: MATERIAL TESTING REPORT

The University of Texas at Austin
Chase M. Slavin
Wassim M. Ghannoum

Sponsored by:
The Charles Pankow Foundation
The Concrete Reinforcing Steel Institute
The American Concrete Institute's Concrete Research Council

August 27, 2015

Defining Structurally Acceptable Properties of High-Strength Steel Bars through Material and Column Testing

CPF Research Grant Agreement #05-14
Funded by
CHARLES PANKOW FOUNDATION
P.O. Box 820631

Vancouver, Washington 98682
Co-funded by
The Concrete Reinforcing Steel Institute, and
The American Concrete Institute's Concrete Research Council

Principal Investigator:	Dr. Wassim M. Ghannoum
Graduate Research Assistants:	Drit Sokoli (PhD student)
	Chase Slavin (Master's student)
	Albert Limantono (Master's Student)
Industry Support:	
Industry Champions:	Mike Mota, VP Engineering, CRSI
	Ron Klemencic, Chairman and CEO, MKA
Advisory Panel:	Dominic Kelly, SGH
	Andrew Taylor, KPFF
	Loring Wyllie, Degenkolb

Acknowledgements

This project was made possible by funding from the Charles Pankow Foundation, the Concrete Reinforcing Steel Institute, and the American Concrete Institute's Concrete Research Council. The steel donations of CMC and NUCOR Steel inc. Seattle are gratefully acknowledged. The assistance of Stephen Zhao in gathering data is gratefully acknowledged.

Abstract

Low-cycle fatigue tests were performed on reinforcing bars in order to assess the acceptability of newly developed high-strength reinforcing bars in seismic applications. The steels tested are classified as grade 60 A706, grade 80 A706, grade 80 A615, and grade 100. The high-strength reinforcing bars tested represent the two most common manufacturing processes used today: microalloying and quenching-and-tempering. The results of these tests are presented along with comparisons between the fatigue life of bars based on steel grade and other bar properties. A statistical analysis of the test results is presented in order to assess the impact of many parameters on the low-cycle fatigue performance of grade 60 A706 and higher-strength reinforcing bars.

Table of Contents

List of Figures

List of Tables

List of Equations

1. Introduction

1.1 MOTIVATION

There is an increasing need for higher grade reinforcing steel in seismic and non-seismic applications. A main driver for higher grades is the need to reduce bar congestion in seismic designs and reduce material quantities generally. Economic and environmental considerations are also major contributors to the demand for higher strength reinforcement. High-strength reinforcing bars (HSRB) are defined in this report as reinforcing bars having a yield strength of 80 ksi or more.

Recently, the reinforcing bar industry adopted a Grade 80 steel that satisfies the ASTM A706 standard. Several mils across the country are able to produce this steel grade, making it available to the structural engineering community. Steel grades higher than Grade 80 and having relatively high ductility (>10% fracture strains) are just emerging. However, the steel industry is producing the high-strength steels with varying mechanical properties. None of the higher steel grades in production are able to match the benchmark mechanical properties of Grade 60 A706 steel; with each high-strength variant diverging from benchmark behavior in different ways. Through the Applied Technology Council (ATC) 115 project (NIST GCR 14-917-30, 2014), structural engineers and steel mills are trying to strike the best balance between needed and feasible properties for high-strength steel.

Nevertheless, current code limits on the strength of reinforcing steel, combined with a lack of understanding of the effects of higher strength steel on the performance of concrete members, are hindering progress in structural designs. Many of today's limits on strength of concrete reinforcing steel have been enforced since the 1950s. The 1956 version of the ACI 318 building code (ACI 318 1956) set the yield-strength limit on

reinforcement at 60 ksi, increasing it from 40 ksi. In the 1971 version of the ACI 318 code, an 80 ksi limit was placed for gravity systems (ACI 318 1971). To this date, the limit remains at 80 ksi for non-seismic systems except for shear, which has to be designed using a maximum yield strength of transverse reinforcement of 60 ksi. For seismic design, the limit currently remains at 60 ksi (ACI 318 2014). Grade 100 steel was recently allowed in the ACI building code but only for designing confinement reinforcement.

Performance concerns that have maintained the code limits on the strength of reinforcing steel span a wide range of behavioral aspects. An increase in steel strength in reinforcing bars is associated with an increase in the strain at yield, and often with a reduction in the fracture strain, the tensile-to-yield strength (T/Y) ratio, and the length of the yield plateau. For a given bar size, higher strength steel implies larger tensile and compressive forces. Larger tensile forces for the same bar size result in an increase in bond demands and the forces at bar hooks or heads. On the other hand, larger compressive forces for the same bar size can increase bar buckling susceptibility given the same lateral bracing. The larger strain at yielding in higher-strength steel can cause larger strains at service loads and therefore increase crack widths and deflections. Larger crack widths in turn can lead to the weakening of the concrete shear-transfer mechanisms and lower shear strengths. Additionally, the lower ductility of high-strength steel may affect seismic design, member deformation capacity, as well as bar-bend performance. There is also evidence that the tensile-to-yield strength ratio affects the spread of plasticity in reinforced concrete members and a low value of the ratio can produce higher strain concentrations in bars at cracks (Aoyama, H. 2001, NEHRP 2013, Macchi et al. 1996). Strain concentrations in the longitudinal reinforcement in turn can reduce member

ductility and cause premature bar fracture. Potentially larger strain demands on high-strength reinforcing bars (HSRB) coupled with the lower fracture strain of HSRB compared with regular strength grade 60 bars, have also raised concerns about their cyclic fatigue performance in concrete structures subjected to seismic demands.

Limited test data exists on the behavior of high-strength reinforcing steel in concrete structures. New experimental data is needed to assess the implication of using high-strength reinforcement in concrete structures and allow the relaxation of code restrictions on the strength of reinforcing bars. The newly published ATC Project 115 report "Roadmap for the use of high-strength reinforcement in reinforced concrete design" outlines a wide range of experimental studies priced at over $26 million that are needed to fully assess the effects of high-strength reinforcements in concrete structures, and allow their adoption by design codes and standards. However, before the bulk of the experimental studies can be undertaken, benchmark structurally desirable properties need to be defined for HSRB so that all testing can be done with the steels satisfying the specifications that will be adopted in the design codes.

1.2 OBJECTIVES AND SCOPE

The overarching objective of this study is to aid the community in defining both feasible and structurally acceptable mechanical properties of HSRB for use in seismic applications. While the main focus to date in developing HSRB has been on the monotonic loading properties (e.g., T/Y ratio and fracture strain), the cyclic fatigue behavior of the newly developed HSRB is unknown. Low-cycle fatigue is defined as the failure in a material due to a relatively small number of load or deformation cycles (< 1000), and typically involves large deformations that exceed the elastic limit.

Cyclic tests are needed to evaluate the low-cycle fatigue performance of HSRB and compare it with that of grade 60 bars. These tests are needed before extensive structural testing is performed using HSRB. If the low-cycle fatigue tests on HSRB show comparable performance with that of grade 60 bars, the structural engineering community can move forward with confidence with structural testing using the HSRB. Alternatively, if poor low-cycle fatigue performance is shown for HSRB, adjustments to manufacturing processes should be implemented to improve the performance and bring it in line with what is needed for acceptable structural performance.

This study was developed to compare the low-cycle fatigue behavior of HSRB and grade 60 reinforcing bars. The low-cycle fatigue performance of HSRB produced with the main two manufacturing techniques currently used in the United-States is investigated. Other variables treated in this study were: bar size, loading history, and bar unsupported length.

2. Background

2.1 METALLURGY

The two main manufacturing processes used in the United-States to produce high-strength reinforcing bars (HSRB) result in differing mechanical properties. These processes are tempering and quenching, and micro-alloying. Steel bars whose strength is increased by quenching and tempering, typically exhibit relatively low tensile-to-yield strength (T/Y) ratios but relatively high strains at fracture. High-strength steel bars produced through micro-alloying, on the other hand, are often characterized by a relatively high T/Y ratio and relatively high strains at fracture. Differences between the production methods, the resulting metallurgy, and its influence on the mechanical properties of reinforcing bars are discussed in this section.

2.1.1. Quenching and Tempering

Two methods traditionally used to produce high-strength rebar are discussed in a paper by J.C. Dotreppe (1997). Both of these methods produce some desirable results but also have detrimental effects on steel bar performance. The first method involves hot rolling of the steel followed by gradual cooling. The second method involves hot rolling of the steel followed by strain hardening.

The method of slow cooling relies heavily on altering the chemical composition of the steel to alter the mechanical properties. For instance, by adding high amounts of carbon and manganese to the steel, the yield strength can be increased significantly. However, above certain concentrations of carbon or manganese, the steel loses much of its ductility as well as its weldability. This issue can be solved by alloying elements at much lower concentrations that have a more potent impact on the material properties,

such as vanadium, niobium, or titanium. These elements have limited detrimental effects on ductility and weldability compared with carbon and manganese, but are much more expensive. This technique is discussed further in section 2.1.2.

The method of strain hardening relies purely on the extent of straining. Increasing the amount of strain hardening increases the yield strength of the bar. Since no chemical modifications are made to the bar in this case, there is no detrimental effect on the weldability of the steel. However, it does produce a stress-strain diagram without an obvious yield plateau and decreases substantially the ductility of the bar.

Dotreppe (1997) also discusses the TEMPCORE process, a patented process that involves quenching the steel immediately after rolling and then allowing the bar to be tempered by the heat remaining in the core while gradually cooling. The quenching process, involves rapidly cooling the bars with water or oil from between 815°C and 870°C (also called the "austenitizing" or "solution-treating" temperature) down to between 150°C and 425°C in order to create a hardened layer of martensite and bainite around the exterior of the bar (Reardon 2011). The rapid cooling causes a change in crystal structure since the amount of carbon which was dissolved in the austenitic phase can no longer be accommodated by the newly formed martensite. As the crystal structure changes from a body-centered cubic lattice to a body-centered tetragonal lattice, there is expansion which leads to the distortion of the lattice structure (Reardon 2011). This lattice distortion inhibits the movement of dislocations in the steel, increasing the hardness. Since the expansion is a function of the amount of carbon dissolved in the steel before quenching, the hardness of quenched and tempered steel is a function of the carbon content.

The core, unlike the rim, cools slowly and remains primarily austenitic in composition. Heat flowing from the hot core to the surface tempers the previously formed martensite surface layer. Martensite is highly sensitive to the temperature at which it is tempered. When tempered at temperatures between 150°C and 200°C, the strength and hardness of the martensite is mostly retained while providing only minor improvements in ductility and fracture toughness. When tempered at a temperature above 425°C, a significant amount of the strength and hardness gained during quenching are lost, but much larger improvements in ductility and fracture toughness are achieved (Reardon 2011). Vanadium can also be added to the steel in order to provide secondary hardening effects during tempering.

Finally, as the bar slowly cools down to ambient temperature on a cooling bed, the austenitic core is transformed into a combination of ferrite, perlite, and bainite. This slow cooling reduces the hardness of the austenite and increases the fracture toughness and ductility.

As a result, the TEMPCORE process produces steel with mechanical properties that vary significantly between its inner core layer and its outer skin layer. TEMPCORE treated bars retain their yield plateau since they have not been strain hardened and, since the overall chemical composition has not been altered, they are still highly weldable if carbon content is limited. The TEMPCORE steel is also highly bendable and ductile compared to steels produced with strain hardening methods. TEMPCORE steel however typically exhibits a low T/Y ratio on the order of 1.15 for grade 100 reinforcing bars.

2.1.2. Micro-alloying

Currently, ASTM A706 grade 80 steel is mainly produced through micro-alloying as that process preserves ductility and weldability of the higher strength bars.

A common approach for increasing yield strength of steel is to alloy it with other elements in order to achieve substitution solid solution strengthening and interstitial solid solution hardening. Traditional elements used in alloying steel for strength improvement are carbon (C), manganese (Mn), and silicon (Si). Manganese and silicon typically contribute to substitution solid solution strengthening and carbon typically contributes to interstitial solid solution hardening. Unfortunately, when added at volumes high enough to produce grade 100 steel, carbon and manganese reduce the weldability and ductility of the material (Deeley et al. 2000).

In order to achieve the same strength gains as those achieved using Mn, Si, or C, one can substitute small amounts of vanadium, niobium, or titanium which is referred to as micro-alloying (NEHRP Consultants Joint Venture 2014). The element that was used as the primary microalloying element in the reinforcing bars studied here is vanadium. By micro-alloying the steel with small amounts of vanadium, the yield strength can be increased past 100 ksi with limited effects on weldability and ductility. However, only small amounts of vanadium are capable of being dissolved in steel and only the vanadium in solution will contribute to the hardenability of the steel. For this reason, steel with high concentrations of vanadium must be held at high austenitizing temperatures for a long time in order to ensure that the vanadium is indeed in solution (Reardon 2011).

Vanadium increases the strength and fracture toughness of steel bars primarily through the inhibition of grain growth during heat-treatment and the precipitation of carbides and nitrides (Reardon 2011 and NEHRP Consultants Joint Venture 2014). Smaller grains result in a higher density of grain boundaries, which inhibit the propagation of dislocations between steel grains.

Micro-alloying can produce a marked yield point and a T/Y ratio larger than that from quenched and tempered steels (on the order of 1.25 for grade 100 reinforcing bars).

2.2 LOW-CYCLE FATIGUE

Mander et al. (1994): Low-Cycle Fatigue Behavior of Reinforcing Steel

The authors of this paper compared the low-cycle fatigue behavior of grade 40 mild steel bars with that of high-strength prestressing threaded bars. The grade 40 steel bars used were all 5/8 inches nominal diameter A615 deformed billet-steel. The prestressing bars used were ASTM A722 type II proof-stressed alloy steel bars with threads hot-rolled into the bars. The prestressing bars had a specified ultimate strength of 157 ksi and no yield plateau. Similarly to the grade 40 bars, all of the prestressed bars had a nominal diameter of 5/8 inches.

The grade 40 bars were attached to the testing machine using steel sleeves, which were welded to the ends of the bars. The prestressing bars were gripped at couplers for testing. The couplers were shown to develop the ultimate tensile strength of the bars.

The authors used only virgin (unmachined) bars so as not to bias fatigue results. The inside and outside layers of reinforcing bars typically have differing mechanical properties. This difference is due to the work hardening of the outer layer from the application of the deformations as well as the different temperature histories of the inside and outside layers of the bars. Furthermore, bar deformation geometry can heavily influence stress concentration at the deformation and hence the fatigue life of bars. Therefore the exterior of the bars tested were not machined to obtain representative fatigue performance of reinforcing bars in concrete members.

All tests were also performed by cycling bars to various constant strain amplitudes, ranging from yield to 6%. A six bar-diameter clear span was used for all tests presented with both ends of the bar fixed against rotation to simulate the effects of transverse reinforcing spaced at 6 bar-diameters. The authors found that, for clear spans greater than 8 bar-diameters, buckling was so severe that the compressive yield strength could not be sustained under cyclic loading for either type of steel.

The low-strength steel bars showed a small amount of hardening over the first few cycles, followed by gradual softening until the formation of a fatigue crack, which was followed soon after by fracture. The high-strength steel bars, on the other hand, showed significant softening over the first few cycles, followed by a more gradual softening until the formation of a fatigue crack and fracture. The authors also found that the effects of mean stress and mean strain were negligible for large strain amplitudes (greater than 1%).

The authors also applied existing strain-based fatigue life models to their low-cycle fatigue results and developed a new energy-based fatigue life model.

Some existing models, such as that proposed by Coffin (1954) and Manson (1953), relate the fatigue life to the plastic strain amplitude. However, the difficulty in calculating plastic strains due to the Bauschinger effect led the researchers to use total strain amplitudes instead. The results of applying these existing models indicated that the high-strength steel threaded bars performed similarly in low-cycle fatigue to the lower-strength steel bars in terms of half-cycles to failure, exhibiting a marginally higher fatigue life.

The authors also explored the option of estimating fatigue life based on the superposition of an elastic component and a plastic component of strain. As the total

strain increases, the elastic contribution to the fatigue life estimate diminishes and the equation approaches that for plastic strain amplitude.

In order to relate the total strain energy dissipation to the strain amplitude, the authors proposed a variety of equations that combined the existing models relating fatigue life to strain amplitude and the relationship between total strain energy dissipation and number of half-cycles to failure proposed by Tong (1989).

Since the maximum stresses reached were so much higher for high-strength steel, the energy dissipated per cycle for a given strain amplitude was much higher. This increase in energy per cycle meant that the energy-based fatigue life models for the two steel types gave very different results. The threaded bars consistently exhibited higher total strain energy dissipation for a given value of: number of half-cycles to failure, total strain amplitude, plastic strain amplitude, maximum stress multiplied by total strain amplitude, or maximum stress multiplied by plastic strain amplitude.

The authors concluded based on these results that the use of high-strength steel in seismic design should not be limited. Another important finding was that the monotonic ductility of the steels did not play an important role in the fatigue performance. The ductility of the high-strength steel was only 17% of that of the grade 40 steel. Conventional wisdom places high value on displacement ductility for seismic applications, but the similar performance of the two steels tested led the authors to conclude that this may not be a very important quantity in seismic applications.

Brown and Kunnath (2004): Low-Cycle Fatigue Failure of Reinforcing Steel Bars

The authors of this paper intended to enhance the understanding of low-cycle fatigue failure of longitudinal reinforcing steel. The authors also note that the ACI 318 code does not directly consider the low-cycle fatigue behavior of reinforcing steel, but

instead uses other factors (such as the tensile properties of the steel) to indirectly control low-cycle fatigue performance of reinforcing bars. In addition to studying the fatigue behavior of the steel, the authors also developed a fatigue life relationship to characterize the response.

The tests were all performed on ASTM A615 grade 60 reinforcing steel. A615 grade 60 steel has a specified minimum yield strength of 60 ksi and a minimum ultimate tensile strength of 90 ksi. Since the tests focused on longitudinal steel, the bar sizes tested were ones representative of typical longitudinal bars: #6, #7, #8, and #9. Virgin (unmachined) bars were used for all tests. All bars were cycled at constant strain amplitudes with fully reversed strain amplitudes varying between 1.5% and 3.0%. The strains were measured over the entire clear span of the coupons, which was selected as 6 bar-diameters. The strain amplitudes measured were, therefore, based on the average strains across the entire clear span.

In order to avoid fracture of the bars at the connections to the grips, a setup similar to that used by Mander et al. (1994) was employed. Instead of a steel sleeve, however, the authors used aluminum sleeves that were not welded to the bars. The aluminum sleeves served to reduce the stress concentrations in the bars due to gripping.

The study was inspired by reports of fracture of longitudinal reinforcing bars from inelastic cyclic strains in bridge columns. The test conditions were, therefore, created to mimic this situation as closely as possible. Since concrete typically spalls at relatively low strains under cyclic loading, the cover concrete can only provide limited resistance against longitudinal bar buckling. To reproduce these *in-situ* conditions for low-cycle fatigue, the authors tested bars in air.

The authors found that the low-cycle fatigue behavior of reinforcing bars generally conforms well to commonly used strain-life models with the best fit coming from the form proposed by Koh and Stephens (1991). They also found that, for low strain amplitudes (less than 2%), bars with larger diameters exhibited longer fatigue life. For high strain amplitudes, however, this relationship is reversed and larger diameter bars exhibited shorter fatigue life. The combination of these two trends indicate that larger diameter bars exhibit a more severe deterioration of fatigue life with increasing strain amplitude when compared to smaller diameter bars. The authors also examined the relationship between fatigue life and plastic strain amplitude. Since all bars tested of the same size had nearly identical elastic strains, using plastic strain amplitude instead of total strain amplitude had little effect on the accuracy of fatigue life predictions. The authors noted, however, these relationships can be useful for modeling fatigue life during random strain amplitudes.

The authors also related the total energy dissipation to failure to the total strain amplitude by using the form of equations proposed by Mander, et al. (1994). They found that these energy based methods of predicting fatigue life were much less reliable than methods based on the number of cycles to failure. The authors postulate that the relationship between the number of cycles to failure and the energy dissipation per cycle may influence the accuracy of energy methods. The energy dissipated in one cycle tends to decrease with an increasing number of cycles to failure. Therefore, the range of cycles to failure can be larger than the range of energy dissipation values, meaning that the total energy dissipation will provide less precise predictions of failure than the number of cycles.

Hawileh, et al. (2010): Evaluation of the Low-Cycle Fatigue Life in ASTM A706 and A615 Grade 60 Steel Reinforcing Bars

The authors of this paper tested steel reinforcing bars under cyclic loading using virgin (unmachined) bars. All of the bars tested were grade 60 #6 bars, and the major difference between bar types was the ASTM classification: either A706 or A615. A706 grade 60 steel has a larger minimum specified fracture strain of 14% compared to the minimum specified fracture strain of 9% for A615 grade 60 steel. The A706 bars had higher ductility than the A615 bars tested. The A706 bars also proved to have a lower ratio of tensile to yield strength than the A615 bars. Unlike in the cyclic tests, machined specimens with a diameter of 0.445 inches were tested monotonically to identify bar material properties.

Constant strain amplitudes were used in the cyclic tests, with non-reversed strain amplitudes ranging between 1% and 3%. Unlike the other studies mentioned here, buckling was prevented during the cyclic tests via a steel collar with an inside diameter just larger than the diameter of the bars. This was done in order to mimic the boundary conditions of unbonded bars in prestressed hybrid frames where grout would prevent bar buckling in compression.

The data for most of the tests showed very similar results between the two different types of steel, despite differing monotonic tensile-test results. In fact, the A615 bars generally required more cycles to failure than the A706 bars. Depending on the strain amplitude, the A615 bars failed after 14% to 43% more cycles than A706 bars. This finding is counter to a commonly held belief that high displacement ductility leads to better low-cycle fatigue performance. Based on the results of these tests, the authors proposed a series of equations intended to estimate the low-cycle fatigue life (as well as the hysteretic energy dissipation) of mild steel bars under particular loading conditions.

Due to the higher stresses experienced by the A706 bars compared to the A615 bars, the amount of strain energy dissipated by the A706 bars per cycle was higher. However, this difference was smaller than the difference in number of cycles so the total strain energy dissipated was higher for the A615 bars.

A major difference between the HSRB produced by the two different manufacturing processes is the monotonic ductility ratio. Results from Hawileh et al. (2010) indicate that, at least when buckling is restrained, the monotonic ductility ratio might not have a significant impact on the fatigue life of HSRB within a practical range of strain amplitudes.

Monti and Nuti (1992): Nonlinear Cyclic Behavior of Reinforcing Bars Including Buckling

The authors of this paper first performed monotonic compressive tests on reinforcing bars with clear spans equal to 5, 8, and 11 times d_b (where d_b = the nominal bar diameter) in order to represent spacing commonly used in construction. For clear spans of $5d_b$, the compressive stress-strain curve closely approximated the tensile stress-strain curve, indicating little impact from buckling. With increasing clear spans, the correspondence between the compressive stress-strain curves and the tensile stress-strain curves decreased drastically. At clear spans of $11d_b$, the bars soften and buckle immediately after yield.

Based on these results, the authors developed an empirical relation for the strain up to which the compressive and tensile stress-strain curves deviated by more than 5%.

The authors also performed cyclic tests with a variety of strain histories on bars with the same clear spans as those used in the monotonic tests. Based on these cyclic tests, they developed an analytical model to represent the cyclic behavior of reinforcing

bars including the effects of buckling. The model updates the stress-strain relationship at every load reversal in order to account for the loading history.

One of the most important parameters identified in the authors' analysis was the hardening ratio, or the ratio of the post-yielding modulus to the initial (elastic) modulus. They found that increasing this ratio would lead to an increase in hardening from one cycle to the next.

The authors found that, in the absence of buckling, their model provided equivalent predictive abilities to previously developed models. For longer clear spans, however, in which buckling was prominent, the new model provided the only accurate predictions of fatigue behavior.

While the model provided significant improvements over previous models, especially in the presence of buckling, it did not provide any estimate of the reinforcing bar fatigue life, which is of critical importance for the assessment of use in seismic applications.

NIST GCR 14-917-30 (2014): Use of High-Strength Reinforcement in Earthquake-Resistant Concrete Structures

This report outlines structural considerations related to bar buckling which are relevant to the low-cycle fatigue behavior of HSRB. Specifically, the report discusses the effect of the ratio of transverse bar spacing to longitudinal bar diameter (s/d_b) and the effect of transverse bar stiffness on reinforcing bar buckling.

The authors identify two potential ways in which premature buckling can reduce the effectiveness of reinforcing bars: decreased energy dissipation, and cracking at the bar deformations. Due to the decrease in compressive load-carrying capacity which is associated with buckling, the total strain energy dissipation of the bar is reduced by

increasing the degree of buckling. In addition, buckling can cause cracks to form at the base of the deformations on the compression side of the bar. These cracks lead to stress concentrations which lead to premature bar fracture.

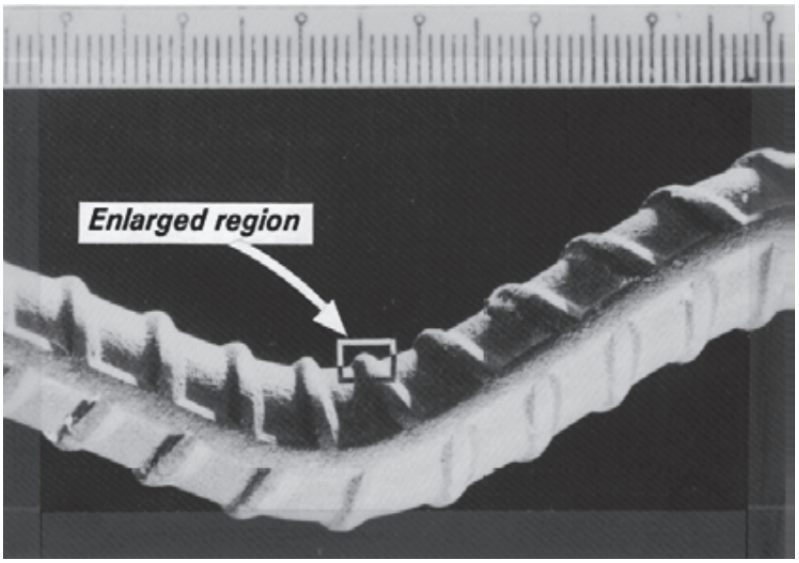

Figure 1: "Cracking along the root of the deformation in the compressed side of a buckled reinforcing bar: overall view of buckled reinforcing bar" (NEHRP Consultants Joint Venture)

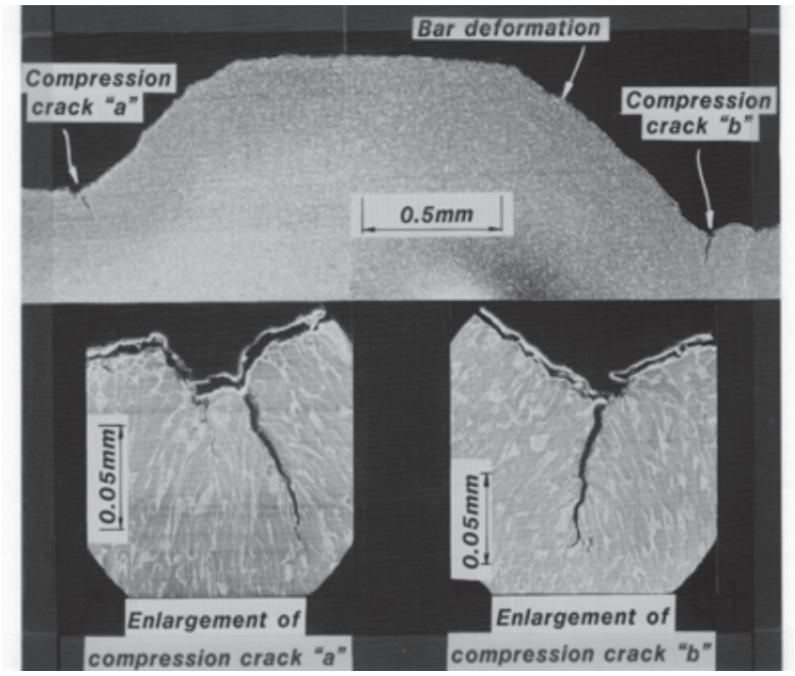

Figure 2: "Cracking along the root of the deformation in the compressed side of a buckled reinforcing bar: electron microscope view of cracking" (NEHRP Consultants Joint Venture)

The authors also performed buckling analyses of grade 60, grade 80, and grade 100 bars based on the expected material properties, discretized fiber cross-sections, and using clear spans of $4d_b$, $5d_b$, and $6d_b$. These clear spans were selected based on the current ACI 318 provision that limits s/d_b to 6 for regions in beams, columns, or the boundary elements of walls at plastic hinges. The bar cross-sections were discretized into fibers in order to evaluate the nonlinear geometric effects of bar buckling. The end conditions were considered to be completely fixed in order to model the idealized conditions provided by the transverse reinforcement. In this way, the effects of transverse reinforcement stiffness, concrete core restraint, and cover restraint were excluded. The analysis primarily focused on strains up to 0.025.

This analysis showed that the response of grade 60 reinforcing bars were practically equivalent for all three clear spans considered prior to a strain of 0.025. Similarly, the response of grade 80 reinforcing bars was practically equivalent for all three clear spans in this strain range. The grade 100 bars, however, showed an equivalent stress-strain response only up to clear spans of $5d_b$ for strains up to 0.025. They observed that the softening behavior of grade 100 bars with a clear span of $5d_b$ was approximately equivalent to the softening behavior of grade 60 and grade 80 bars with clear spans of $6d_b$.

Based on this analysis, the authors concluded that: the current ACI 318 provisions limiting clear spans could be directly applied to grade 80 reinforcing bars, and reducing the clear span limit for grade 100 reinforcing bars from $6d_b$ to $5d_b$ would suffice to overcome the differences in performance.

The current ACI 117 limits spacing tolerances to the lesser of ±3 inches, ±1 inch per foot of beam depth, or ±1 inch per least column width (ACI 117 2010). The authors note, however, that these spacing tolerances would need to be decreased if the limits of $6d_b$ and $5d_b$ were adopted for grade 80 and grade 100 respectively. They note that, for an element which is 3 feet or deeper with grade 80 #8 bars as longitudinal reinforcement, spacing of up to 9 inches, or $9d_b$, would be acceptable. Likewise, for an element which is 3 feet or deeper with grade 100 #8 bars as longitudinal reinforcement, spacing of up to 8 inches, or $8d_b$, would be acceptable. The higher strength reinforcing bars were seen to be more prone to buckling with increases in clear span than grade 60 bars and clear spans as high as $8d_b$ and $9d_b$ would cause significant decreases in fatigue performance.

The report also discusses the possibility of buckling of longitudinal bars across multiple hoops. If grade 60 hoops are replaced with higher strength bars of a smaller size,

the decreased stiffness may allow buckling to occur over multiple hoops, greatly increasing the buckling length of the longitudinal bars. This issue has not yet been resolved and the authors suggest further investigation of the issue.

Finally, they note that a limited number of tests on beams and columns using HSRB and detailed to ensure the development of a plastic hinge have been performed. All of these tests have used s/d_b ratios of less than or equal to 4.6, and almost all have shown excellent deformation capacity. This does not necessarily indicate that members with the suggested s/d_b ratio of 5 or 6 would perform as desired, but neither does it indicate a deficiency in this recommendation.

The clear span suggestions provided here helped guide the development of the test matrix used in the material testing study performed at UTA.

Restrepo-Posada et al. (1994): Variables Affecting Cyclic Behavior of Reinforcing Steel

The authors of this paper performed cyclic tests on virgin bars with clear spans of 4 times the bar diameter as well as machined specimens with clear spans of 2.5 times the machined bar diameter. The low aspect ratios were selected in order to minimize the effects of buckling so that the material properties could be examined. For each specimen type, bars were tested with nominal yield strengths of 40 and 60 ksi.

The researchers applied an analytical model originally proposed by Dodd and Restrepo-Posada (1995) and calibrated the model based on the results of the machined specimens. They then compared the predictions of this model to the results of the virgin bars and found a high degree of correspondence. They concluded, therefore, that when buckling is absent, neither the geometry nor the existence of rolled-on deformations affect the cyclic behavior of reinforcing bars.

The effects of strain rate on monotonic and cyclic behavior were also investigated. From the monotonic tests, an increase in the yield and ultimate strengths were noticed with an increase in strain rate. The fracture strain, however, decreased with an increase in strain rate. A difference was noticed in the strain rate effects based on the grade of steel tested, with the lower strength steel exhibiting higher strain rate effects, but none of the effects were very large. By increasing the strain rate by two orders of magnitude, the yield stress only increased by a maximum of 10%.

The authors also investigated the effects of strain aging on the two different strength steels. They noted that the vanadium content of the higher strength steel (0.034% to 0.040% by mass) was sufficient to altogether eliminate the effects of strain aging due to its ability to reduce the amount of soluble nitrogen in the steel.

3. Experimental Program

3.1 TEST MATRIX

Low-cycle fatigue tests were conducted on HSRB representative of current production methods and practices in the United-States. In the experimental program, the following influential parameters were varied: 1) production method, 2) steel strength or grade, 3) bar size, 4) loading protocol, and 5) bar unbraced span.

Bars produced by two manufacturers utilizing the two main production methods for HSRB in the United-States were tested. The high-strength steel bars produced by the two manufacturers had significant differences in their material properties. Manufacturer 1 produces HSRB using micro-alloying, while Manufacturer 2 produces HSRB using a combination of micro-alloying and quenching and tempering.

Four different grades of steel were tested for this research: grade 60 and grade 80 satisfying ASTM A706, grade 80 satisfying ASTM A615, and a relatively ductile grade 100 that does not have standard specifications at this time. The term grade is used in this document to refer to the specified yield strength of a reinforcing bar.

In order to assess the low-cycle fatigue behavior of bars typically used as longitudinal reinforcement, as well as those typically used as transverse reinforcement, three different bar sizes were tested: #5, #8, and #11.

A total of three loading protocols were used in order to represent realistic strains for each particular bar size. For all bar sizes, a partially reversed cyclic loading protocol bound by +4% and -1% strains was used. A positive strain value indicates a tensile strain and a negative strain value indicates a compressive strain. The partially reversed loading protocol was used to allow for direct comparison between different bar sizes. This partially reversed loading protocol with a high tensile strain target and a relatively low

compression strain target is representative of the strains experienced by longitudinal bars of flexural members in plastic hinge regions sustaining large inelastic deformations (Sokoli 2015).

For #11 bars, representing the larger end of commonly used longitudinal bar, only this partially reversed loading protocol was used. For #8 bars, representing the smaller end of commonly used longitudinal bars, a fully reversed loading protocol cycling between strains of +2% and -2% was also used (for comparison with previous low-cycle fatigue tests identified in the literature). For #5 bars, representing transverse bars, a partially reversed loading protocol cycling between strains of +4% and 0% was used. This partially reversed loading protocol with only tensile strains is representative of the strains experienced by transverse bars of flexural members in plastic hinge regions sustaining large inelastic deformations (Sokoli 2014). For this reason, very few tests were performed on #5 bars at the loading protocol of (+4%, -1%) and the (+4%, 0%) loading protocol was used primarily.

Bars were gripped at three clear spans where possible: $4d_b$, $5d_b$, and $6d_b$ (where d_b = the nominal bar diameter). Current code provisions for seismically detailed frame members, given in ACI 318-14, limit the spacing between transverse hoops to $6d_b$ (six times the diameter of the longitudinal bar) to limit buckling of the longitudinal bars braced by the hoops during severe inelastic demands. Since bars of higher strength will experience higher loads for the same bar diameter and buckling strength, higher strength bars may need to be braced at a closer interval than is currently prescribed for grade 60 bars in ACI 318-14 (NEHRP 2013). Bars were tested at various clear spacing to explore the interactions between bar buckling and low-cycle fatigue performance. Due to geometric constraints, #5 bars could not be tested at clear spans of $4d_b$ or smaller.

Therefore, tests were performed at only $5d_b$ and $6d_b$. Based on the consistent relationship between fatigue life and clear span shown in the #8 bars, only the two extremes ($4d_b$ and $6d_b$) were used for #11 bars.

3.2 TESTING PROTOCOLS AND INSTRUMENTATION

3.2.1 Monotonic Testing Protocol

In order to identify the material properties of the steel bars, monotonic tension tests were performed conforming to the procedures specified in *ASTM A370 – Standard Methods and Definitions for Mechanical Testing of Steel Products* and *ASTM E8 – Standard Test Methods for Tension Testing of Metallic Materials*. The complete force-strain response of a bar was recorded during each monotonic test. Stresses were calculated as the bar force divided by the nominal bar area. All strains used to generate bar stress-strain relations were measured over an 8 inch gage length as specified in ASTM A370. The material properties obtained include: the modulus of elasticity, the yield strength, the tensile strength, the tensile-to-yield strength (T/Y) ratio, the uniform strain, and the fracture strain. The modulus of elasticity was measured as the slope of the initial elastic region of the stress-strain curve. Since all of the bars tested exhibited a clear yield plateau, the end of this elastic region was clear. Yield stress was calculated by the 0.2% offset method as detailed in ASTM E8. The ultimate tensile strength was measured as the maximum stress recorded in a test. The tensile-to-yield strength ratio was taken as the ratio of the ultimate tensile strength to the yield strength. Uniform strain is defined as the strain reached at tensile strength and immediately prior to the initiation of necking. Since the stress-strain curve is nearly flat in this region (Figure 3), the uniform strain was taken, in accordance with ASTM E8, as the middle point of the range of strains that led to

stresses of at least 99.5% of the ultimate tensile strength (Figure 3). Fracture strain was measured just prior to loss of load-carrying capacity and, therefore, includes both the plastic and the elastic components of strain.

Two additional monotonic stress/strain properties were also calculated from those discussed above. These parameters are the strain at the elastic limit and the ductility ratio. The elastic limit strain was obtained by dividing the yield strength by the elastic modulus to obtain the strain at which yielding began. The ductility ratio was obtained by dividing the fracture strain by the elastic limit.

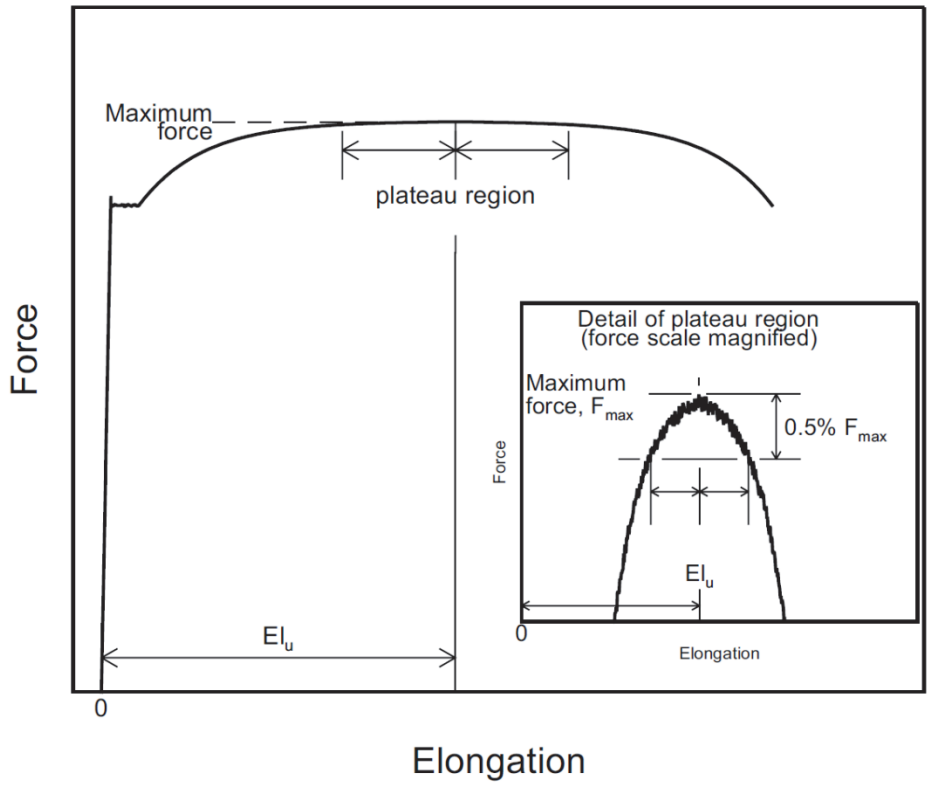

Figure 3: Method of calculating uniform strain (ASTM E8)

3.2.2 Low-Cycle Fatigue Testing Protocols

All tests were performed in a universal test machine with a capacity of 550 kips in compression and tension with two independent hydraulic gripping mechanisms. The machine is capable of static and fatigue testing under load or deformation control. Hydraulic grips are six inches long such they were able to generate rotational fixity at both ends of the bars tested. Rotational fixity at bar ends was intended to replicate boundary conditions of longitudinal reinforcing bars between two transverse bars.

Bar deformation geometry has been proven to have significant impacts on the fatigue life of reinforcing bars. Furthermore, most bars typically exhibit significant gradients in strengths across their thickness. This strength gradient is especially pronounced in quenched steels as the rapid cooling of the outer layer leads to the formation of martensite, a high-strength, low ductility steel crystalline structure, which eliminates the yield plateau. The work hardening of the outer layer of steel bars also causes strength gains and reductions in ductility closer to the bar surface. The bars were therefore tested in their virgin (un-machined) state to obtain low-cycle fatigue data that is representative of their in-situ low-cycle fatigue performance.

To minimize bar fracture at the edge of the grips due to stress concentrations generated by the gripping, bars were swaged with ASTM 6063 aluminum tubing. Tubes were halved length-wise and placed around the bars where they were gripped (Figure 4). The aluminum tubing material is softer than the steel bars such that it deformed upon griping and distributed gripping stresses more evenly on the bars. Swaging the bars significantly reduced the number of failures at the grips. However, because the aluminum has a low yield strength (16 ksi) and low relative stiffness, deformations in the aluminum during cyclic testing lead to discrepancies between the displacement readings of the

loading head and bar deformations. Thus deformation readings from the testing machine could not be used reliably and tests were controlled using strains measured directly on the bar surface. All cyclic tests were performed at a strain rate of about 0.001/second.

Figure 4: Aluminum tubing temporarily attached to the ends of a bar with tape.

In order to measure the number of cycles to failure in a low-cycle fatigue test, one must first define failure. Some options are: the point at which peak stress within a cycle no longer occurs at the peak strain, the initiation of a fatigue crack, or fracture of the bar. For the tests conducted in this study, fracture of the bar was selected as the failure threshold. Due to the relatively high strain ranges used in in this study (and, therefore, the low number of cycles to failure) the difference between fatigue crack initiation and bar fracture was found to be at most two full cycles. The number of half-cycles to failure, not full cycles, was selected as a unit for measuring fatigue life.

3.2.3 Instrumentation

Loads applied to the bars were recorded from the load cell of the testing machine. Strains and deformations of the bars were obtained from high-resolution images recorded using a monochrome digital camera. A typical photograph taken by this camera is shown

in Figure 5. A Digital Image Correlation (DIC) software (Sokoli et al. 2014) was used to monitor the two-dimensional location of surface targets on the bars. Surface targets tracked by the system can either be affixed paper targets with a high-contrast random pattern or any surface area with a unique pattern with sufficient contrast. The DIC system is capable of tracking an unlimited number of targets during testing and in post-processing, and produce strain resolutions on the order of 10^{-4}. Real time strain data obtained from the system were used to control the tests. The targets nearest to the grips on both ends of the bars were used to calculate the average strain along the entire clear span of bars. This average strain was used to control the tests and achieve the intended strain ranges. All bars were oriented such that weak axis buckling would occur in the plane perpendicular to the direction of the camera to measure the extent of bar buckling.

Figure 5: Typical photograph from the DIC System.

3.2.4 Other Data Collection

In addition to the variables which were directly controlled in these tests, other parameters were derived from direct measurement of the reinforcing bars. These

parameters consist of the geometric properties of the bar deformations and the steel chemical composition.

Geometric Properties of Deformations

Previous researchers have identified the importance of transverse deformation geometry for cyclic fatigue life. Specifically, the ratio of the radius at the base of the deformation to the height of that deformation has been shown to correlate with fatigue life (Helgason et al. 1976). Therefore, the radii at the base of either side of the deformations as well as the height of the deformations were measured using the same high resolution monochrome digital camera as was used for measuring strains. An example image used to measure these deformation geometry parameters is shown in Figure 6.

Three parameters which were determined to be correlated to the cyclic performance of the reinforcing bars tested were: the ratio of the smaller of the two radii at the base of the deformation (R_{min}) to the height of the deformation (H), the ratio of the larger of the two radii at the base of the deformation (R_{max}) to the height of the deformation, and the ratio of the height of the deformation to the nominal diameter of the bar (d_b).

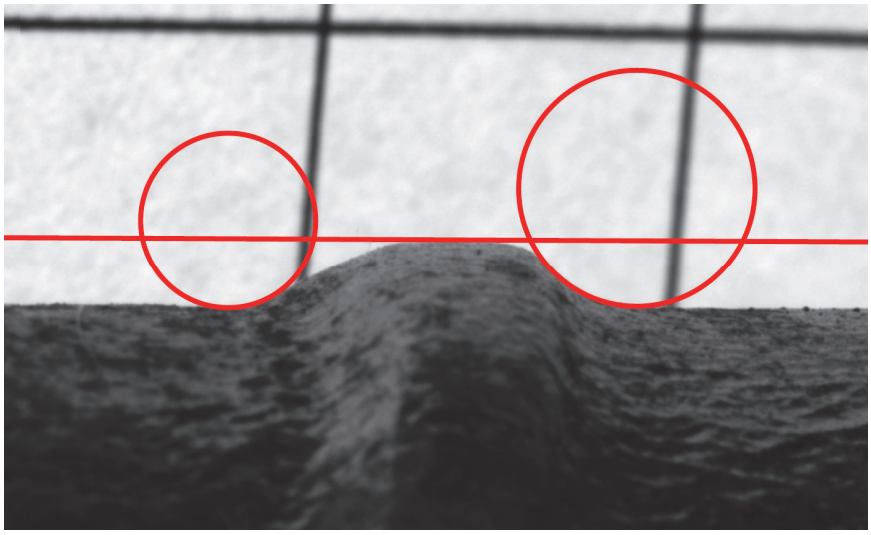

Figure 6: Example image of bar deformation detail. The red circles represent the measured minimum and maximum radii of curvature at the base of the deformation. The red line represents the location the height of the deformation was measured.

A summary of these geometric properties for every bar type is provided in Table 1.

Bar Size	Manufacturer	Grade	R_{min}/H	R_{max}/H	H/d_b
#11	1	**60**	1.32	1.81	0.0500
		100	2.27	2.31	0.0604
	2	**60**	0.89	1.10	0.0604
		100	0.66	0.89	0.0665
#8	1	**60**	2.72	2.97	0.0617
		80	3.54	3.81	0.0756
		100	3.22	4.94	0.0632
	2	**60**	1.30	2.59	0.0611
		100	0.63	0.86	0.0753
#5	1	**60**	2.55	3.00	0.0618
		80	1.27	2.18	0.0813
		100	1.32	1.72	0.0707
	2	**60**	1.13	2.06	0.0639
		80	3.01	3.52	0.0755
		100	0.43	0.69	0.0735

Table 1: Summary of deformation geometry for all types of bars tested

Steel Chemical Composition

The mill test reports for the bars studied indicate the percent composition of twelve elements in the steel: carbon, manganese, phosphorus, sulfur, silicon, copper, chromium, nickel, molybdenum, vanadium, niobium, and tin. The impact of the concentrations of these elements on the cyclic performance of the reinforcing bars was studied and is discussed in chapter 5.

4. Test Results and General Observations

4.1 MONOTONIC TENSION TESTS

Monotonic tests were conducted on at least three coupons for each bar type used in the cyclic tests. Mechanical properties for each bar type averaged over all coupons are summarized in Table 2. Figure 7 to Figure 9 present the stress-strain relations obtained for all monotonic tension tests.

Bar Size	Manuf-acturer	Grade	Yield Strength (ksi)	Tensile Strength (ksi)	T/Y Ratio (unitless)	Elastic Modulus (ksi)	Uniform Strain (%)	Fracture Strain (%)	Percent Difference in Fracture and Uniform Strains
#11	1	**60**	67.0	97.1	1.45	28,300	11.9	21.7	82%
		100	103.4	128.8	1.27	28,300	8.3	11.7	42%
	2	**60**	62.7	91.1	1.45	29,200	11.4	18.1	59%
		100	99.6	118.9	1.19	28,300	6.7	9.9	48%
#8	1	**60**	63.2	93.7	1.48	26,900	11.6	18.8	73%
		80	80.3	110.0	1.37	27,400	10.0	16.7	67%
		100	101.5	128.5	1.27	30,100	8.1	11.6	42%
	2	**60**	61.5	103.1	1.68	25,800	9.5	14.5	53%
		100	104.6	123.8	1.18	31,400	6.2	9.8	58%
#5	1	**60**	68.5	95.8	1.40	30,700	10.0	14.4	45%
		80	83.3	107.1	1.28	26,900	9.5	13.7	45%
		100	111.0	134.9	1.22	26,000	8.8	11.6	32%
	2	**60**	72.4	104.3	1.44	28,300	10.0	15.3	54%
		80	83.6	105.0	1.26	26,900	9.7	13.9	43%
		100	106.8	127.7	1.20	28,100	7.6	10.8	43%

Table 2: Summary of material properties calculated from monotonic tension tests (average across all coupons per bar type)

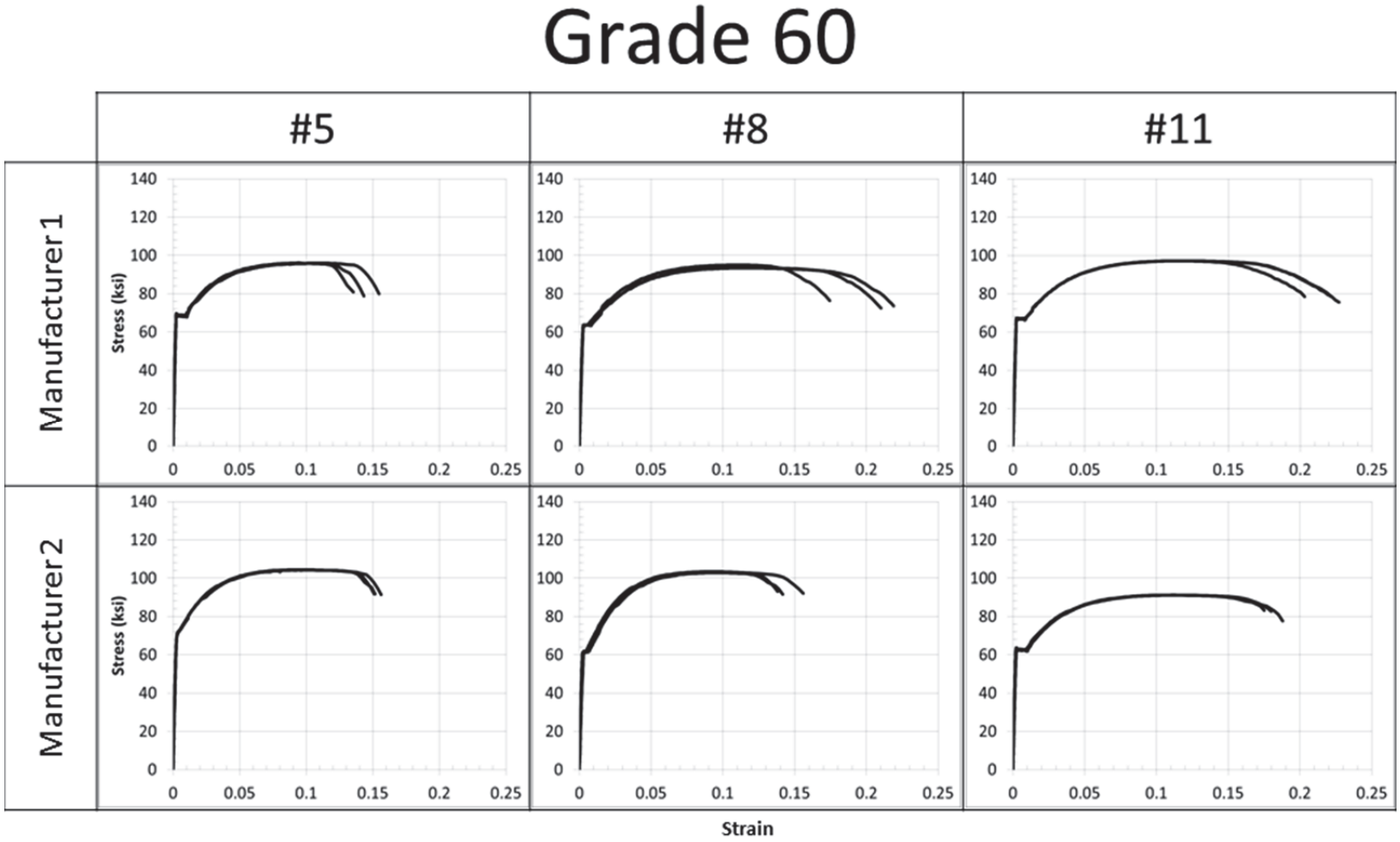

Figure 7: Stress-strain curves from monotonic tension tests of grade 60 A706 bars

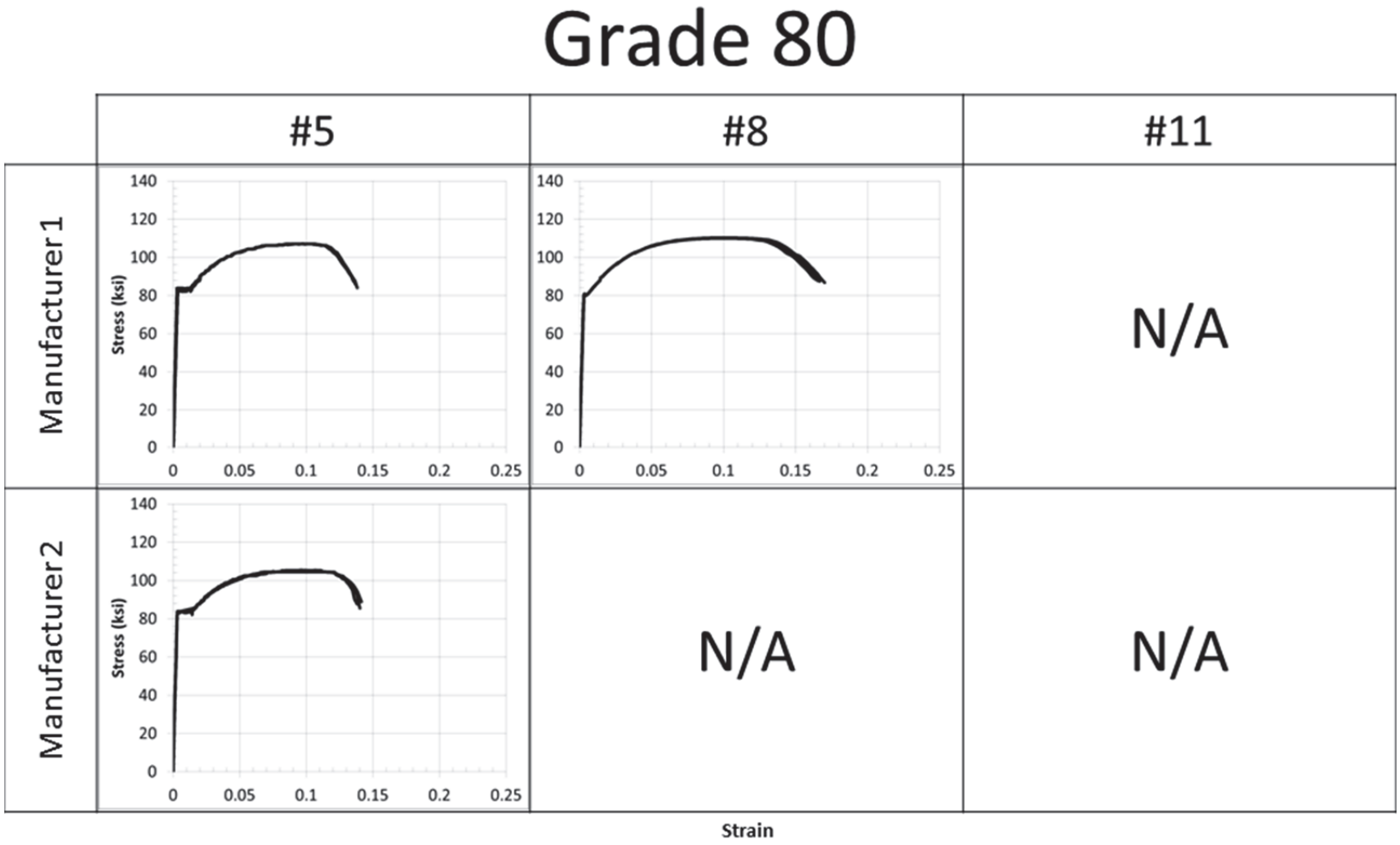

Figure 8: Stress-strain curves from monotonic tension tests of grade 80 bars

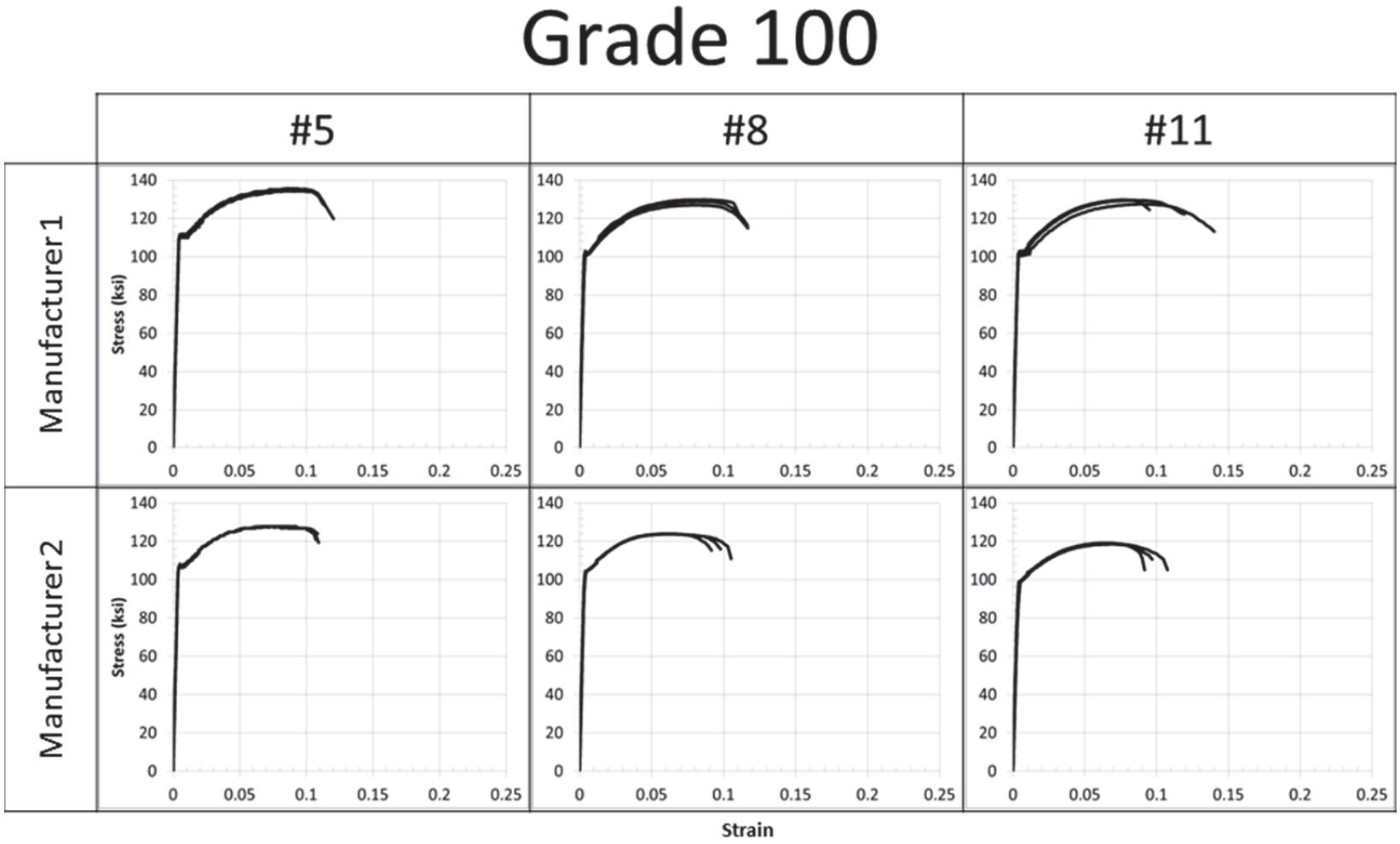

Figure 9: Stress-strain curves from monotonic tension tests of grade 100 bars

4.1.1 Effects of the Manufacturing Process

For #8 and #11 grade 100 bars, the manufacturing process had a significant impact on the T/Y ratio. Namely, Manufacturer 1 produced bars with higher T/Y ratios (1.27 for #8 and #11 bars) than Manufacturer 2 (1.18 for #8 bars and 1.19 for #11 bars). These differences are likely a result of the different production methods used by the two manufacturers to increase the strength of the steel. The quenching-and-tempering process used by Manufacturer 2 typically increases yield strength by a larger amount than tensile strength, which causes bars produced using that process to have a relatively low T/Y ratio (Grimaldi 2000). Micro-alloying, on the other hand, typically has a greater impact on tensile strength than quenching and tempering and produces a larger T/Y ratio (Nikolaou 2005).

The #5 bars, however, exhibited much less difference between the two manufacturers. For both grade 80 and 100, the difference in T/Y ratio was below 3%.

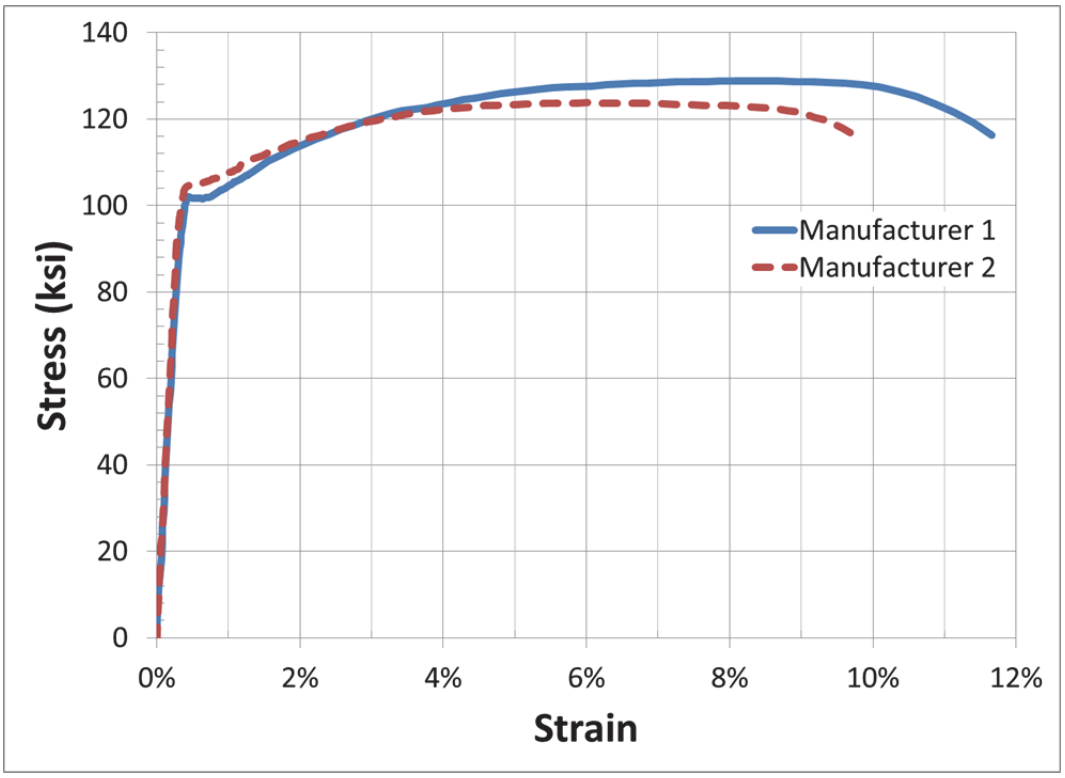

Figure 10: Comparison of stress-strain curves for typical grade 100 #8 bars

In addition, the uniform strains measured were 15.8% to 30.7% higher for grade 100 #8 and #11 bars from Manufacturer 1 than for grade 100 bars from Manufacturer 2.

The fracture strains measured were 7.2% to 18.7% higher for grade 100 #8 and #11 bars from Manufacturer 1 than for grade 100 bars from Manufacturer 2.

The grade 80 #5 bars from each manufacturer exhibited uniform and fracture strains that were very similar to each other. The bars from Manufacturer 2 show only 2.9% and 1.7% higher uniform and fracture strains, respectively, than those of Manufacturer 1.

Both grade 60 #5 and #11 bars had very similar T/Y ratios, with less than a 4% difference between manufacturers. However, despite the similarities in chemistry, the

grade 60 #8 bars exhibited significantly differing T/Y ratios from one manufacturer to the next. Both #8 bars displayed yield strengths just above the specified minimum of 60 ksi, but the steel from Manufacturer 2 exhibited a larger ultimate tensile strength of 103.1 ksi compared to 93.7 ksi for Manufacturer 1.

Similarly to the trend in T/Y ratios, the uniform strain was very similar (less than 5% different) for grade 60 #5 and #11 bars while the difference was much larger for grade 60 #8 bars (Manufacturer 1 having 22.3% larger uniform strain).

The fracture strain varied dramatically for grade 60 bars based on manufacturer. The grade 60 bars produced by Manufacturer 1 had significantly higher fracture strains for the larger bars (20.0% and 38.5% higher for #8 bars and #11 bars respectively). The grade 60 #5 bars from Manufacturer 2, however, had a slightly (5.9%) higher fracture strain than those from Manufacturer 1.

4.1.2 Effects of the Steel Grade

For both manufacturers and all bar sizes, increasing the steel grade resulted in: higher yield strength, higher ultimate strength, lower T/Y ratios, lower uniform strains, and lower fracture strains (Figure 11). In addition, the percent difference between uniform and fracture strains tends to be lower for higher grade bars (Table 2). This indicates that the higher grade bars experienced less necking prior to fracture.

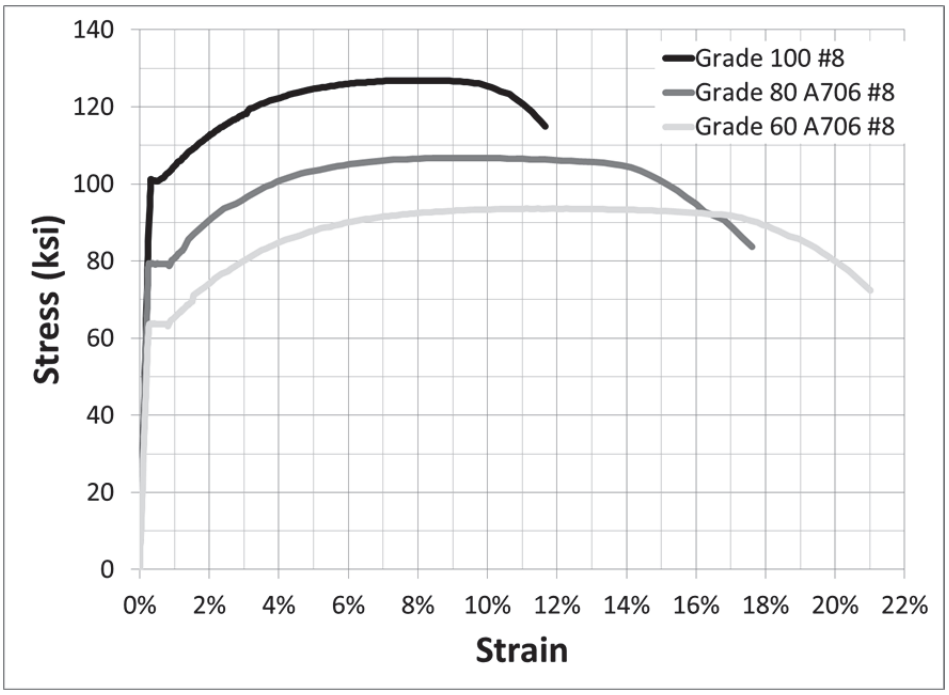

Figure 11: Stress-strain curves representative of different steel grades (all bars are produced by Manufacturer 1)

4.1.3 Effects of Bar Size

As shown in Table 2, the mechanical properties of grade 60 bars produced by Manufacturer 1 varied with respect to bar size as expected. The yield and ultimate strengths were similar for #5, #8, and #11 bars, but the larger bars had considerably larger fracture strains than the smaller bars, likely due to the slower cooling rate of the larger bars, which leads to decreased hardness and increased ductility. The larger diameter also allows for a greater degree of necking prior to fracture, which, over a fixed gage length of 8 inches, leads to a perceived increase in fracture strain for larger bars. The bar-size effect was less pronounced with respect to the uniform strain, with #11 bars only showing 4%, higher uniform strains than the #5 bars of the same grade and produced by the same manufacturer.

Similarly, the grade 80 bars produced by Manufacturer 1 varied in their monotonic test properties with respect to bar size in the same way that the grade 60 bars did.

However, the mechanical properties of grade 100 bars produced by Manufacturer 1 were nearly identical, with all parameters except for the elastic modulus varying by less than 9% between bar sizes. The fact that the uniform and fracture strains were similar for all bar sizes in grade 100 bars indicates that the necking stage extends over a much smaller strain range in grade 100 bars than in grade 60 bars. This observation is also corroborated by the smaller difference between uniform and fracture strains in grade 100 bars (6% average strain difference) than in grade 60 bars (20% average strain difference).

The mechanical properties of grade 60 bars produced by Manufacturer 2 varied significantly based on bar size. The #5 bars had larger yield strength than the larger bars, while the #11 bars had larger uniform and fracture strain values (due to the same two factors mentioned above).

The mechanical properties of grade 100 bars produced by Manufacturer 2 were also very similar, with all parameters except for elastic modulus and uniform strain varying by 11% or less between bar sizes. The uniform strain of grade 100 #5 bars was nearly 22% larger than that of grade 100 #8 bars.

4.2 LOW-CYCLE FATIGUE TESTS

Table 3 to Table 5 provide the numbers of half-cycles to fracture for all bar coupons tested in the program. Table 6 summarizes the overall average number of half-cycles to fracture and the coefficients of variation (COV) for all values of four parameters that were controlled in the study: 1) manufacturing process, 2) clear span, 3) steel grade, 4) and loading protocol. As can be seen in Table 6, for a given set of parameter values,

large scatter exists in the number of cycles to fracture. Significant changes in the numbers of half-cycles to failure were also recorded across the controlled parameters in the testing program. It is important to note that the test matrixes for manufacturer, grade, clear span, and total strain ranges were mostly complete across other parameters such that little bias is expected in the results in Table 6. For bar size, however, #11 bars were only tested at the larger 5% total strain range while #5 bars were mostly tested at a total strain range of 4%. For this reason, results for bar size are not presented in Table 6.

Table 7 summarizes the changes in low-cycle fatigue performance of bars with respect to all controlled parameters. The differences in the coefficients of variation (COV) are also reported in Table 7. These differences are not calculated based on the average values presented in Table 6, but based on the average difference between sets of tests for which all other variables are held constant.

		Loading Protocol		
		+4%, 0%		**+4%, -1%**
		Clear-Span		**Clear-Span**
Manufacturer	**Grade**	**$5d_b$**	**$6d_b$**	**$6d_b$**
1	60	30.6 (3)	43.2 (5)	N/A
	80	N/A	16 (3)	N/A
	100	39 (4)	36.5 (4)	12 (3)
2	60	55 (4)	19.3 (3)	N/A
	80	N/A	85.5(4)	N/A
	100	23 (4)	33.3 (3)	14 (3)

Table 3: Mean number of half-cycles to fracture for #5 bars with the number of coupons tested per bar type noted in parentheses.

		Loading Protocol					
		+2%, -2%			+4%, -1%		
		Clear-Span			Clear-Span		
Manufacturer	Grade	$4d_b$	$5d_b$	$6d_b$	$4d_b$	$5d_b$	$6d_b$
1	60	46.7 (3)	44 (3)	32 (3)	33.3 (3)	25 (2)	20 (3)
	80	36.7 (3)	N/A	14.7 (3)	18 (3)	N/A	11.3 (3)
	100	68 (4)	42 (5)	28.5 (4)	27.3 (3)	18.5 (4)	12.7 (3)
2	60	69.3 (4)	36 (3)	24 (4)	25.3 (3)	17.3 (3)	14.7 (3)
	100	57.3 (3)	N/A	26.7 (3)	28.5 (4)	18 (3)	12 (3)

Table 4: Mean number of half-cycles to fracture for #8 bars with the number of coupons tested per bar type noted in parentheses.

		Loading Protocol	
		+4%, -1%	
		Clear-Span	
Manufacturer	Grade	$4d_b$	$6d_b$
1	60	25 (4)	15.6 (5)
	100	13.3 (3)	6.4 (5)
2	60	28 (3)	10.7 (3)
	100	13.5 (4)	12.5 (4)

Table 5: Mean number of half-cycles to fracture for #11 bars with the number of coupons tested per bar type noted in parentheses.

		Mean Number of Half-Cycles to Fracture	Coefficient of Variation
Manufacturing Technique	Manufacturer 1	27.6	0.31
	Manufacturer 2	29.7	0.28
Clear Span	$4d_b$	35.0	0.25
	$5d_b$	31.7	0.29
	$6d_b$	22.8	0.33
Steel Grade	Grade 60	30.8	0.21
	Grade 80	30.4	0.35
	Grade 100	25.9	0.37
Total Strain Range	4%	39.5	0.32
	5%	18.0	0.27

Table 6: Mean number of half-cycles to fracture and coefficients of variation for tests having certain values of the controlled variables.

		Percent Difference in Half-Cycles to Fracture	Percent Difference in Coefficient of Variation of Half-Cycles to Fracture
Manufacturing Process	(Manufacturer 2 - Manufacturer 1) / Manufacturer 1	19%	32%
Clear Span	$(5d_b - 4d_b) / 4d_b$	-31%	25%
	$(6d_b - 5d_b) / 5d_b$	-16%	7%
	$(6d_b - 4d_b) / 4d_b$	-47%	18%
Steel Grade (Manufacturer 1)	(grade 80 - grade 60) / grade 60	-46%	119%
	(grade 100 - grade 60) / grade 60	-14%	211%
Steel Grade (Manufacturer 2)	(grade 80 - grade 60) / grade 60	342%	67%
	(grade 100 - grade 60) / grade 60	-3%	88%
Steel Grade (Both Manufacturers)	(grade 80 - grade 60) / grade 60	19%	108%
	(grade 100 - grade 60) / grade 60	-9%	150%
Total Strain Range	(5% - 4%) / 4%	-49%	0%
Bar Size	(#5 - #8) / #8	10%	82%
	(#11 - #8) / #8	-27%	178%

Table 7: Percent difference in half-cycles to fracture and coefficients of variation.

4.2.1 Effect of the Manufacturing Process

Overall, the fatigue life of bars produced using the two manufacturing processes considered in this study were comparable. The bars produced by Manufacturer 2 exhibited fatigue lives that were only 19% higher than those produced by Manufacturer 1 (Table 7). The coefficient of variation for the numbers of half-cycles to fracture was slightly lower for bars produced by Manufacturer 2. However, the performance of

equivalent bars varied significantly from one set of parameters to another depending on the manufacturing process.

The effect of the manufacturing process on fatigue life is discussed next for grade 100 #5 bars, grade 100 #8 bars, grade 100 #11 bars, and finally, grade 80 #5 bars.

As shown in Table 3, the grade 100 #5 bars made using the two manufacturing processes exhibited significant differences in their cyclic performance depending on the loading protocol and clear span. For the loading protocol of (+4%, -1%), the bars produced by Manufacturer 1 exhibited a slightly lower mean fatigue life than those produced by Manufacturer 2 (14% lower). This difference, however, represents only two half-cycles (or one full cycle). Likewise, for the loading protocol of (+4%, 0%) and clear spans of $6d_b$, the bars produced by Manufacturer 1 exhibited a 9% higher mean fatigue life than those produced by Manufacturer 2. For the loading protocol of (+4%, 0%) with clear spans of $5d_b$, however, there was a marked difference in the fatigue life of the bars produced by the two manufacturers. The bars produced by Manufacturer 1 exhibited a 41% higher mean fatigue life than those produced by Manufacturer 2.

No significant differences were observed in the low-cycle fatigue life of grade 100 #8 bars produced by the two manufacturers, despite significant differences in their monotonic mechanical properties (Table 2). The average difference in mean fatigue life between bars produced by the two manufacturers was just over 5% for all #8 bars tested (Manufacturer 2 bars failed, on average, at 5% fewer half-cycles than bars of Manufacturer 1) (Table 4).

Likewise, the grade 100 #11 bars produced by both manufacturers exhibited significant differences in their monotonic mechanical properties (Table 2). However, the difference in cyclic fatigue behavior between #11 bars from the two manufacturers was

much larger than between #8 bars (Table 5). Manufacturer 1 bars had a mean fatigue life of only 1% less than Manufacturer 2 for clear spans of $4d_b$ but 48% less for clear spans of $6d_b$ (Table 6).

The grade 80 #5 bars exhibited the largest difference in cyclic fatigue life based on manufacturer. While the bars produced by Manufacturer 2 had the largest range of fatigue life of any set of bars, the mean was more than 4 times that of the bars produced by Manufacturer 1. This extreme difference is in spite of the high degree of similarity in the monotonic properties of the two bar types.

4.2.2 Effect of the Clear Span

For almost every combination of grade, loading protocol, and manufacturer origin, the bars tested at higher clear spans had a lower average fatigue life (Table 3, Table 4, and Table 5). As seen in Table 7, bars tested at clear spans of $5d_b$ had average fatigue lives of 31% less than those tested at clear spans of $4d_b$. Likewise, bars tested at clear spans of $6d_b$ had average fatigue lives of 47% less than those tested at clear spans of $4d_b$. This is due to the relationship between clear span and the amount of buckling to which bars were subjected. Longer clear spans reduce the buckling load of the reinforcing bars and increase the lateral sway experienced under cyclic loading (Figure 12). The bars with longer clear spans, therefore, sustained higher curvatures due to buckling and associated higher local strains. Figure 13 illustrates the increase in local strains due to increasing amounts of lateral buckling. Even the small amounts of buckling seen during the first compressive cycle for clear spans of $6d_b$ were observed to increase local strains by up to five times the average bar strain (e.g., -10% vs. -2% strains in Figure 13). In general these increased local strains generated shorter fatigue lives. However, some tests on #5 bars did not show this same relationship (namely Manufacturer 1 grade 60, and

Manufacturer 2 grade 100). In both cases, the ranges of fatigue life values for each clear span overlapped significantly, indicating that the relationship between clear span and fatigue life was not very strong.

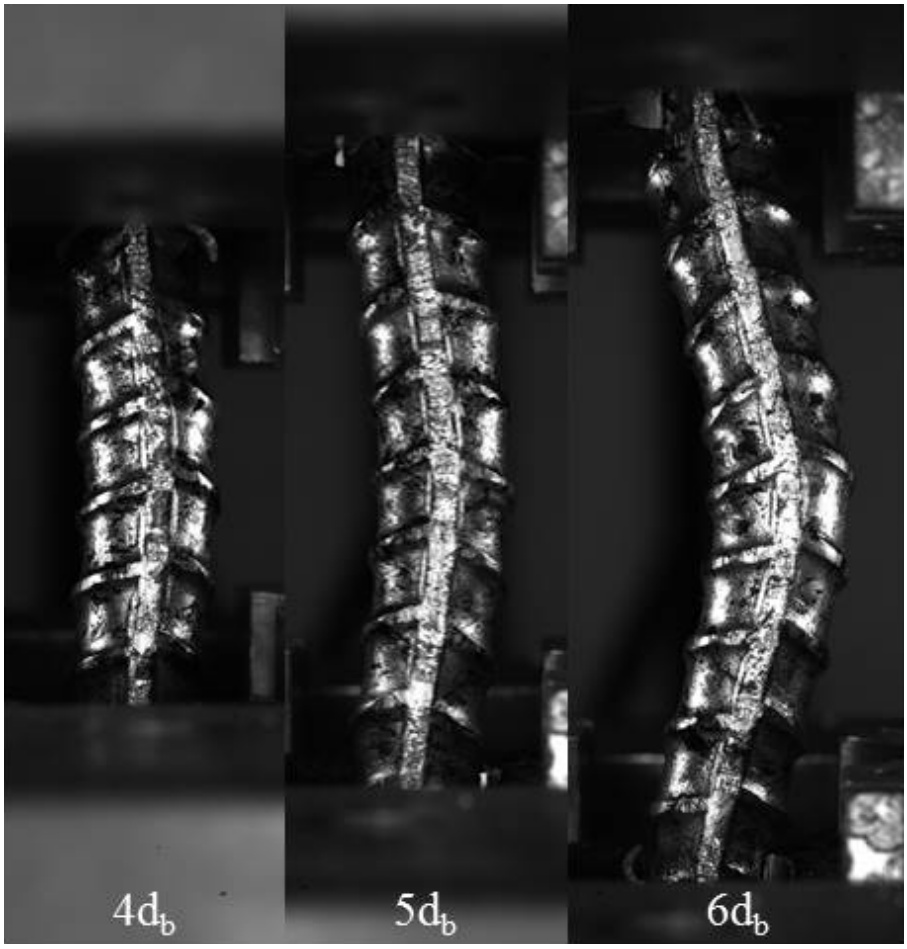

Figure 12: Photographs showing the maximum lateral buckling in grade 100 #8 bars from Manufacturer 1 tested cyclically under the loading protocol of (+4%, -1%) for clear spans of $4d_b$, $5d_b$, and $6d_b$. The photographs were taken during the final cycle prior to fracture. All three photographs are at the same scale.

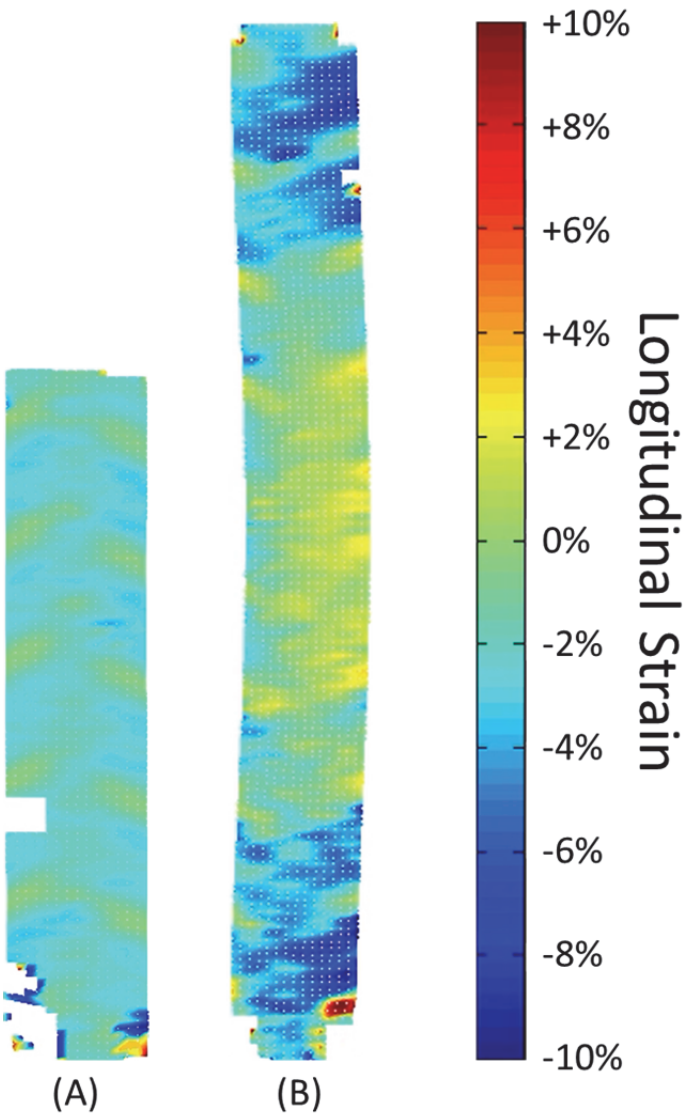

Figure 13: Illustration of longitudinal surface strains during the first compressive cycle. Both images depict a grade 80 #8 bar produced by Manufacturer 1 and tested under the (+2%, -2%) loading protocol. (A) Clear span of $4d_b$. (B) Clear span of $6d_b$. The white areas represent locations where strains could not be measured because the aluminum collar blocked the view of the bar, or the targets were otherwise not able to be tracked.

4.2.3 Effect of the Steel Grade

For a majority of the combinations of manufacturer, loading protocol, clear span, and bar size that were studied, the grade 100 bars surpassed or matched the fatigue life of the corresponding grade 60 bars. Overall, however, the grade 100 bars exhibited 91% of the fatigue life of the grade 60 A706 bars (Table 7). This was due to some parameter combinations producing significantly poorer performance in grade 100 bars than in their grade 60 counterparts.

The variability in the numbers of cycles to failure (as measured by the COV) was much higher for high-strength bars than it was for the grade 60 bars (Table 6 and Table 7). Similarly, the error bars plotted in Figure 14 to Figure 25 indicate this trend in variability.

Grade 80 bars showed mixed fatigue performance compared with grade 60 bars. Unlike the grade 100 bars, the grade 80 bars performed very differently depending on the manufacturer. Those produced by Manufacturer 1 exhibited on average only 54% of the fatigue life of the grade 60 A706 bars from the same manufacturer. Those produced by Manufacturer 2, on the other hand, exhibited on average 4.4 times the fatigue life of the grade 60 A706 bars from the same manufacturer.

The effects of steel grade on fatigue life are discussed next in more detail for #5 bars, #8 bars, and finally, #11 bars.

#5 Bars

Tests on #5 bars were performed primarily at one loading protocol: (+4%, 0%). The results of the tests on #5 bars produced by Manufacturer 1 indicate a comparable fatigue life between grade 100 bars and grade 60 A706 bars (Figure 14). The grade 80 #5 bars

produced by Manufacturer 1, however, had significantly lower fatigue life than the grade 60 analogues (more than 60% lower on average). The grade 80 #5 bars produced by Manufacturer 1, however, performed comparably to the grade 60 #5 bars produced by Manufacturer 2, indicating satisfactory fatigue life if the lesser performance of the grade 60 bars is used as the benchmark.

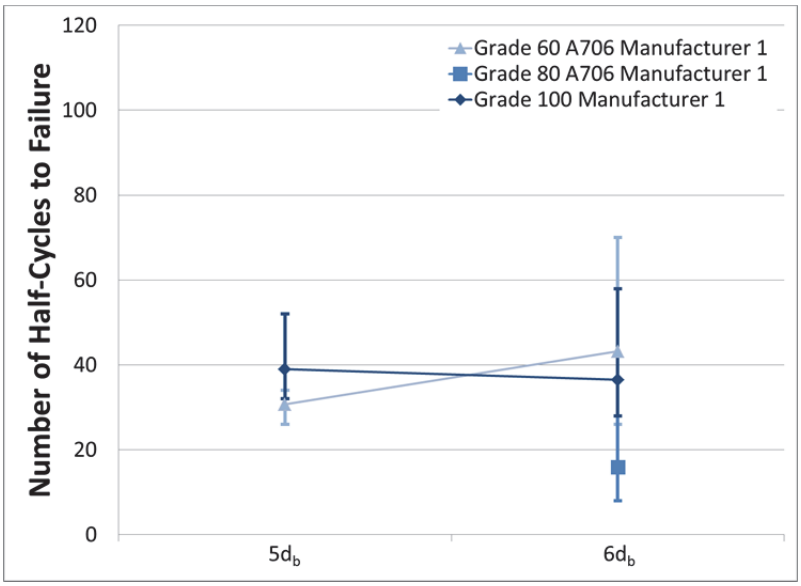

Figure 14: Effects of steel grade and clear span on low-cycle fatigue life for #5 bars produced by Manufacturer 1 and tested under the (+4%, 0%) loading protocol. (Points indicate the mean value of half-cycles to failure for each bar type, while the error bars indicate the maximum and minimum values)

As seen in Figure 15, the grade 100 #5 bars produced by Manufacturer 2 performed comparably to, or much better than the grade 60 A706 bars for the larger clear span of $6d_b$, but significantly worse for clear spans of $5d_b$ (nearly 60% worse). When compared to the grade 60 #5 bars produced by Manufacturer 1, however, the grade 100 bars from Manufacturer 2 exhibited only 25% lower mean fatigue life at clear spans of $5d_b$ (Figure 16). Unlike the grade 80 #5 bars produced by Manufacturer 1, those produced

by Manufacturer 2 exhibited superior fatigue life compared to the grade 60 #5 bars. They averaged a fatigue life of nearly 440% that of the grade 60 bars from Manufacturer 2 (Figure 15).

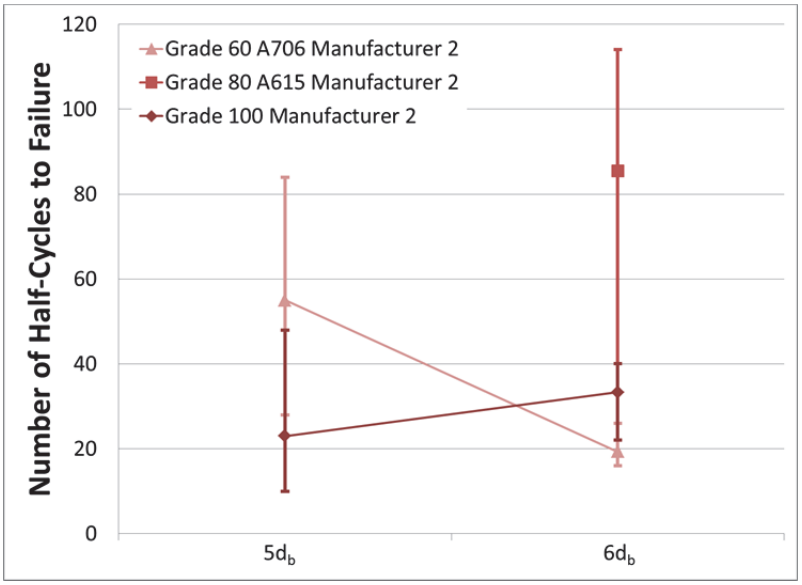

Figure 15: Effects of steel grade and clear span on low-cycle fatigue life for #5 bars produced by Manufacturer 2 and tested under the (+4%, 0%) loading protocol. (Points indicate the mean value of half-cycles to failure for each bar type, while the error bars indicate the maximum and minimum values)

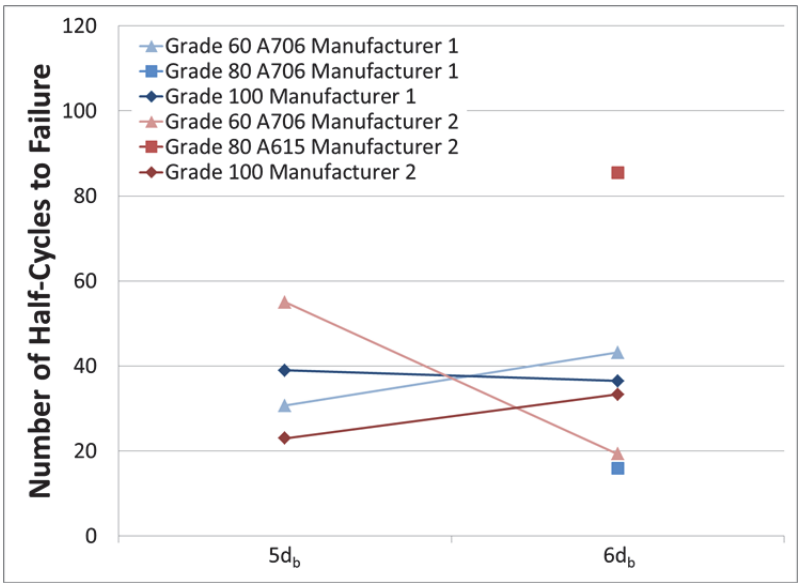

Figure 16: Effects of steel grade and clear span on low-cycle fatigue life for #5 bars tested under the (+4%, 0%) loading protocol. (Points indicate the mean value of half-cycles to failure for each bar type)

#8 Bars

Results for #8 bars are organized into four different combinations of steel manufacturer and loading protocol in Figure 17 to Figure 20 (i.e., Manufacturer 1 & Loading Protocol 1, Manufacturer 1 & Loading Protocol 2, etc.). No significant difference in cyclic performance was observed between the grade 60 and grade 100 bars for 3 out of 4 of the combinations as seen in Figure 17, Figure 18, and Figure 20. However, the #8 bars from Manufacturer 1 tested at (+4%, -1%) showed consistent difference between the two grades. As seen in Figure 19, the grade 100 #8 bars performed significantly worse than the grade 60 #8 bars (having a mean fatigue life between 18% and 37% less than their lower strength analogues). However, when compared to grade 60 #8 bars from Manufacturer 2, the grade 100 #8 bars from Manufacturer 1 performed nearly equivalently (Figure 22).

Unlike the grade 100 #8 bars tested, the grade 80 #8 bars produced by Manufacturer 1 performed significantly worse than grade 60 A706 #8 bars produced by the same manufacturer. Figure 17 depicts this inferior performance of grade 80 steel which, on average, failed 21% to 54% sooner than grade 60 A706 steel when subjected to strains of (+2%, -2%). Testing to strains of (+4%, -1%) also yielded inferior performance of grade 80 #8 bars when compared to grade 60 A706 #8 bars, as shown in Figure 19. At these strains, the decrease in fatigue life for grade 80 #8 bars was greater than 40% when compared to grade 60 A706. When compared to the grade 60 #8 bars produced by Manufacturer 2, however, the decrease in fatigue life was only between 23% and 29%. Since the chemical composition of the grade 80 bars falls directly between that of lesser and greater strength bars, the reduced fatigue life compared to both other grades is not fully understood.

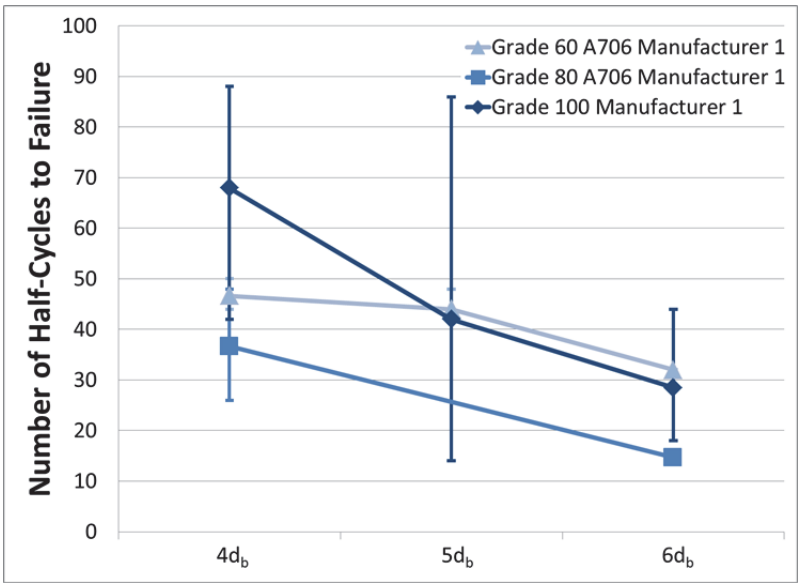

Figure 17: Effects of steel grade and clear span on low-cycle fatigue life for #8 bars produced by Manufacturer 1 and tested under the (+2%, -2%) loading protocol. (Points indicate the mean value of half-cycles to failure for each bar type, while the error bars indicate the maximum and minimum values)

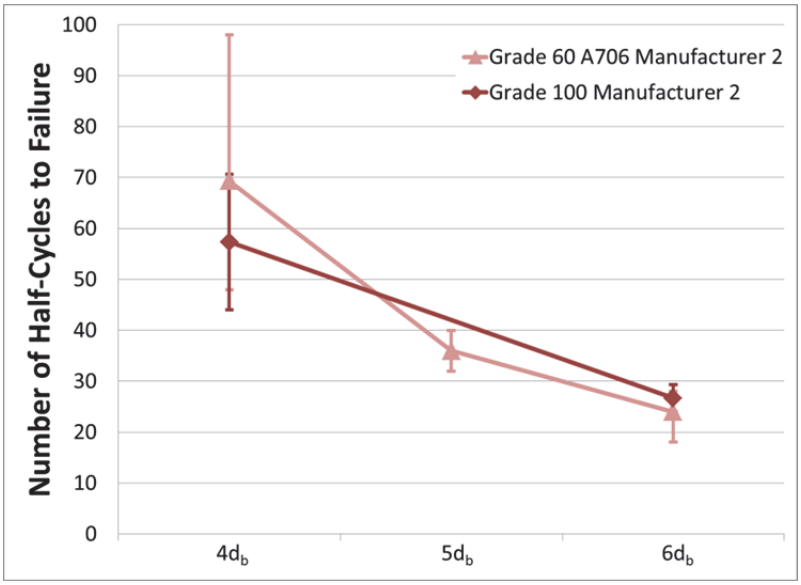

Figure 18: Effects of steel grade and clear span on low-cycle fatigue life for #8 bars produced by Manufacturer 2 and tested under the (+2%, -2%) loading protocol. (Points indicate the mean value of half-cycles to failure for each bar type, while the error bars indicate the maximum and minimum values)

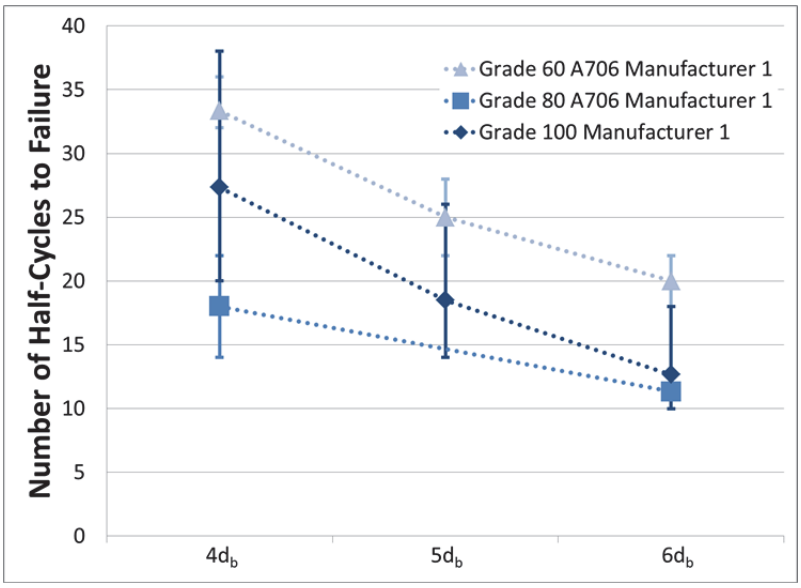

Figure 19: Effects of steel grade and clear span on low-cycle fatigue life for #8 bars produced by Manufacturer 1 and tested under the (+4%, -1%) loading protocol. (Points indicate the mean value of half-cycles to failure for each bar type, while the error bars indicate the maximum and minimum values)

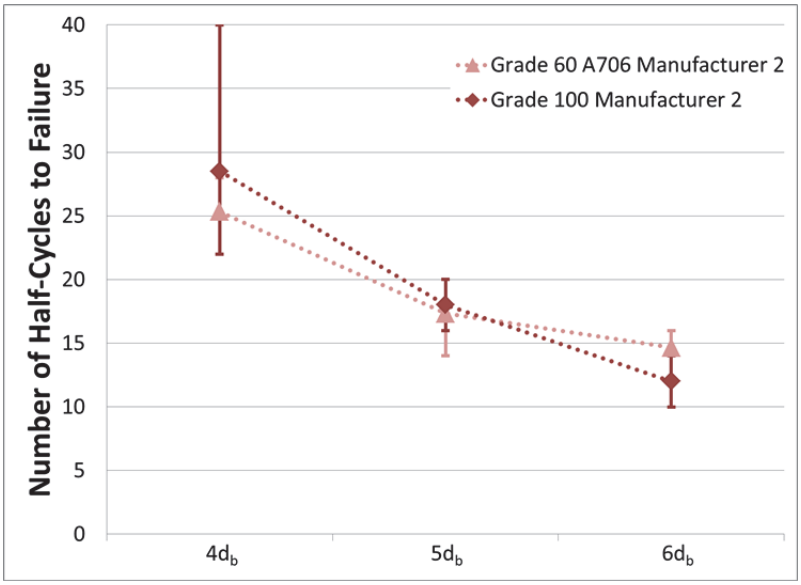

Figure 20: Effects of steel grade and clear span on low-cycle fatigue life for #8 bars produced by Manufacturer 2 and tested under the (+4%, -1%) loading protocol. (Points indicate the mean value of half-cycles to failure for each bar type, while the error bars indicate the maximum and minimum values)

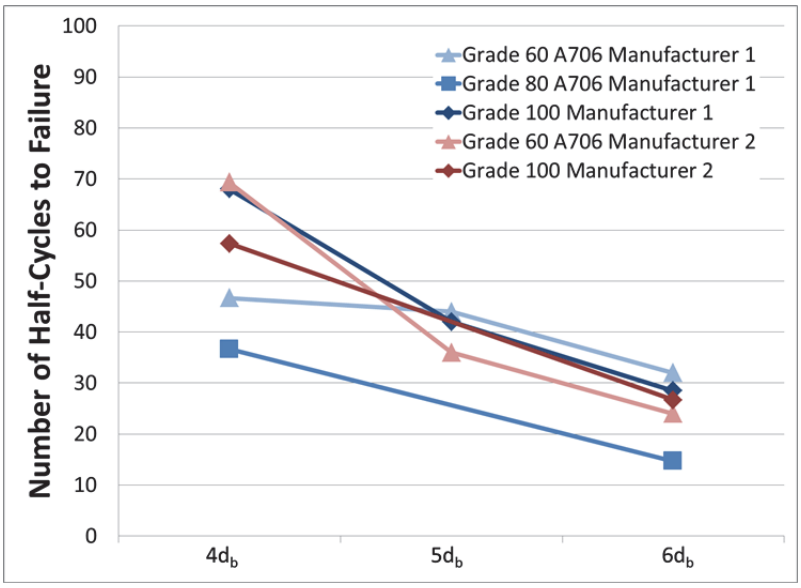

Figure 21: Effects of steel grade and clear span on low-cycle fatigue life for #8 bars tested under the (+2%, -2%) loading protocol. (Points indicate the mean value of half-cycles to failure for each bar type)

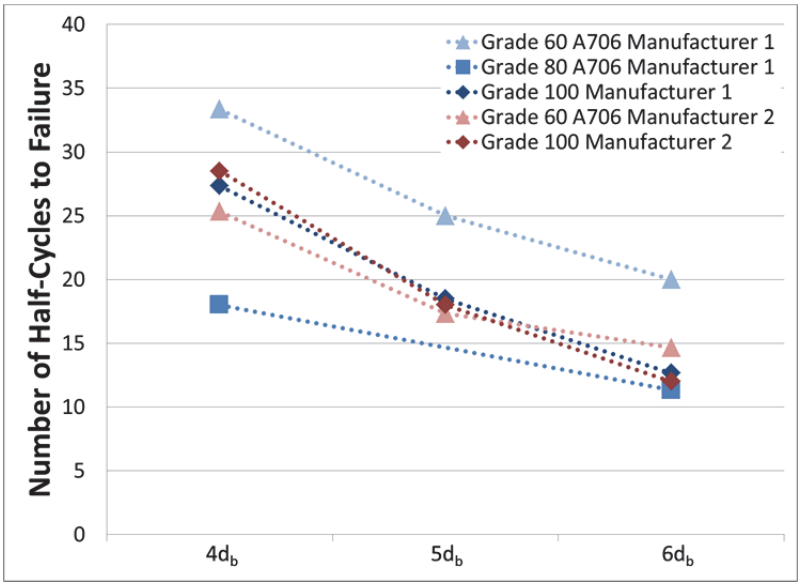

Figure 22: Effects of steel grade and clear span on low-cycle fatigue life for #8 bars tested under the (+4%, -1%) loading protocol. (Points indicate the mean value of half-cycles to failure for each bar type)

#11 Bars

Tests on #11 bars were performed at only one loading protocol: (+4%, -1%). The results of the tests on #11 bars produced by Manufacturer 1 indicate a significant decrease in fatigue life of grade 100 bars when compared to grade 60 bars (Figure 23). Specifically, the mean of grade 100 #11 bars fractured at between 41% and 53% of the number of half-cycles required to fracture the corresponding grade 60 #11 bars. When compared to the grade 60 bars produced by Manufacturer 2, the grade 100 bars from Manufacturer 1 still exhibit a significantly shorter fatigue life at all clear spans (Figure 25).

The grade 100 #11 bars produced by Manufacturer 2 performed comparably to the grade 60 A706 #11 bars at a clear span of $6d_b$ (Figure 24). However, at a clear span of $4d_b$, the mean fatigue life of grade 100 bars was less than 50% of that for grade 60 bars.

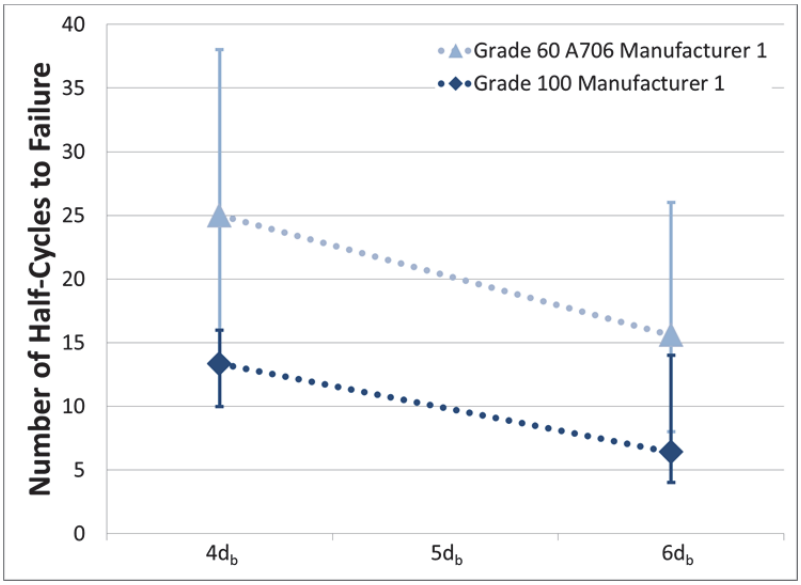

Figure 23: Effects of steel grade and clear span on low-cycle fatigue life for #11 bars produced by Manufacturer 1 and tested under the (+4%, -1%) loading protocol. (Points indicate the mean value of half-cycles to failure for each bar type, while the error bars indicate the maximum and minimum values)

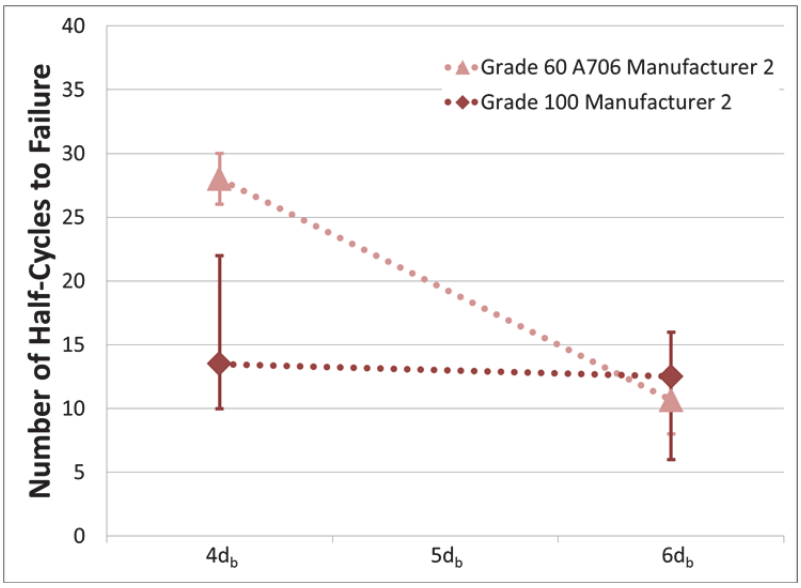

Figure 24: Effects of steel grade and clear span on low-cycle fatigue life for #11 bars produced by Manufacturer 2 and tested under the (+4%, -1%) loading protocol. (Points indicate the mean value of half-cycles to failure for each bar type, while the error bars indicate the maximum and minimum values)

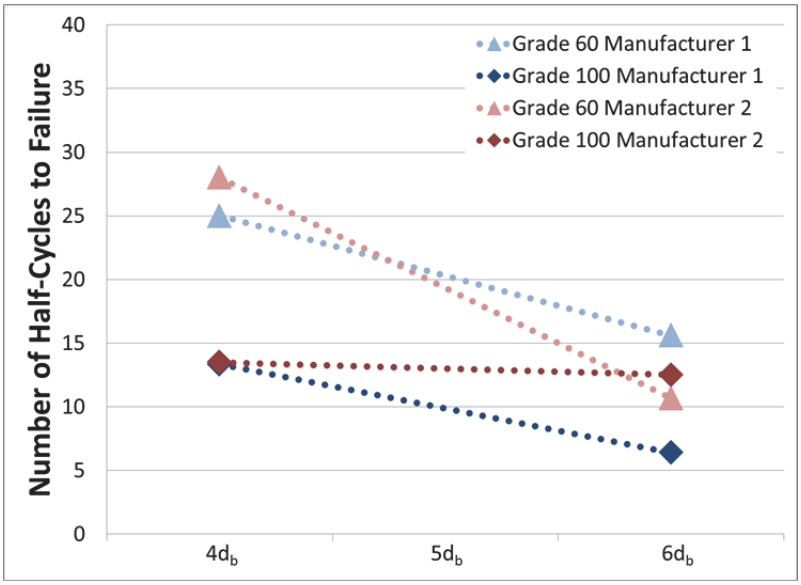

Figure 25: Effects of steel grade and clear span on low-cycle fatigue life for #11 bars tested under the (+4%, -1%) loading protocol. (Points indicate the mean value of half-cycles to failure for each bar type)

Tests performed on concrete columns reinforced with HSRB indicate that the strain demands on grade 100 bars can exceed those for grade 60 bars by as much as 100% (Sokoli, Drit 2014). Since the relationship between reinforcing bar fatigue life and total strain range is exponential (Brown and Kunnath 2004), this 100% increase in strain can lead to a dramatic decrease in fatigue life and column drift capacity for HSRB compared to grade 60 A706 bars.

4.2.4 Effect of the Loading Protocols

The loading protocols exhibited the same effect on half-cycles to fracture that has been identified by other researchers. Namely, higher total strain ranges resulted in fewer half-cycles to fracture.

Mean stress and strain effects have been shown to be negligible at high strain ranges (>1%) (Koh and Stephens 1991), because plastic strains reduce mean stresses to essentially zero barring significant bar buckling. Since all of the strain targets used in the low-cycle fatigue loading protocols discussed here exceed 0.5%, the total strain range was used to account for the differences in behavior under the two loading protocols (Mander et al. 1994).

The total strain range is greater for the (+4%, -1%) loading protocol (=5%) than for the (+2%, -2%) and (+4, 0%) loading protocols (=4%). As past low-cycle fatigue testing on reinforcing bars has demonstrated, increasing the total strain range reduces the number of half-cycles to fracture of a bar exponentially (Mander et al. 1994, Brown and Kunnath 2004). As shown in Figure 26 and Figure 27, bars tested under the (+4%, -1%) loading protocol had a significantly reduced fatigue life compared with those tested under the (+2%, -2%) protocol. Likewise, a similar reduction in fatigue life is shown in Figure 28 for bars tested under the (+4%, -1%) and (+4%, 0%) loading protocols.

This trend can also be seen from the average percent difference in number of half-cycles to fracture: bars tested at a total strain range of 5% exhibited only 51% of the fatigue life of those tested at a total strain range of 4% (Table 7).

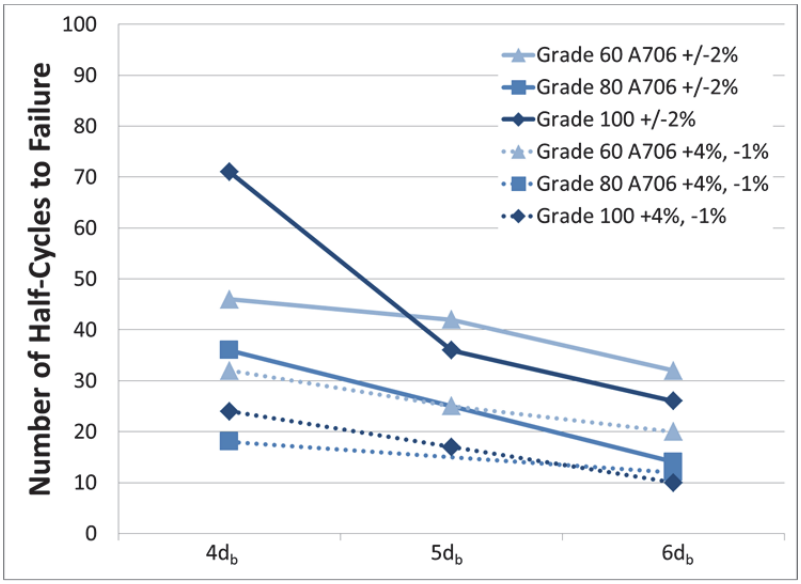

Figure 26: Relationship between loading protocol and low-cycle fatigue life for #8 bars produced by Manufacturer 1. (Points indicate the mean value of half-cycles to failure for each bar type)

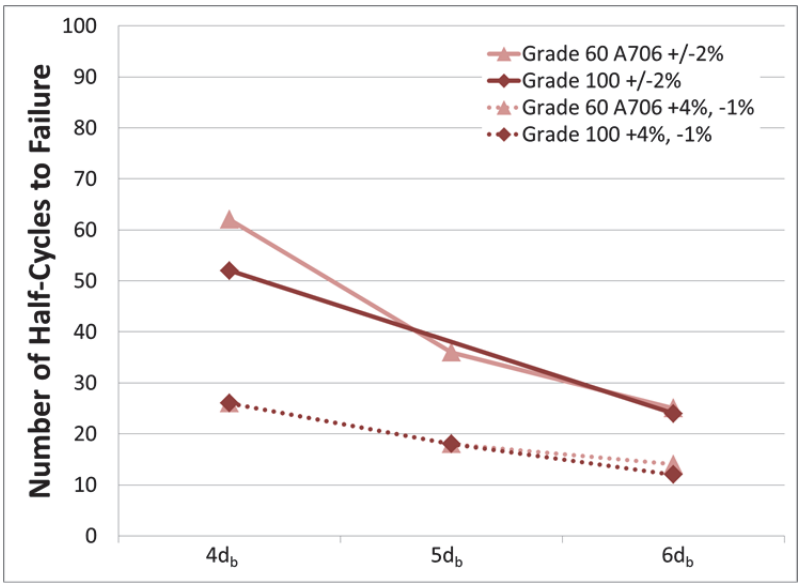

Figure 27: Relationship between loading protocol and low-cycle fatigue life for #8 bars produced by Manufacturer 2. (Points indicate the mean value of half-cycles to failure for each bar type)

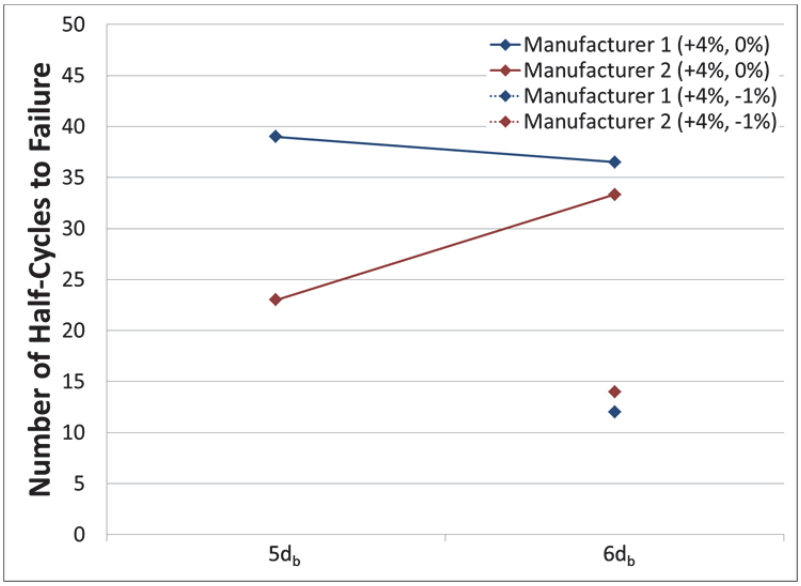

Figure 28: Relationship between loading protocol and low-cycle fatigue life for #5 grade 100 bars. (Points indicate the mean value of half-cycles to failure for each bar type)

4.2.5 Effect of Bar Size

The overall effect of bar size on fatigue life appears to be less significant than other factors. A general trend was observed that indicates lower fatigue life for larger bars within the spectrum of bar sizes measured in this study. Specifically, the fatigue life of #11 bars was 27% lower than that of the #8 bars and the fatigue life of #8 bars was 10% lower than that of the #5 bars.

The #11 bars tested exhibited a mean fatigue life of between 47% and 111% of that of the #8 bars (Figure 29 and Figure 30). The mean of these differences indicates a 27% lower fatigue life for the #11 bars compared to the #8 bars (tested at the same strain range of 5%) (Table 7). Following the same trend, the fatigue life of #5 bars was higher than that of #8 bars. The #5 bars exhibited a mean fatigue life between 70% and 152% of that of the #8 bars (Figure 29, Figure 30, Figure 31, and Figure 32). The mean of these differences indicates a 10% higher fatigue life for the #5 bars compared to the #8 bars (tested at the same strain range of 4%) (Table 7).

The effect appears to be more significant for the grade 100 bars tested. When comparing tests performed on grade 100 bars only, the fatigue life of the #11 bars was 37% lower than that of the #8 bars (tested at the same strain range of 5%) and the fatigue life of the #5 bars was 11% higher than that of the #8 bars (tested at the same strain range of 4%).

Results of other studies on fatigue of metals (Weisman 1969 and Tetelman et al. 1967) indicate a decrease in fatigue life with larger surface areas. As discussed in (Helgason et al. 1976), this relationship could be due to “a statistical size effect related to the probability of finding a critical notch on the bar surface”.

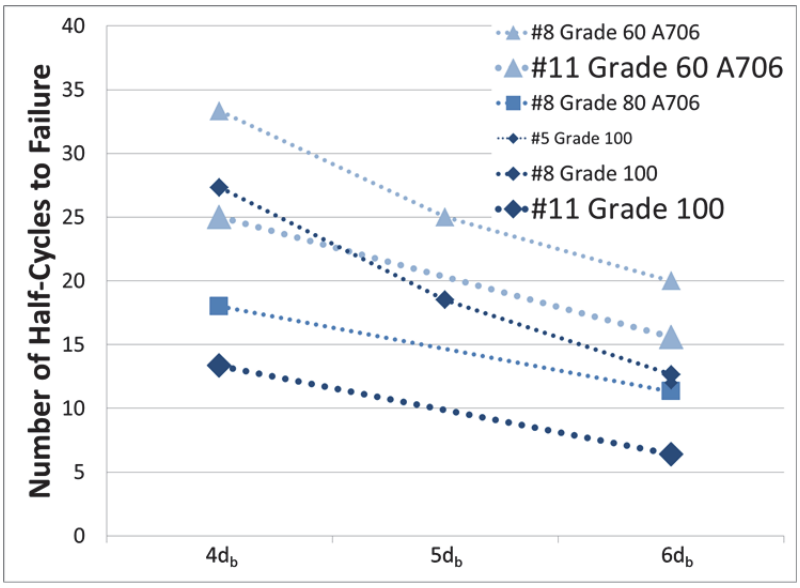

Figure 29: Effects of bar size and clear span on low-cycle fatigue life for #5, #8, and #11 bars produced by Manufacturer 1 and tested with a total strain range of 5%. (Points indicate the mean value of half-cycles to failure for each bar type)

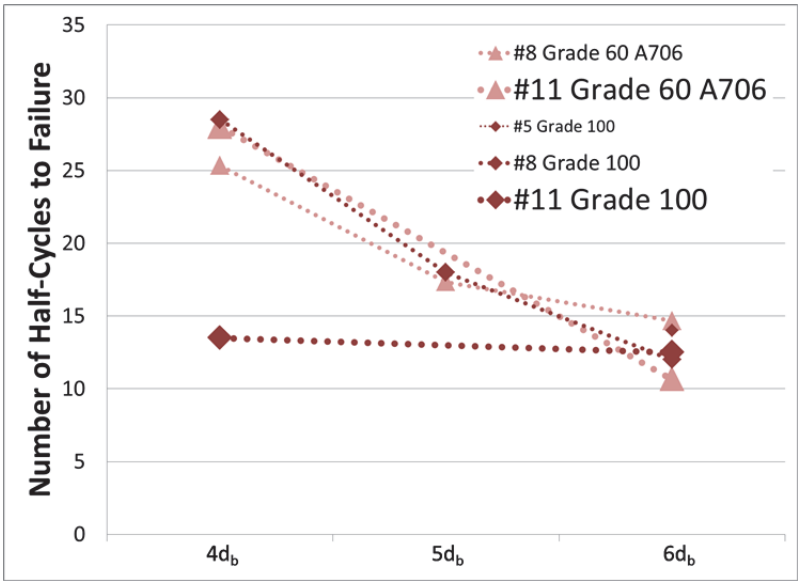

Figure 30: Effects of bar size and clear span on low-cycle fatigue life for #5, #8, and #11 bars produced by Manufacturer 2 and tested with a total strain range of 5%. (Points indicate the mean value of half-cycles to failure for each bar type)

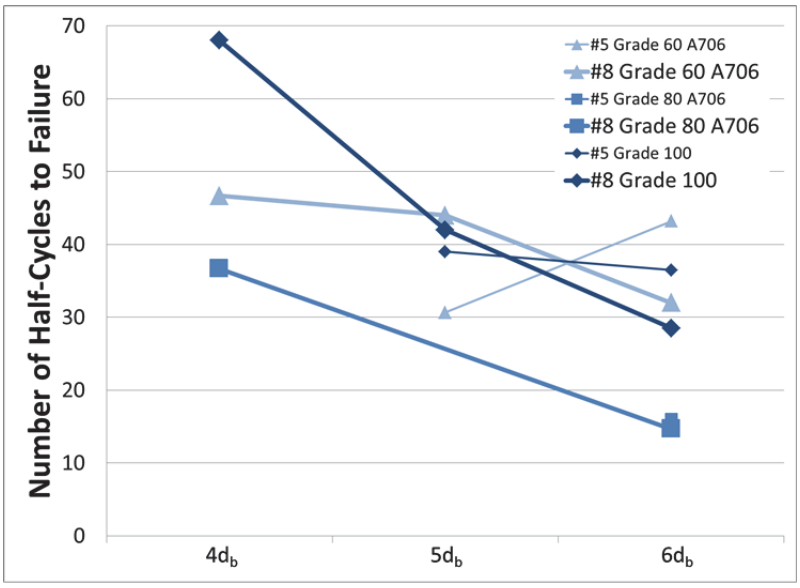

Figure 31: Effects of bar size and clear span on low-cycle fatigue life for #5 and #8 bars produced by Manufacturer 1 and tested with a total strain range of 4%. (Points indicate the mean value of half-cycles to failure for each bar type)

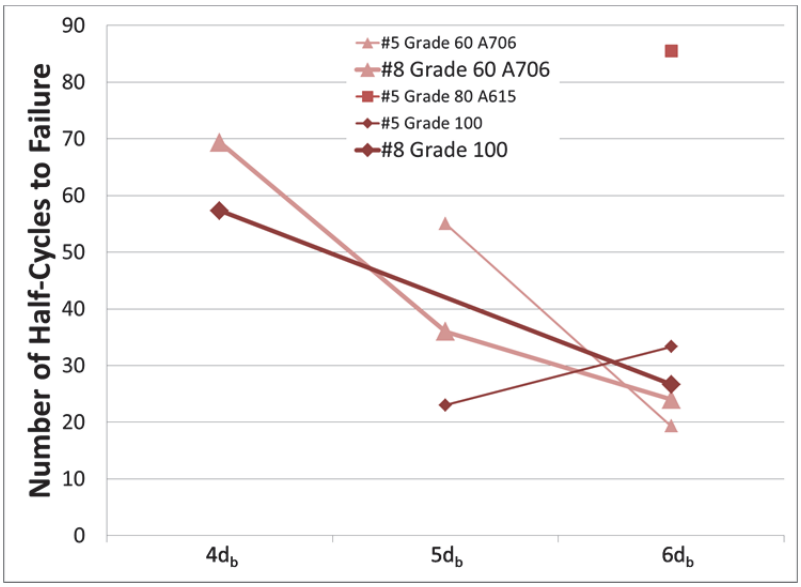

Figure 32: Effects of bar size and clear span on low-cycle fatigue life for #5 and #8 bars produced by Manufacturer 2 and tested with a total strain range of 4%. (Points indicate the mean value of half-cycles to failure for each bar type)

5. Analysis of Test Results

Test results and general trends are discussed in Chapter 4. In this chapter, possible explanations for those trends are examined systematically.

5.1 Influential Parameters

The influence on low-cycle fatigue performance of the five variables that were directly controlled through the experimental program was investigated. These parameters are: manufacturing process, clear span, steel grade, loading protocol (or total cyclic strain range), and bar size. In addition to the controlled parameters, the influence on low-cycle performance of a suite of non-controlled parameters was investigated. Each bar type, consisting of bars having a specific manufacturing process, steel grade, and bar size was produced from a single heat. Therefore, each of these bar types had characteristic monotonic stress/strain properties, deformation geometries, and chemistry. The non-controlled parameters considered in the analyses were measured as discussed in sections 3.2.1 and 3.2.4.

5.2 Performance Measures

To compare the low-cycle fatigue performance of the bars, several performance measures were defined in addition to that performance measure used previously (i.e., the number of half-cycles to bar fracture):

1. the total strain energy dissipated before fracture, defined as the cumulative area under the stress-strain curve up to fracture
2. softening and hardening parameters:
    a. Second Tension-Cycle Stress / First Tension-Cycle Stress
    b. Maximum Tension Stress / First Tension-Cycle Stress

c. Last Tension-Cycle Stress / First Tension-Cycle Stress
d. Second Compression-Cycle Stress / First Compression-Cycle Stress
e. Maximum Compression-Cycle Stress / First Compression-Cycle Stress
f. Last Compression-Cycle Stress / First Compression-Cycle Stress

3. the fracture type and location determined by visual inspection
4. the amount of lateral buckling observed, defined as the maximum lateral movement of a bar during a test

The derivation of these parameters is discussed in section 5.3.

5.3 Additional Performance Measures Derived from Cyclic Tests

5.3.1 Lateral Buckling

By tracking the location of the targets affixed on the bars as described in section 3.2.3, the amount of lateral sway of many points along the longitudinal ribs of bars were measured. This measurement was only obtained when the buckling occurred in the minor axis direction, and therefore within the plane of the photograph. The buckling measurement was then normalized by dividing the sway by the diameter of the bar in order to compare displacements across multiple bar sizes. The critical target, showing the highest lateral sway, was considered to represent the amount of buckling for a bar. The maximum normalized lateral sway of the critical target was used to compare the amount of buckling between various bars, and was termed the maximum buckling amplitude. An example plot of the lateral sway versus the average bar strain is shown in Figure 33.

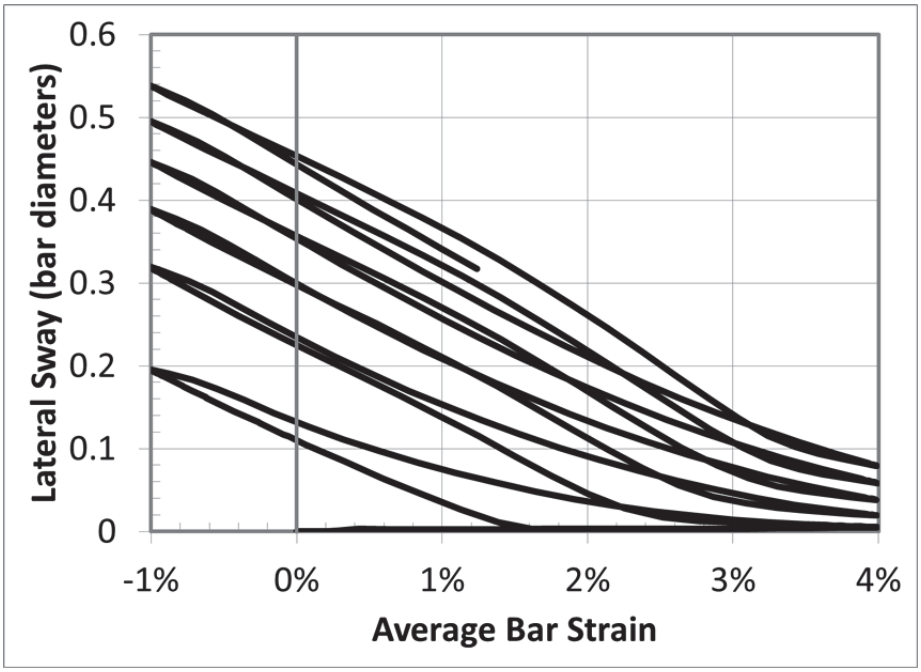

Figure 33: Lateral sway of a target versus the average strain measured over the length of the bar for a test performed at the (+4%, -1%) loading protocol.

5.3.2 Strain Energy Dissipated

The total strain energy dissipated throughout a cyclic test can be assessed by integrating the area under the cyclic stress-strain plot. The total strain energy can be divided by the yield strength of the bar to obtain the normalized strain energy.

One application of HSRB is to replace regular strength reinforcing bars with a smaller area of high-strength bars in order to achieve a comparable total strength. Since strain energy is measured per unit volume of the reinforcing steel, if the steel area is reduced, the total capacity for strain energy dissipation would also be reduced. By normalizing the strain energy dissipation by the yield stress, one can compare the amount of strain energy dissipation provided by the reinforcing bars per unit of force capacity.

5.3.3 Softening or Hardening Parameters

Throughout a low-cycle fatigue test, the peak stress exhibited per cycle can vary significantly. A decrease in this peak stress will result in a loss of force-carrying capacity and a decrease in strain energy dissipation per cycle. In order to quantify this hardening or softening behavior, three peak tensile and compressive stresses were measured in addition to the peak tensile and compressive stresses during the first cycle:

The peak tensile and compressive stresses were measured during the second strain cycle to assess the rate of hardening or softening at the beginning of the test. Secondly, the largest tensile and compressive peak stresses were measured to assess the maximum amount of hardening a bar experienced. Finally, the tensile and compressive peak stresses were measured during the last complete cycle to assess the total amount of softening the bar experienced throughout the test.

To compare stresses across different bar strengths, the peak tensile and compressive stresses were divided by the respective tensile and compressive peak stresses from the first cycle.

5.3.4 Fracture Type

The point at which a fatigue crack initiated in the reinforcing bars studied was almost always located at the base of a deformation. However, two distinct fracture propagation patterns were observed. In one case, the fatigue crack would propagate along the base of the deformation until the bar fractured (Figure 34). In the other case, the fatigue crack would propagate horizontally through the barrel of the bar (Figure 35).

Figure 34: Photograph of a fractured bar where the fatigue crack initiated at, and propagated along the base of a transverse deformation.

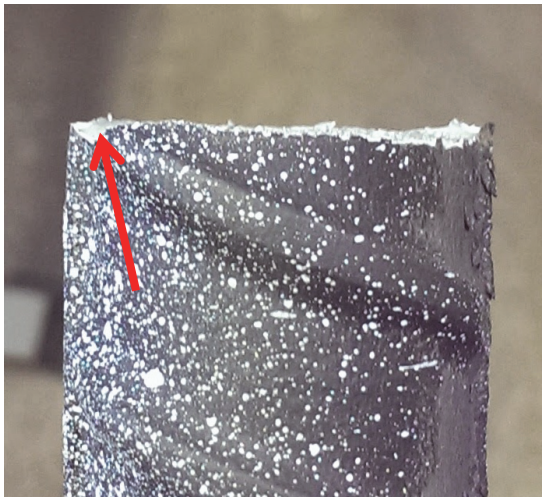

Figure 35: Photograph of a fractured bar where the fatigue crack initiated at the base of a transverse deformation and propagated horizontally through the barrel of the bar. The red arrow indicates the point at which the fatigue crack initiated.

5.4 DATA ANALYSIS

In order to quantify the effects of the potentially influential variables on the performance measures, ordinary least squares regression was used. For each performance measure, four regression models were fitted to four groups of potentially influential variables. The first of these groups included the controlled test parameters: manufacturing technique, bar size, and grade. The second group included the monotonic stress/strain properties of the bars listed in Table 8. The third group included the geometric parameters of the bar deformations listed in Table 8. The fourth group included the chemical composition of the steel, which consisted of the concentrations of the twelve elements in the steel listed in Table 8.

The regression models isolate the effects of each variable by holding all other variables constant. Since the effects of clear span and strain range on fatigue life are well known and highly significant, these variables were included in every model so that their effects could be separated from the effects of the other variables.

Collinearity of variables had to be considered in the assessment of correlations so as not to misattribute possible causalities. Many of the parameters studied here were highly correlated with each other. A summary of the correlation coefficients between these variables (based on linear correlations) is shown in Appendix A. A few groups of variables exhibited particularly high correlations. High degrees of correlation were identified between most of the monotonic material properties as well as between the concentrations of many chemical elements. In addition, high degrees of correlation were identified between the monotonic stress/strain properties and the steel chemical concentrations.

The variance inflation factor (VIF) is a parameter that quantifies this collinearity, which results from linear regressions between each variable and all other variables in the model. The VIF can be calculated from Equation 1,

Equation 1: Calculation of the variance inflation factor based on R^2

$$VIF = \frac{1}{1 - R^2}$$

where R^2 is the coefficient of determination found from the aforementioned regression analysis. A VIF of 2.0 indicates that the variance for that regression coefficient is twice as high as it would be if that variable were not correlated at all with the other variables. For this reason, when developing the regression models between groups of variables and the performance measures, variables which exhibited a VIF greater than 2.0 were not included in the regression model.

The slopes of the linear correlations were then normalized so that they could be directly compared across variables. This normalization was done by multiplying the slope by the total range of observations for a given variable and dividing that result by the total range of observations for the performance measure. Thus, a slope of 100% indicates that changing the variable from its minimum value to its maximum value would correlate with increasing the performance measure from its minimum value to its maximum value. The maximum, minimum, and range of each variable and performance measure are presented in Table 8 and Table 9.

		Minimum Value	Maximum Value	Range
Basic Bar Properties	**Manufacturer**	1	2	1
	Bar Size	5	11	6
	Steel Grade	60	100	40
Test Procedure	**Clear Span**	4	6	2
	Strain Range	4	5	1
Monotonic Stress/Strain Properties	**Yield Strength**	61.46	111.00	49.53
	Tensile Strength	91.1	134.92	43.81
	T/Y Ratio	1.183	1.679	0.496
	Elastic Modulus	25,800	31,400	5,600
	Ductility Ratio	27.2	91.7	64.6
	Elastic Limit Strain	0.215	0.427	0.212
	Uniform Strain	6.21	11.90	5.69
	Fracture Strain	9.8	21.7	11.9
Geometry	**R_{min}/H**	0.43	3.54	3.10
	R_{max}/H	0.69	4.94	4.25
	H/d_b	0.0500	0.0813	0.0312
Chemistry	**C**	0.260	0.350	0.090
	Mn	0.810	1.430	0.620
	P	0.007	0.020	0.013
	S	0.014	0.045	0.031
	Si	0.180	0.330	0.150
	Cu	0.180	0.340	0.160
	Cr	0.070	0.160	0.090
	Ni	0.060	0.130	0.070
	Mo	0.010	0.053	0.043
	V	0.001	0.355	0.354
	Nb	0.000	0.032	0.032
	Sn	0.008	0.020	0.012

Table 8: Maximum, minimum, and range of bar variables

		Minimum Value	Maximum Value	Range
Fatigue Life	**Half-Cycles to Failure**	4	114	110
	Total Strain Energy Dissipated (k-in/in^3)	16.8	243	226
	Normalized Strain Energy Dissipated	0.162	3.63	3.47
Softening / Hardening Parameters	**Second Tension Cycle Stress / First Tension Cycle**	0.962	1.125	0.163
	Maximum Tension Stress / First Tension Cycle	1.000	1.299	0.299
	Last Tension Cycle Stress / First Tension Cycle	0.313	1.299	0.986
	Second Compression Cycle Stress / First Compression Cycle	0.882	1.054	0.172
	Maximum Compression Cycle Stress / First Compression Cycle	1.000	1.079	0.0794
	Last Compression Cycle Stress / First Compression Cycle	0.579	1.032	0.453
Fracture Type	**Fracture Propagation Along the Base of Deformation**	FALSE	TRUE	1
Buckling Amount	**Max Buckling Amplitude (d_b)**	0.125	0.639	0.514

Table 9: Maximum, minimum, and range of performance measures

For all regression models, a relationship was considered statistically significant if the regression p-value was less than 5%. The normalized correlation coefficients found for p-values of less than 5% are summarized in Table 10 and Table 11. In addition, a summary of the normalized correlation coefficients found for p-values less than 1% is shown in Table 12 and Table 13. The color scales in these tables are determined for each performance measure, with green shades and bold type indicating correlations resulting in

more desirable performance and red shades and underlined type indicating correlations resulting in less desirable performance.

Subsets of Table 10 and Table 11are repeated in this chapter as specific relationships are discussed (Tables 14 to 28).

			Performance Measures											
			Fatigue Life			Softening / Hardening						Fracture Type	Buckling Amount	
			Half-Cycles to Fracture	Total Strain Energy Dissipated	Normalized Strain Energy Dissipated	Second Tension Cycle Stress / First Tension Cycle	Maximum Tension Cycle Stress / First Tension Cycle	Last Tension Cycle Stress / First Tension Cycle	Second Compression Cycle Stress / First Compression Cycle	Maximum Compression Cycle Stress / First Compression Cycle	Last Compression Cycle Stress / First Compression Cycle	Fracture Propogation Along the Base of Deformation[1]	Max Buckling Amplitude[2]	
Influential Parameters	Test Variables	Manufacturer				-26%	-14%	-17%	-11%	-12%	-13%	71%		
		Bar Size	-10%	-12%		**37%**	**23%**	**17%**	-11%				**-31%**	
		Grade			-10%	-19%	-6%		-8%	-5%		**-36%**	**-35%**	
		Clear Span	-14%	-23%	-19%		-8%		-32%	-29%	-25%		42%	
		Total Strain Range	-18%	-14%	-11%	-33%	-21%	-6%	-6%	-7%				
	Monotonic Stress/Strain Properties	Yield Strength			-12%								**-36%**	
		Tensile Strength									**11%**	**-83%**		
		T/Y Ratio						**17%**						
		Elastic Modulus										32%		
		Ductility Ratio												
		Elastic Limit Strain												
		Uniform Strain							**21%**	**17%**				
		Fracture Strain				**48%**	**22%**							

[1]Positive values indicate a higher precent of crack propogation along the base of a deformation and are colored red and underlined since they represent a less desirable fracture type.

[2]Positive values are colored red and underlined because higher amounts of buckling are considered less desirable.

Table 10: Normalized slopes of linear regression for performance measures as a function of test variables with p-values less than 5%. Red shading and underlined type indicate correlations resulting in undesirable performance while green shading and bold type indicate correlations resulting in desirable performance.

			Performance Measures											
			Fatigue Life			Softening / Hardening						Fracture Type	Buckling Amount	
			Half-Cycles to Failure	Total Strain Energy Dissipated	Normalized Strain Energy Dissipated	Second Tension Cycle Stress / First Tension Cycle	Maximum Tension Cycle Stress / First Tension Cycle	Last Tension Cycle Stress / First Tension Cycle	Second Compression Cycle Stress / First Compression Cycle	Maximum Compression Cycle Stress / First Compression Cycle	Last Compression Cycle Stress / First Compression Cycle	Fracture Propogation Along the Base of Deformation[1]	Max Buckling Amplitude[2]	
Influential Parameters	Deformation Geometry	R_{min}/H				43%	27%			18%		-100%		
		R_{max}/H						25%	7%		9%			
		H/d_b			-14%	-41%	-13%	-12%						
	Chemical Composition	C^3	14%				-56%						-18%	
		Mn^3							9%	-24%				
		P^3			13%		18%			11%				
		S^3							16%					
		Si^3								12%				
		Cu^3			16%									
		Cr^3					-41%							
		Ni^3	-23%		-46%				-20%	-16%				
		Mo^3												
		V^3	-23%		-33%							-71%	-28%	
		Nb^3												
		Sn^3	-11%	-8%	-15%			9%						

[1]Positive values indicate a higher precent of crack propogation along the base of a deformation and are colored red and underlined since they represent a less desirable fracture type.

[2]Positive values are colored red and underlined because higher amounts of buckling are considered less desirable.

[3]Concentrations are measured as a percent of the total mass of steel

Table 11: Normalized slopes of linear regression for performance measures as a function of deformation geometry and chemical composition with p-values less than 5%. Red shading and underlined type indicate correlations resulting in undesirable performance while green shading and bold type indicate correlations resulting in desirable performance.

			Performance Measures											
			Fatigue Life			Softening / Hardening						Fracture Type	Buckling Amount
			Half-Cycles to Fracture	Total Strain Energy Dissipated	Normalized Strain Energy Dissipated	Second Tension Cycle Stress / First Tension Cycle	Maximum Tension Cycle Stress / First Tension Cycle	Last Tension Cycle Stress / First Tension Cycle	Second Compression Cycle Stress / First Compression Cycle	Maximum Compression Cycle Stress / First Compression Cycle	Last Compression Cycle Stress / First Compression Cycle	Fracture Propogation Along the Base of Deformation[1]	Max Buckling Amplitude[2]
Influential Parameters	Test Variables	Manufacturer				-26%	-14%	-17%	-11%	-12%	-13%	71%	
		Bar Size				**37%**	**23%**	**17%**	-11%				
		Grade			-10%	-19%	-6%		-8%			**-36%**	**-35%**
		Clear Span	-14%	-23%	-19%		-8%		-32%	-29%	-25%		42%
		Total Strain Range	-18%	-14%	-11%	-33%	-21%		-6%				
	Monotonic Stress/Strain Properties	Yield Strength			-12%								**-36%**
		Tensile Strength									**11%**	**-83%**	
		T/Y Ratio						**17%**					
		Elastic Modulus										32%	
		Ductility Ratio											
		Elastic Limit Strain											
		Uniform Strain							**21%**	**17%**			
		Fracture Strain				**48%**	**22%**						

[1]Positive values indicate a higher precent of crack propogation along the base of a deformation and are colored red and underlined since they represent a less desirable fracture type.

[2]Positive values are colored red and underlined because higher amounts of buckling are considered less desirable.

Table 12: Normalized slopes of linear regression for performance measures as a function of test parameters and material properties with p-values less than 1%. Red shading and underlined type indicate correlations resulting in undesirable performance while green shading and bold type indicate correlations resulting in desirable performance.

			Performance Measures											
			Fatigue Life			Softening / Hardening						Fracture Type	Buckling Amount
			Half-Cycles to Failure	Total Strain Energy Dissipated	Normalized Strain Energy Dissipated	Second Tension Cycle Stress / First Tension Cycle	Maximum Tension Cycle Stress / First Tension Cycle	Last Tension Cycle Stress / First Tension Cycle	Second Compression Cycle Stress / First Compression Cycle	Maximum Compression Cycle Stress / First Compression Cycle	Last Compression Cycle Stress / First Compression Cycle	Fracture Propogation Along the Base of Deformation[1]	Max Buckling Amplitude[2]
Influential Parameters	Deformation Geometry	R_{min}/H				43%	27%			18%		-100%	
		R_{max}/H						25%	7%		9%		
		H/d_b			-14%	-41%	-13%	-12%					
	Chemical Composition	C^3	14%				-56%						
		Mn^3								-24%			
		P^3			13%		18%						
		S^3							16%				
		Si^3											
		Cu^3			16%								
		Cr^3					-41%						
		Ni^3	-23%		-46%				-20%				
		Mo^3											
		V^3	-23%		-33%							-71%	-28%
		Nb^3											
		Sn^3	-11%		-15%			9%					

[1]Positive values indicate a higher precent of crack propogation along the base of a deformation and are colored red and underlined since they represent a less desirable fracture type.

[2]Positive values are colored red and underlined because higher amounts of buckling are considered less desirable.

[3]Concentrations are measured as a percent of the total mass of steel

Table 13: Normalized slopes of linear regression for performance measures as a function of deformation geometry and chemical composition with p-values less than 1%. Red shading and underlined type indicate correlations resulting in undesirable performance while green shading and bold type indicate correlations resulting in desirable performance.

5.5 Observed Trends

5.5.1 Effects of the Controlled Test Parameters

		Fatigue Life		
		Half-Cycles to Fracture	Total Strain Energy Dissipated	Normalized Strain Energy Dissipated
Test Variables	Manufacturer			
	Bar Size	-10%	-12%	
	Grade			-10%
	Clear Span	-14%	-23%	-19%
	Total Strain Range	-18%	-14%	-11%

Table 14: Normalized slopes of linear regression for fatigue life parameters as a function of test parameters with p-values less than 5%

Effects on Half-Cycles to Failure

The relationships between the test parameters and the number of half-cycles to failure were discussed qualitatively in section 4.2 and are discussed in more detail here. Three controlled parameters were found to correlate with the numbers of half-cycles to failure. These are in order of highest normalized regression slope: 1) strain range, 2) clear span, and 3) bar size.

The total cyclic strain range had a significant negative relationship with fatigue life. An increase in strain range from 4% to 5% resulted in an average decrease in fatigue life of 19.8 half-cycles to failure (Equation 2).

Equation 2: Example calculation for interpreting the normalized linear regression slopes

$$\Delta_{half\text{-}cycles\ to fracture}$$
$$= Normalized\ linear\ regression\ slope * Range_{half\text{-}cycles\ to\ fracture} * \frac{\Delta_{strain\ range}}{Range_{strain\ range}}$$
$$= (-18\%) * (110\ half\text{-}cycles\ to\ fracture) * \frac{1\%}{1\%}$$
$$= 19.8\ half\text{-}cycles\ to\ fracture$$

As discussed in Chapter 4, a clear relationship exists between the number of half-cycles to failure and the clear span. This correlation was found to be statistically significant. Namely, increasing the clear span from $4d_b$ to $6d_b$ resulted in an average decrease in fatigue life of 15.7 half-cycles to fracture. A significant relationship was also identified between half-cycles to failure and the bar size. Specifically, larger bars had smaller fatigue lives than the smaller bars. Increasing the bar size from a #5 bar to a #11 bar caused an average decrease in fatigue life of 10.5 half-cycles across all steel grades. As discussed in section 4.2.5, this effect is even more pronounced when only considering the grade 100 bars tested.

Effects on Total Strain Energy Dissipated

The effects of the test parameters on the total strain energy dissipated are of similar type and scale to those seen on the number of half-cycles to failure. However, the clear span was found to have a greater effect on total strain energy than numbers of half-cycles. By increasing the clear span from $4d_b$ to $6d_b$, a decrease in the total strain energy dissipated of 51.3 ksi is expected. This decrease is due in part to the decrease in the number of cycles to failure, but the energy dissipated per cycle is also decreased due to

decreased compressive stresses caused by higher amounts of buckling at clear spans of $6d_b$.

Effects on Normalized Strain Energy Dissipated

Similarly to the half-cycles to failure and the non-normalized strain energy dissipation, negative relationships were found connecting clear span and strain range to normalized strain energy.

The increased height of hysteresis loops due for higher strength bars increases the amount of energy dissipation per cycle. Normalizing the strain energy dissipated by the yield strength of the steel compensates for these positive effects of high yield strengths on strain energy dissipation. A negative relationship was found between steel grade and normalized energy dissipation. Namely, an increase in the grade of the steel from grade 60 to grade 100 resulted in a decrease in normalized strain energy of 0.34 (a 33% decrease compared to the mean normalized strain energy dissipation of grade 60 bars). This result implies that the strain energy dissipation is lower when a lower area of HSRB is used to replace grade 60 bars of equivalent strength.

5.5.2 Effects of Monotonic Stress/Strain Properties

		Fatigue Life		
		Half-Cycles to Fracture	Total Strain Energy Dissipated	Normalized Strain Energy Dissipated
Monotonic Stress/Strain Properties	Yield Strength			-12%
	Tensile Strength			
	T/Y Ratio			
	Elastic Modulus			
	Ductility Ratio			
	Elastic Limit Strain			
	Uniform Strain			
	Fracture Strain			

Table 15: Normalized slopes of linear regression for fatigue life parameters as a function of material properties with p-values less than 5%

No statistically significant relationships were identified between the stress/strain properties identified through monotonic testing and the number of half-cycles to failure or the amount of strain energy dissipated.

Similar to the effect of steel grade on the normalized strain energy dissipation, the measured yield strength displayed a negative relationship with normalized strain energy dissipation. An increase in the yield strength of the steel from 61.5 ksi to 111.0 ksi resulted in a decrease in normalized strain energy of 0.42.

5.5.3 Effects of Deformation Geometry

		Fatigue Life		
		Half-Cycles to Fracture	Total Strain Energy Dissipated	Normalized Strain Energy Dissipated
Deformation Geometry	R_{min}/H			
	R_{max}/H			
	H/d_b			-14%

Table 16: Normalized slopes of linear regression for fatigue life parameters as a function of deformation geometry with p-values less than 5%

No statistically significant relationships were identified between the geometry of the deformations and the number of half-cycles to failure or the amount of strain energy dissipated.

A statistically significant relationship was identified between the normalized strain energy dissipation and the ratio of deformation height to nominal bar diameter (H/d_b). This relationship indicated that an increase in the deformation height to bar diameter ratio from the minimum value observed (0.05) to the maximum value observed (0.0813) would result in a decrease in normalized strain energy of 0.48. It is noteworthy that the H/d_b ratio was highly correlated with steel grade in this study (Appendix A).

5.5.4 Effects of Chemical Composition

		Fatigue Life		
		Half-Cycles to Fracture	Total Strain Energy Dissipated	Normalized Strain Energy Dissipated
Chemical Composition	C[1]	14%		
	Mn[1]			
	P[1]			13%
	S[1]			
	Si[1]			
	Cu[1]			16%
	Cr[1]			
	Ni[1]	-23%		-46%
	Mo[1]			
	V[1]	-23%		-33%
	Nb[1]			
	Sn[1]	-11%	-8%	-15%

[1]Concentrations are measured as a percent of the total mass of steel

Table 17: Normalized slopes of linear regression for fatigue life parameters as a function of chemical composition with p-values less than 5%

Effects on Half-Cycles to Failure

Statistically significant correlations were found between the number of half-cycles to failure and the concentrations of four elements: carbon, nickel, vanadium, and tin.

A positive relationship was found between fatigue life and carbon. Namely, by increasing carbon content from the minimum value measured (0.26% by mass) to the

maximum value measured (0.35% by mass), the average fatigue life would increase by 15.8 half-cycles.

The relationship between fatigue life and the remaining elements was negative. Increasing nickel from its minimum value to its maximum value (a change of 0.07% nickel by mass) resulted in a decrease in fatigue life of 25.5 half-cycles. Increasing vanadium from its minimum value to its maximum value (a change of 0.354% vanadium by mass) resulted in a decrease in fatigue life of 25.8 half-cycles. Increasing tin from its minimum value to its maximum value (a change of 0.01% tin by mass) resulted in a decrease in fatigue life of 11.9 half-cycles.

Effects on Total Strain Energy Dissipation

The only statistically significant correlation identified between strain energy dissipation and the concentration of an element was tin. This effect was of a very similar scale to that observed in the half-cycles to failure. Increasing tin from its minimum value to its maximum value (a change of 0.01% tin by mass) resulted in a decrease in strain energy dissipation of 17.0 ksi.

Effects on Normalized Strain Energy Dissipation

Positive relationships were identified between normalized strain energy dissipation and phosphorous as well as copper. Increasing these two elements from their smallest observed concentrations to their highest observed concentrations resulted in an increase in normalized strain energy dissipation of 0.45 and 0.55 respectively.

Negative relationships on normalized strain energy dissipation were identified from nickel vanadium and tin. The impact of increasing each of these elements from its

smallest observed value to its largest observed value was 1.58, 1.16, and 0.53 respectively.

5.6 Changes in Hardening or Softening Behavior

5.6.1 Effects of Controlled Test Parameters

		Softening / Hardening					
		Second Tension Cycle Stress / First Tension Cycle	Maximum Tension Cycle Stress / First Tension Cycle	Last Tension Cycle Stress / First Tension Cycle	Second Compression Cycle Stress / First Compression Cycle	Maximum Compression Cycle Stress / First Compression Cycle	Last Compression Cycle Stress / First Compression Cycle
Test Variables	Manufacturer	-26%	-14%	-17%	-11%	-12%	-13%
	Bar Size	**37%**	**23%**	**17%**	-11%		
	Grade	-19%	-6%		-8%	-5%	
	Clear Span		-8%		-32%	-29%	-25%
	Total Strain Range	-33%	-21%	-6%	-6%	-7%	

Table 18: Normalized slopes of linear regressions for hardening / softening performance measures as a function of test variables with p-values less than 5%

A significant negative relationship exists between performance measures relating to cyclic hardening and the strain range. This effect is especially pronounced on the second-cycle hardening parameter. This trend indicates that bars tested at larger strain ranges sustained relatively high damage during the first cycle. Increasing the strain range also decreased the maximum amount of hardening throughout a test in addition to slightly decreasing the amount of net hardening at the last cycle of the test.

As would be expected, increasing the clear span, and therefore the amount of buckling, resulted in significant amounts of softening in compression. Namely, an increase in clear span from $4d_b$ to $6d_b$ resulted in an average increase in the compression softening ratio over the first two cycles of 0.05.

The manufacturing technique played a statistically significant role in hardening and softening behavior as well. Bars produced by Manufacturer 2 consistently exhibited less hardening in tension and more softening in compression between cycles than bars produced by Manufacturer 1.

A significant positive relationship was identified between the bar size and the amount of cyclic hardening. Most notably, the hardening ratio between the first two cycles could be expected to increase by 0.10 by increasing the size of the bar from #5 to #11.

A significant negative relationship was identified between the steel grade and cyclic hardening ratio between the first two cycles with grade 100 bars exhibiting a hardening ratio 0.03 lower than grade 60 bars.

5.6.2 Effects of Monotonic Stress/Strain Properties

		Softening / Hardening					
		Second Tension Cycle Stress / First Tension Cycle	Maximum Tension Cycle Stress / First Tension Cycle	Last Tension Cycle Stress / First Tension Cycle	Second Compression Cycle Stress / First Compression Cycle	Maximum Compression Cycle Stress / First Compression Cycle	Last Compression Cycle Stress / First Compression Cycle
Monotonic Stress/Strain Properties	Yield Strength						
	Tensile Strength						11%
	T/Y Ratio			17%			
	Elastic Modulus						
	Ductility Ratio						
	Elastic Limit Strain						
	Uniform Strain				21%	17%	
	Fracture Strain	48%	22%				

Table 19: Normalized slopes of linear regression for hardening / softening performance measures as a function of monotonic stress/strain properties with p-values less than 5%

The largest statistically significant relationships between softening or hardening and monotonic material properties came from the uniform and fracture strains. Positive correlations were identified between fracture strain and the amount of hardening that occurred over the first two cycles as well as the maximum amount of cyclic hardening. Likewise, negative correlations were identified between uniform strain and the amount of softening that occurred in compression between the first two cycles.

5.6.3 Effects of Deformation Geometry

		Softening / Hardening					
		Second Tension Cycle Stress / First Tension Cycle	Maximum Tension Cycle Stress / First Tension Cycle	Last Tension Cycle Stress / First Tension Cycle	Second Compression Cycle Stress / First Compression Cycle	Maximum Compression Cycle Stress / First Compression Cycle	Last Compression Cycle Stress / First Compression Cycle
Deformation Geometry	R_{min}/H	43%	27%			18%	
	R_{max}/H			25%	7%		9%
	H/d_b	-41%	-13%	-12%			

Table 20: Normalized slopes of linear regression for hardening / softening performance measures as a function of deformation geometry with p-values less than 5%

A positive correlation was identified between the ratio of R_{min}/H and the hardening over the first two cycles as well as the maximum total hardening in both tension and compression. In addition, a negative correlation was identified between the ratio of H/d_b and several of the hardening parameters considered. Specifically, higher deformation heights relative to the bar diameter correlated with decreases in hardening after the first cycle, decreases in maximum hardening, and decreases in net hardening at the last cycle of the test.

5.6.4 Effects of Chemical Composition

		Softening / Hardening					
		Second Tension Cycle Stress / First Tension Cycle	Maximum Tension Cycle Stress / First Tension Cycle	Last Tension Cycle Stress / First Tension Cycle	Second Compression Cycle Stress / First Compression Cycle	Maximum Compression Cycle Stress / First Compression Cycle	Last Compression Cycle Stress / First Compression Cycle
Chemical Composition	C[1]		-56%				
	Mn[1]				9%	-24%	
	P[1]		18%			11%	
	S[1]				16%		
	Si[1]					12%	
	Cu[1]						
	Cr[1]		-41%				
	Ni[1]				-20%	-16%	
	Mo[1]						
	V[1]						
	Nb[1]						
	Sn[1]			9%			

[1]Concentrations are measured as a percent of the total mass of steel

Table 21: Normalized slopes of linear regression for hardening / softening performance measures as a function of chemical composition with p-values less than 5%

A strong negative correlation was identified between the maximum amount of hardening in tension and the concentration of carbon in the bars. For an increase in only 0.08% carbon by mass, a decrease in the maximum tensile hardening ratio of 0.17 was observed. Similarly, an increase in 0.09% chromium by mass led to a decrease in the maximum tensile hardening ratio of 0.12.

Although few statistically significant relationships were identified between the net tensile hardening at the last cycle and chemical composition, when bars from the two manufacturers were assessed separately, clear correlations were observed. Specifically, increases in vanadium and sulfur both exhibited positive normalized regression slopes of 10% with net tensile hardening, but only for bars produced by Manufacturer 1. Carbon

content, however exhibited a negative normalized regression slope of 25% with net tensile hardening for bars produced by Manufacturer 2. In addition, a negative normalized regression slope of 26% was identified between copper and net tensile hardening for bars produced by Manufacturer 2.

Finally, a positive correlation was identified between sulfur concentration and the initial hardening between the first two cycles. For most cases, this correlation actually indicated that increasing sulfur concentrations decreased the amount of softening, but did not actually lead to compression hardening.

5.7 CHANGES IN FRACTURE TYPE

5.7.1 Effects of Test Parameters

		Fracture Type
		Fracture Propogation Along the Base of Deformation[1]
Test Variables	Manufacturer	71%
	Bar Size	
	Grade	-36%
	Clear Span	
	Total Strain Range	

[1]Positive values indicate a higher precent of crack propogation along the base of a deformation and are colored red and underlined since they represent a less desirable fracture type.

Table 22: Normalized slopes of linear regression for fracture type as a function of test parameters with p-values less than 5%

A distinct relationship was identified between the manufacturing process and type of fracture. Namely, for bars produced by Manufacturer 1, 23% of fatigue cracks propagated along the base of the deformation and 77% propagated horizontally through the barrel of the bar. For bars produced by Manufacturer 2, however, every single fatigue crack propagated along the base of the deformation with none propagating horizontally through the barrel of the bar. The steel grade was also found to have a statistically significant impact on the fracture type. Increasing the steel grade tended to decrease the probability of fatigue crack propagation along the base of a deformation.

When fatigue crack propagation path was included in the regression model between half-cycles to fracture and the five controlled test variables, the p-value for fatigue crack propagation path was 0.42, indicating that no statistically significant relationship was found between fatigue life and fatigue crack propagation path. However, providing a distinct path of weakness along which a fatigue crack can propagate may have hindered the fatigue performance of bars produced by Manufacturer 2.

5.7.2 Effects of Monotonic Stress/Strain Properties

		Fracture Type
		Fracture Propogation Along the Base of Deformation[1]
Monotonic Stress/Strain Properties	Yield Strength	
	Tensile Strength	-83%
	T/Y Ratio	
	Elastic Modulus	32%
	Ductility Ratio	
	Elastic Limit Strain	
	Uniform Strain	
	Fracture Strain	

[1]Positive values indicate a higher precent of crack propogation along the base of a deformation and are colored red and underlined since they represent a less desirable fracture type.

Table 23: Normalized slopes of linear regression for fracture type as a function of monotonic stress/strain properties with p-values less than 5%

A significant negative correlation was found between the likelihood of fracture propagation along the base of a deformation and the ultimate tensile strength of the steel.

5.7.3 Effects of Deformation Geometry

		Fracture Type
		Fracture Propogation Along the Base of Deformation[1]
Deformation Geometry	R_{min}/H	-100%
	R_{max}/H	
	H/d_b	

[1]Positive values indicate a higher precent of crack propogation along the base of a deformation and are colored red and underlined since they represent a less desirable fracture type.

Table 24: Normalized slopes of linear regression for fracture type as a function of deformation geometry with p-values less than 5%

The ratio of R_{min}/H had a significant impact on the fatigue crack propagation direction. On average an increase in this ratio of 3.1 (which is roughly equal to the range of values observed) correlated with a change in fatigue crack propagation from horizontally through the barrel of the bar to along the base of the deformation.

For values of R_{min}/H greater than 3.01, none of the bars tested exhibited fatigue crack propagation along the base of a deformation.

5.7.4 Effects of Chemical Composition

		Fracture Type
		Fracture Propogation Along the Base of Deformation[1]
Chemical Composition	C[2]	
	Mn[2]	
	P[2]	
	S[2]	
	Si[2]	
	Cu[2]	
	Cr[2]	
	Ni[2]	
	Mo[2]	
	V[2]	-71%
	Nb[2]	
	Sn[2]	

[1]Positive values indicate a higher precent of crack propogation along the base of a deformation and are colored red and underlined since they represent a less desirable fracture type.

[2]Concentrations are measured as a percent of the total mass of steel

Table 25: Normalized slopes of linear regression for fracture type as a function of chemical composition with p-values less than 5%

A negative correlation was also found between the likelihood of fracture propagation along the base of a deformation and the concentration of vanadium.

5.8 CHANGES IN BUCKLING AMPLITUDE

5.8.1 Effects of Controlled Test Parameters

		Buckling Amount
		Max Buckling Amplitude[1]
Test Variables	Manufacturer	
	Bar Size	-31%
	Grade	-35%
	Clear Span	42%
	Total Strain Range	

[1]Positive values are colored red and underlined because higher amounts of buckling are considered less desirable.

Table 26: Normalized slopes of linear regression for buckling amplitude as a function of controlled test parameters with p-values less than 5%

As would be expected, the clear span exhibited a large and highly significant positive correlation with the maximum amount of buckling. By increasing the clear span from $4d_b$ to $6d_b$, the maximum buckling amplitude tended to increase by 42% of the range of values observed, or $0.22d_b$. Increasing bar size had a significant negative relationship with buckling, with #11 bars predicted to buckle $0.16d_b$ less than #5 bars. The steel grade also proved to have a significant negative correlation with buckling amplitude, with higher grade bars buckling to a lesser degree, even though higher grade steel was observed to result in less hardening or more softening (section 5.6.1).

5.8.2 Effects of Monotonic Stress/Strain Properties

		Buckling Amount
		Max Buckling Amplitude[1]
Monotonic Stress/Strain Properties	Yield Strength	-36%
	Tensile Strength	
	T/Y Ratio	
	Elastic Modulus	
	Ductility Ratio	
	Elastic Limit Strain	
	Uniform Strain	
	Fracture Strain	

[1]Positive values are colored red and underlined because higher amounts of buckling are considered less desirable.

Table 27: Normalized slopes of linear regression for buckling amplitude as a function of monotonic stress/strain properties with p-values less than 5%

Following the same relationship seen between buckling amplitude and grade, the measured steel yield stress exhibited a negative relationship with buckling amplitude. The relationship related to actual yield stress was slightly steeper than that related to grade, with an increase in yield from 61.5ksi to 111ksi resulting in a decrease in buckling of $0.18d_b$.

5.8.3 Effects of Deformation Geometry

No statistically significant relationships were identified between the geometry of the deformations and the amplitude of buckling experienced.

5.8.4 Effects of Chemical Composition

		Buckling Amount
		Max Buckling Amplitude[1]
Chemical Composition	C[2]	-18%
	Mn[2]	
	P[2]	
	S[2]	
	Si[2]	
	Cu[2]	
	Cr[2]	
	Ni[2]	
	Mo[2]	
	V[2]	-28%
	Nb[2]	
	Sn[2]	

[1]Positive values are colored red and underlined because higher amounts of buckling are considered less desirable.

[2]Concentrations are measured as a percent of the total mass of steel

Table 28: Normalized slopes of linear regression for buckling amplitude as a function of chemical composition with p-values less than 5%

Carbon exhibited a shallow but significant negative relationship with buckling amplitude. Increasing carbon concentration by 0.08% by mass decreased the maximum buckling displacement by only $0.09d_b$.

Similar negative relationships which steel grade and measured yield strength exhibited to buckling were exhibited in the relationship between vanadium and buckling. An increase in vanadium of 0.354% by mass correlated with a decrease in buckling amplitude of $0.14d_b$.

5.9 RELATING FATIGUE LIFE TO TOTAL STRAIN RANGE

Several relationships between the low-cycle fatigue life of reinforcing bars and the total strain range have been proposed (Mander et al. 1994, Brown and Kunnath 2004, Hawileh et al. 2010), but none apply for the new HSRB in production. The proposed relationships closely follow a power function of the form described in Equation 3 or Equation 4, where the parameters "a", "b", "c", and "d" are material properties for a given bar. The results of this study have enabled the development of such equations for different grades of reinforcing bars so that the relationships can be compared and an estimate of the fatigue life for these bars can be inferred for any strain range. Specifically, the form shown in Equation 4 was selected as it is more convenient for use by engineers assessing the fatigue life of bars given a strain history.

Equation 3: Form of equation for fatigue life modeling with strain range as the dependent variable

$$Total\ Strain\ Range = a * (Half-Cycles\ to\ Failure)^b$$

Equation 4: Form of equation for fatigue life modeling with fatigue life as the dependent variable

$$Half-Cycles\ to\ Failure = c * (Total\ Strain\ Range)^d$$

Since the tests on #5 bars and #11 bars were primarily conducted for one value of cyclic strain range, reliable relationships could not be developed for these bar sizes. However, nearly all of the #8 bars represented in this study were tested under two cyclic total strain ranges (4% and 5%). In addition, previous researchers (Mander et al. 1994) have utilized the fracture strain obtained from monotonic tension tests to represent the total strain range which corresponds to a fatigue life of half of one half-cycle. Using these three sets of data, relationships were developed using regression analyses for each

combination of manufacturer, grade, and clear span based on the results of at least nine cyclic or monotonic tension tests.

The test results and the relationships identified from these tests are displayed in Figure 36 to Figure 40. The material coefficients, "c" and "d", used in Equation 4 are summarized in Table 29 for various parameter combinations.

Manufacturer	Grade	Clear Span	c	d
1	60	**4db**	5.14E-03	-2.87
		5db	5.92E-03	-2.77
		6db	7.92E-03	-2.59
	80	**4db**	2.48E-03	-2.97
		6db	6.60E-03	-2.43
	100	**4db**	2.40E-05	-4.62
		5db	8.14E-05	-4.06
		6db	1.49E-04	-3.77
2	60	**4db**	3.59E-04	-3.75
		5db	8.49E-04	-3.31
		6db	1.49E-03	-3.03
	100	**4db**	1.90E-06	-5.42
		5db	2.60E-06	-5.25
		6db	1.65E-05	-4.46

Table 29: Summary of material coefficients for fatigue life equations for #8 bars

Using these equations, one can estimate the fatigue life of a #8 bar studied here simply based on the manufacturer, grade, clear span, and strain range. For example, a grade 60 #8 bar produced by Manufacturer 1 and tested at a clear span of $6d_b$ and a total strain range of 2% would be predicted to have a fatigue life around 201 half-cycles (Equation 5).

Equation 5: Example calculation for fatigue life of grade 60 #8 bar produced by Manufacturer 1, tested at $6d_b$ and 2% strain range

$$Half\text{-}Cycles\ to\ Failure_{grade\ 60,6db} = c * (Total\ Strain\ Range)^d$$

$$= 7.92 * 10^{-3} * (2\%)^{-2.59} = 201\ Half\text{-}Cycles$$

Due to strain concentrations at cracks, HSRB used as longitudinal reinforcement in concrete columns have been shown to sustain strains as much as 100% larger than grade 60 A706 bars when subjected to the same drift cycles (Sokoli and Ghannoum 2015). This observation indicates that the cyclic fatigue life of HSRB may be much lower than that of grade 60 bars for a given lateral drift loading history. For example, if grade 60 #8 bars are expected to be cycled at a total strain range of 2% in a column design, then grade 100 bars replacing the grade 60 bars would be expected to be cycled at a strain range of 4%. The fatigue life of the grade 100 bars having a clear span of $6d_b$ would then only be 27 half-cycles (Equation 6) compared with 201 half-cycles for the grade 60 counterparts (Equation 5).

The relations summarized in Table 29 also indicate that the low-cycle fatigue life of bars, particularly HSRB, can be improved by narrowing the span between transverse ties. For the example in Equation 6, changing the clear span from $6d_b$ to $4d_b$ for the grade 100 bar would result in an increase of 41 half-cycles to fracture (from 27 to 68) (Equation 7). However, while reducing the clear span limit from $6d_b$ to $4d_b$ for HSRB may improve the fatigue life, it may not be sufficient to counteract the expected increase in strain demands on HSRB compared to grade 60 bars. Furthermore, since buckling was almost eliminated for clear spans of $4d_b$, a decrease in clear span below $4d_b$ is unlikely to provide significant gains in low-cycle fatigue performance.

Equation 6: Example calculation for fatigue life of grade 100 #8 bar produced by Manufacturer 1, tested at $6d_b$ and 4% strain range

$$Half-Cycles\ to\ Failure_{grade\ 100,6db} = c * (Total\ Strain\ Range)^d$$

$$= 1.49 * 10^{-4} * (4\%)^{-3.77} = 27\ Half-Cycles$$

Equation 7: Example calculation for fatigue life of grade 100 #8 bar produced by Manufacturer 1, tested at $4d_b$ and 4% strain range

$$Half-Cycles\ to\ Failure_{grade\ 100,4db} = c * (Total\ Strain\ Range)^d$$

$$= 2.40 * 10^{-5} * (4\%)^{-4.62} = 68\ Half-Cycles$$

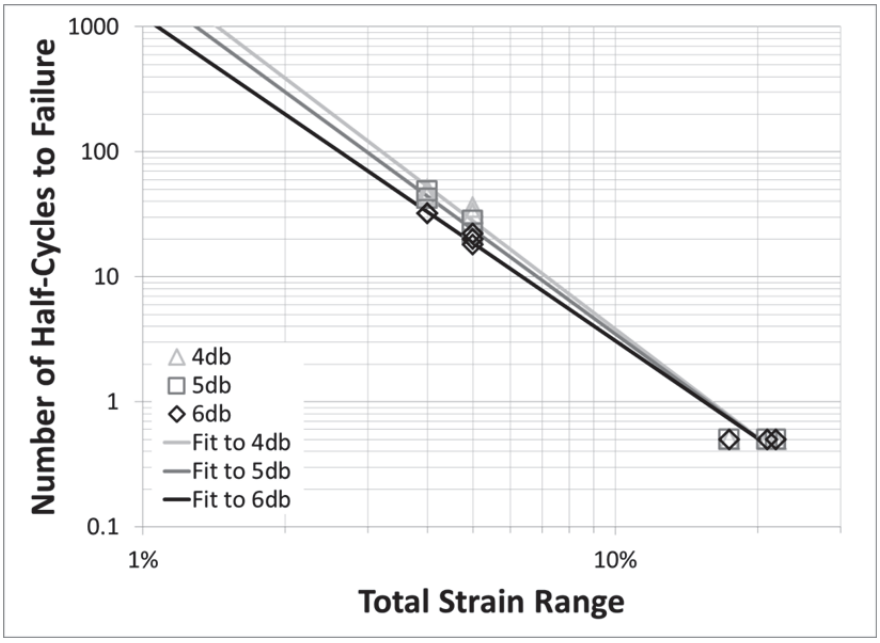

Figure 36: Relationship between half-cycles to failure and total strain range for grade 60 #8 bars produced by Manufacturer 1

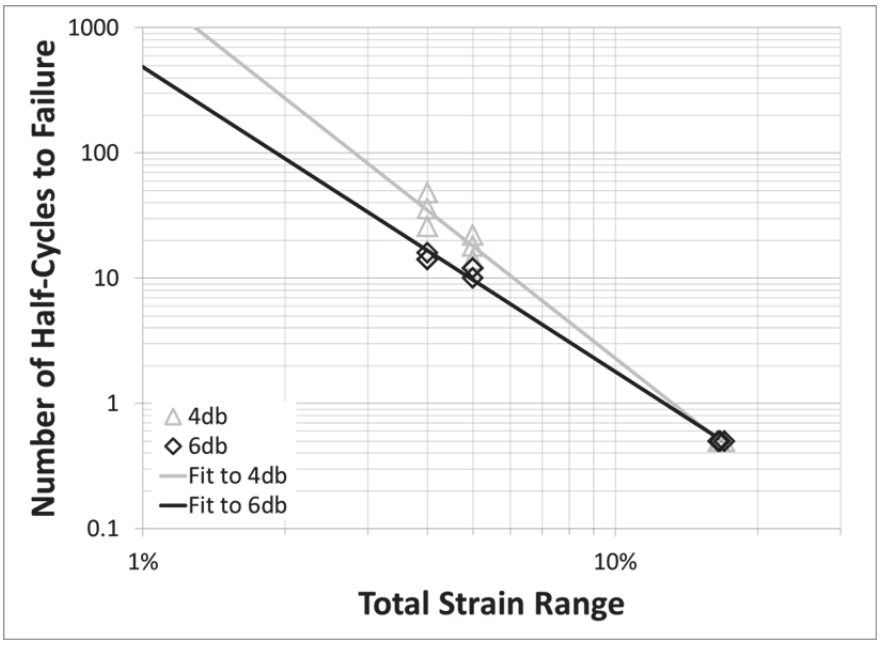

Figure 37: Relationship between half-cycles to failure and total strain range for grade 80 #8 bars produced by Manufacturer 1

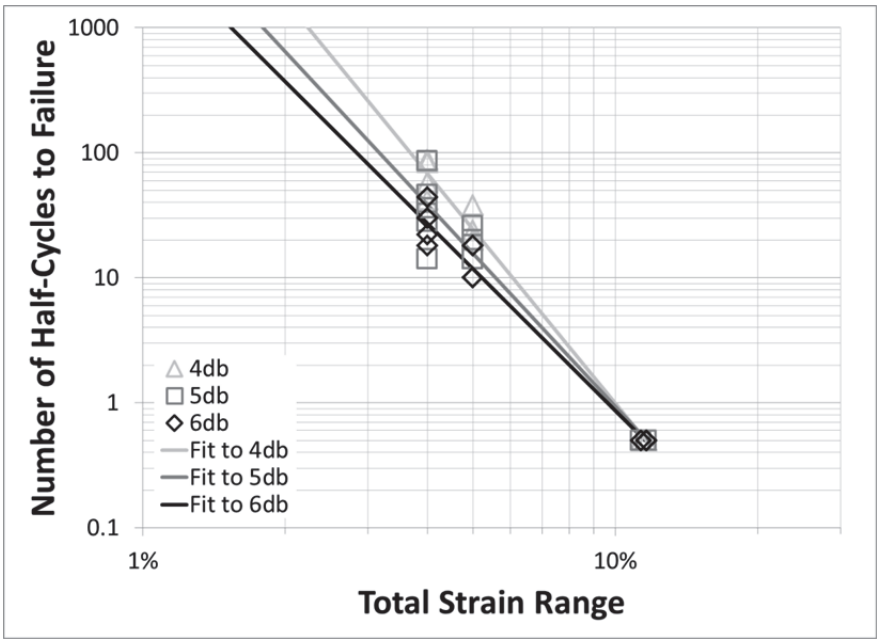

Figure 38: Relationship between half-cycles to failure and total strain range for grade 100 #8 bars produced by Manufacturer 1

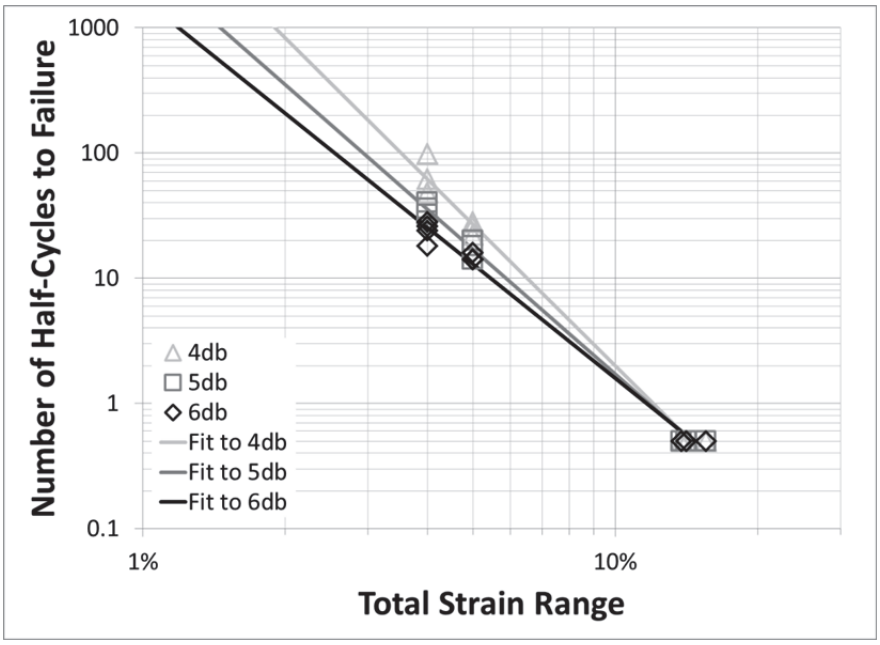

Figure 39: Relationship between half-cycles to failure and total strain range for grade 60 #8 bars produced by Manufacturer 2

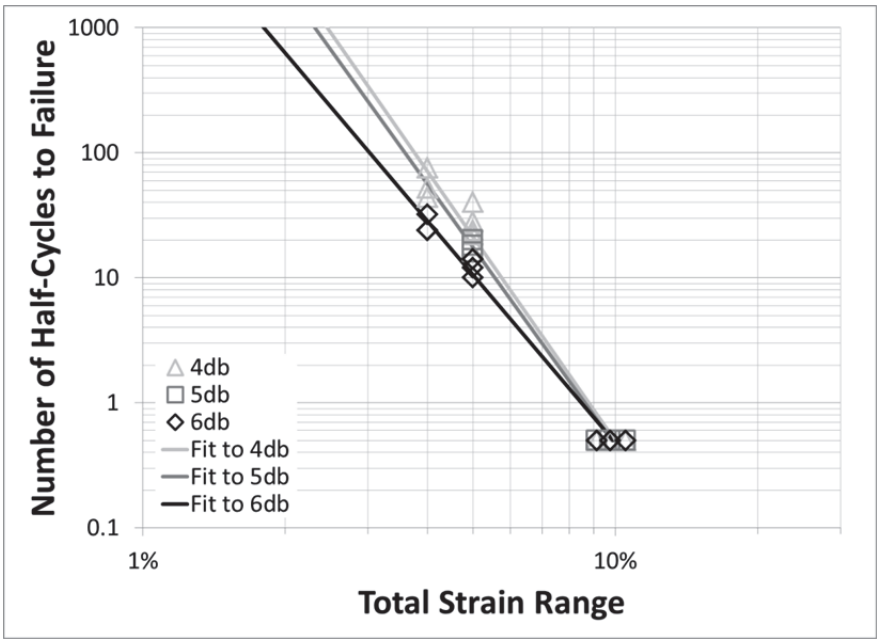

Figure 40: Relationship between half-cycles to failure and total strain range for grade 100 #8 bars produced by Manufacturer 2

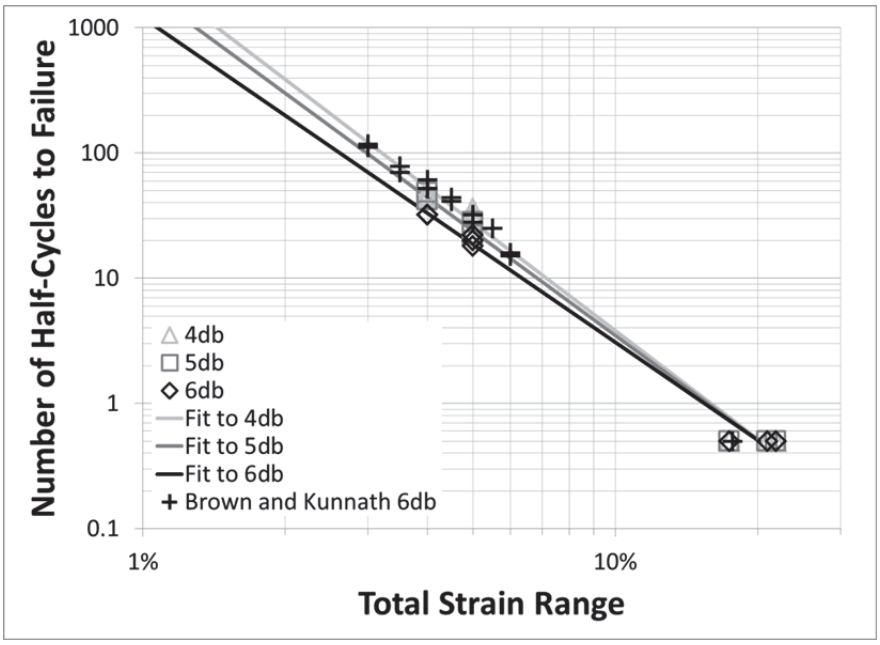

Figure 41: Results from Brown and Kunnath (2004) overlaid with data from grade 60 #8 bars produced by Manufacturer 1

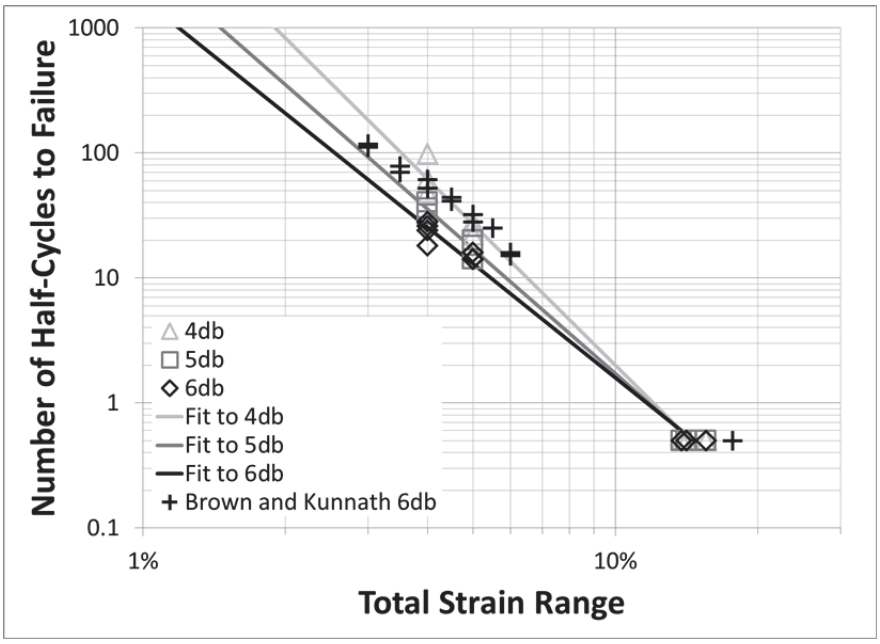

Figure 42: Results from Brown and Kunnath (2004) overlaid with data from grade 60 #8 bars produced by Manufacturer 2

In Figure 41 and Figure 42, the low cycle fatigue data from Brown and Kunnath (2004) for total strain ranges of 2% to 6% and clear spans of $6d_b$ is displayed with the data from this study. The results of monotonic tension tests performed by Brown and Kunnath are also displayed as representing half of one half-cycle to fracture. The figures indicate that results from this study are comparable to those of the Brown and Kunnath study for those particular parameters. In particular, the grade 60 #8 bars produced by Manufacturer 1 correspond well to the data produced by Brown and Kunnath (2004).

5.10 Potential Causes of Fatigue Life Outliers

The majority of the reinforcing bars tested in low-cycle fatigue experienced similar fatigue life regardless of grade. However, four combinations of manufacturer, grade, and bar size gave results that departed significantly from the general observed trends. The bars types of interest were the grade 80 #5 and #8 bars, and grade 100 #11 bars produced by Manufacturer 1, as well as the grade 80 #5 bars produced by Manufacturer 2. The potential causes of these differences are investigated in the subsequent sections.

5.10.1 Manufacturer 1, Grade 80, #5 and #8 Bars

The fatigue life of grade 80 bars produced by Manufacturer 1 exhibited significantly lower fatigue life when compared to similar grade 60 and grade 100 bars. As discussed in section 5.5.4, a positive relationship was observed between fatigue life and carbon content. Manufacturer 1's grade 80 bars of both sizes had very low carbon concentrations. In addition, these bars contained concentrations of sulfur which approach the upper level deemed acceptable for ASTM A706 steel (0.045%). While the analysis of the bars tested in this study did not reveal a statistically significant relationship between

fatigue life and sulfur concentration, other studies on the fatigue of steel have shown a negative relationship (Cyril et al. 2008). Lastly, both sets of grade 80 bars exhibited high levels of tin, which was found to have a small but significant negative effect on fatigue life as discussed in section 5.5.4.

5.10.2 Manufacturer 1, Grade 100, #11 Bars

Most of the properties of the grade 100 #11 bars produced by Manufacturer 1 fall in the middle of the range exhibited by all of the other bars. This makes the deficient fatigue life of these bars difficult to explain based on material and geometric properties alone. The one way in which these bars differ significantly from the other bars of the same size is the amount of vanadium. Due to the size of the bar, there is a decrease in the amount of strength gained during cooling and, therefore, large amounts of vanadium must be added in order to reach a yield strength above 100ksi. The grade 100 #11 bars produced by Manufacturer 1 contain the highest amount of vanadium of any of the bars tested. The lower fatigue life exhibited by these bars may be an indication of a negative impact on fatigue life of high amounts of vanadium.

5.10.3 Manufacturer 2, Grade 80, #5 Bars

Unlike the other anomalous fatigue results, the grade 80 #5 bars produced by Manufacturer 2 exhibited much higher fatigue life than the other bars of the same size. One possible contribution to the superior fatigue life is the high ratio of the smaller of the two radii at the base of the deformation to the height of the deformation. This R_{min}/H value was the highest of any of the #5 bars tested.

Another potential source of this high fatigue life is the relatively high carbon content of the bars, which was found to correlate with increased fatigue life. These bars

also contained the second lowest concentration of vanadium of any bar tested and the lowest concentration of any #5 bar tested, which may have contributed to their higher than average fatigue life.

6. Summary and Conclusions

6.1 Summary of the Experimental Program

The use of high-strength reinforcing bars (HSRB) in reinforced concrete structures subjected to earthquakes has the potential to reduce reinforcement congestion, accelerate construction, and allow designs not currently possible with grade 60 reinforcement. However, the current ACI 318-14 design code restricts reinforcing steel yield strengths to 60 ksi for shear, 100 ksi for confinement, and 80 ksi for all other non-seismic applications. For seismic designs, the yield-strength limit provided by the code remains at 60 ksi. Similar limits exist in the AASTHO LRFD 2015 code (American Association of State Highway and Transportation Officials, 2015).

To assess the acceptability of newly developed high-strength reinforcing bars in seismic applications, the low-cycle fatigue performance of HSRB produced using the two most common manufacturing processes was investigated. HSRB are defined in this study as bars having a specified yield strength not less than 80 ksi.

Low-cycle fatigue tests were performed on grade 60 A706, grade 80 A706 and A615, and grade 100 reinforcing bars from two manufacturers. #5, #8, and #11 bars were tested in order to represent a range of typically used transverse and longitudinal bars. The bars were gripped at multiple clear spans in order to modify the amount of buckling experienced. Two total strain ranges were also used to examine the relationships between strain range and fatigue life of HSRB: 4% and 5%. In this study, each type of grade 100 bar had a comparable grade 60 bar type tested under the same clear span and loading protocol. The study focused on comparing the performance of grade 100 bars with that of grade 60 bars. Limited tests were conducted on grade 80 bars.

The effects of the controlled variables on the low-cycle fatigue performance of HSRB were explored. In addition, the effects of the monotonic tension-test properties, deformation geometry, and chemical composition were explored to identify any possible relationships with fatigue life. Relations for estimating the fatigue life of #8 bars within the parameter ranges of this study were developed.

6.2 CONCLUSIONS

Overall, the fatigue performance, defined in terms of the number of half-cycles to failure and the total strain energy dissipation, was marginally poorer for HSRB than for grade 60 bars. Over all tests performed, the average number of half-cycles to failure of the grade 100 bars was 91% of that for the grade 60 A706 bars.

However, relatively large discrepancies between the performance of high-strength and grade 60 bars were observed for certain bars types, sizes, and loading protocols. Four of the nine bar types tested with yield strengths greater than 80ksi performed substantially differently from their grade 60 A706 counterparts. Of those four, three HSRB types performed significantly worse than the equivalent grade 60 A706 bars. These three were the grade 80 #5 and #8 bars as well as the grade 100 #11 bars produced by Manufacturer 1.

The grade 80 bars produced by Manufacturer 1 exhibited only 54% of the half-cycles to failure of the grade 60 A706 bars from the same manufacturer, while those produced by Manufacturer 2 exhibited 4.4 times the cycles to failure of the grade 60 A706 bars from the same manufacturer. These results indicate a very wide range of low-cycle fatigue performance for grade 80 bars. Only a limited number of grade 80 bars were tested, however. More tests are needed to fully assess the highly variable and sometimes inferior low-cycle fatigue results observed for grade 80 bars.

The larger bar sizes failed, in general, at lower numbers of cycles than the smaller bars. This effect was more pronounced for grade 100 bars, with grade 100 #11 bars fracturing on average at 37% of the half-cycles to fracture of grade 100 #8 bars.

As expected, the total strain range to which the bars were subjected affected the low-cycle fatigue life of the bars significantly. An increase in cyclic strain range reduced the numbers of cycles to fracture.

Decreasing the clear spacing between grips on the bars was found to reduce the buckling amplitudes in the bars and significantly improve the low-cycle fatigue performance.

A strong correlation was observed between fracture propagation along the base of a deformation and the manufacturer. Namely, all but one of the bars produced by Manufacturer 2 exhibited fracture propagation along a deformation. While this did not appear to have a substantial negative impact on the low-cycle fatigue performance of those bars, the results indicate that increasing the ratio of the base-radius to height of the deformations may improve the low-cycle fatigue performance of the bars produced by the manufacturer.

Test results have indicated that the concentration of vanadium may have a negative impact on the low-cycle fatigue life of high-strength reinforcing bars. However, the concentration of vanadium is correlated with steel grade and other variables that negatively impact the low-cycle fatigue performance of bars. Other variables that were not investigated in this study, such as the heat history of the bars may also play a role in the amount of vanadium in solution and the austenitizing process. Other chemical concentrations that were observed to be negatively correlated with fatigue performance

were nickel and tin. Chemicals showing a positive correlation with fatigue performance were carbon, phosphorus, and copper.

It is important to note that, except for yield strength, the monotonic stress-strain parameters were not found to correlate with fatigue performance of reinforcing bars.

6.3 IMPLICATIONS OF TEST RESULTS

High-strength reinforcing bars have been shown to experience significantly higher strains for a given drift demand than grade 60 bars in concrete columns (up to two times those experienced by grade 60 A706 bars) (Sokoli and Ghannoum 2015). Based on the fatigue life equations developed in this study for grade 100 #8 bars, a doubling of total strain range can lead to a decrease in the number of half-cycle to fracture of approximately 93%. This means that the HSRB tested in this study may fracture at significantly lower drift-cycle demands in concrete members than grade 60 A706 bars.

As test results demonstrated, decreasing the buckling length of bars, which can be achieved by decreasing the spacing of transverse reinforcement in concrete members, can improve their low-cycle fatigue performance significantly. Therefore, reducing the clear span limit of $6d_b$ currently in ACI 318-14 for HSRB in seismic applications can partially counteract the detrimental effects of potential increases in strain demands on higher-strength bars. However, since buckling was almost eliminated in this study for clear spans of $4d_b$, benefits from decreasing the buckling length can likely only be achieved down to spans of $4d_b$.

A large demand for HSRB is in applications where grade 60 bars are needed at the upper limit of the bars sizes in production. In such applications, HSRB are substituted without going beyond the #18 bar size limit. Test results have demonstrated a moderate but significant negative correlation between bar size and fatigue life, particularly in grade

100 bars. This study, however, only investigated the fatigue behavior of bars up to #11 in size. Larger HSRB may have more a pronounced decrease in fatigue life compared with the smaller bars tested in this study.

7. Recommendations for Future Work

Additional tests need to be conducted to fully understand the inferior results and the large scatter in low-cycle fatigue results of this study. More advanced chemical analyses should be conducted on bars to uncover any correlations between fatigue life and the concentration of elements that are not commonly reported. Likewise, bar rolling procedures and heat history should be investigated to explore any possible relations to the low-cycle fatigue performance of the HSRB.

Only two cyclic total strain ranges were tested in this study: 4% and 5%. In order to increase the range of total strain ranges represented, cyclic tests should be performed on bars at total strain ranges outside of the range tested in this study.

The poor performance of the grade 80 bars produced by Manufacturer 1 would indicate that major revisions to the manufacturing of these bars are required. However, only two bar sizes (and only one heat per bar size) were used to draw this conclusion. In order to identify the severity and cause of this problem, tests should be performed on grade 80 bars covering a wider size range and from different heats.

Since larger bars were shown to have worse low-cycle fatigue performance than smaller bars, larger bars up to #18 should be tested.

The current ASTM A706 specifications for reinforcing bars does not place limits on most of the parameters that were found to correlate with low-cycle fatigue of bars. ASTM A706 is focused on limiting chemistry for weldability and monotonic stress/strain parameters that were shown not to correlate with low-cycle fatigue performance. Given the large variability in the low-cycle fatigue of high-strength and grade 60 reinforcing bars, it seems warranted to introduce additional specifications to improve the reliability

of the low-cycle fatigue performance of reinforcing bars intended for seismic applications. Results from this study and the additional recommended testing should be used to guide new specifications and improve production techniques for reinforcing bars intended for seismic applications.

8. Appendix A

Appendix A1: Linear coefficients of determination between variables. Absolute values greater than 0.5 are colored (red for negative and green for positive).

	Manufacturer	Bar Size	Steel Grade	Clear Span	Strain Range	Yield Strength	Tensile Strength	T/Y Ratio	Elastic Modulus	Ductility Ratio	Elastic Limit Strain	Uniform Strain	Fracture Strain	R_{min}/H	R_{max}/H	H/D	C	Mn	P	S	Si	Cu	Cr	Ni	Mo	V	Nb	Sn
Manufacturer		-0.02	-0.04	-0.03	0.06	-0.04	-0.05	0.10	0.02	-0.18	-0.07	-0.39	-0.34	-0.73	-0.61	0.18	0.32	-0.26	-0.27	-0.16	0.44	0.50	0.00	0.69	0.36	-0.49	-0.40	-0.44
Bar Size	-0.02		-0.03	-0.24	0.57	-0.14	-0.15	0.12	0.12	0.23	-0.21	0.07	0.21	0.00	-0.04	-0.47	-0.27	-0.04	0.04	0.29	0.08	-0.02	0.16	0.06	0.25	-0.07	0.05	0.11
Steel Grade	-0.04	-0.03		0.03	0.08	0.98	0.95	-0.88	0.40	-0.92	0.93	-0.83	-0.82	-0.06	-0.05	0.50	0.62	-0.61	-0.42	-0.54	0.10	-0.07	-0.75	-0.10	-0.36	0.68	0.35	-0.66
Clear Span	-0.03	-0.24	0.03		-0.09	0.07	0.05	-0.09	-0.07	-0.08	0.11	0.01	-0.06	-0.05	-0.06	0.09	0.11	-0.01	0.02	-0.03	-0.02	0.07	0.01	0.01	0.00	0.06	-0.08	-0.05
Strain Range	0.06	0.57	0.08	-0.09		0.04	0.01	-0.04	0.10	0.05	0.00	-0.06	0.03	-0.17	-0.20	-0.26	0.00	-0.12	-0.04	0.06	0.16	0.06	0.02	0.09	0.16	-0.01	-0.03	-0.05
Yield Strength	-0.04	-0.14	0.98	0.07	0.04		0.96	-0.90	0.40	-0.92	0.96	-0.81	-0.82	-0.13	-0.13	0.49	0.67	-0.59	-0.37	-0.56	0.14	-0.03	-0.74	-0.07	-0.34	0.69	0.29	-0.67
Tensile Strength	-0.05	-0.15	0.95	0.05	0.01	0.96		-0.75	0.27	-0.93	0.95	-0.80	-0.83	-0.08	-0.01	0.41	0.52	-0.38	-0.37	-0.50	0.15	-0.12	-0.65	-0.17	-0.37	0.80	0.38	-0.75
T/Y Ratio	0.10	0.12	-0.88	-0.09	-0.04	-0.90	-0.75		-0.54	0.74	-0.82	0.67	0.64	0.08	0.18	-0.53	-0.75	0.76	0.25	0.53	0.00	-0.04	0.74	-0.03	0.27	-0.47	-0.18	0.39
Elastic Modulus	0.02	0.12	0.40	-0.07	0.10	0.40	0.27	-0.54		-0.30	0.12	-0.48	-0.39	-0.01	0.02	0.08	0.44	-0.45	-0.39	-0.50	0.05	-0.25	-0.64	-0.01	-0.30	0.12	0.38	-0.13
Ductility Ratio	-0.18	0.23	-0.92	-0.08	0.05	-0.92	-0.93	0.74	-0.30		-0.89	0.92	0.96	0.19	0.11	-0.55	-0.57	0.52	0.45	0.50	-0.20	-0.07	0.62	-0.05	0.25	-0.60	-0.24	0.78
Elastic Limit Strain	-0.07	-0.21	0.93	0.11	0.00	0.96	0.95	-0.82	0.12	-0.89		-0.71	-0.75	-0.14	-0.15	0.50	0.59	-0.49	-0.25	-0.43	0.13	0.05	-0.58	-0.07	-0.25	0.72	0.18	-0.67
Uniform Strain	-0.39	0.07	-0.83	0.01	-0.06	-0.81	-0.80	0.67	-0.48	0.92	-0.71		0.96	0.35	0.25	-0.49	-0.62	0.63	0.58	0.59	-0.33	-0.14	0.66	-0.22	0.20	-0.36	-0.16	0.73
Fracture Strain	-0.34	0.21	-0.82	-0.06	0.03	-0.82	-0.83	0.64	-0.39	0.96	-0.75	0.96		0.31	0.18	-0.47	-0.55	0.50	0.57	0.53	-0.29	-0.09	0.57	-0.13	0.19	-0.47	-0.22	0.82
R_{min}/H	-0.73	0.00	-0.06	-0.05	-0.17	-0.13	-0.08	0.08	-0.01	0.19	-0.14	0.35	0.31		0.92	-0.03	-0.40	0.28	0.20	0.15	-0.60	-0.56	-0.04	-0.69	-0.43	0.29	0.52	0.39
R_{max}/H	-0.61	-0.04	-0.05	-0.06	-0.20	-0.13	-0.01	0.18	0.02	0.11	-0.15	0.25	0.18	0.92		-0.15	-0.47	0.42	0.00	0.07	-0.61	-0.72	-0.07	-0.77	-0.56	0.35	0.74	0.17
H/D	0.18	-0.47	0.50	0.09	-0.26	0.49	0.41	-0.53	0.08	-0.55	0.50	-0.49	-0.47	-0.03	-0.15		0.48	-0.52	-0.05	-0.18	0.16	0.39	-0.43	0.34	0.02	0.09	-0.22	-0.12
C	0.32	-0.27	0.62	0.11	0.00	0.67	0.52	-0.75	0.44	-0.57	0.59	-0.62	-0.55	-0.40	-0.47	0.48		-0.76	-0.39	-0.78	0.25	0.26	-0.76	0.18	-0.30	0.10	-0.13	-0.46
Mn	-0.26	-0.04	-0.61	-0.01	-0.12	-0.59	-0.38	0.76	-0.45	0.52	-0.49	0.63	0.50	0.28	0.42	-0.52	-0.76		0.38	0.54	-0.03	-0.29	0.62	-0.33	0.10	0.12	0.17	0.20
P	-0.27	0.04	-0.42	0.02	-0.04	-0.37	-0.37	0.25	-0.39	0.45	-0.25	0.58	0.57	0.20	0.00	-0.05	-0.39	0.38		0.73	-0.04	0.34	0.62	0.26	0.53	-0.10	-0.39	0.52
S	-0.16	0.29	-0.54	-0.03	0.06	-0.56	-0.50	0.53	-0.50	0.50	-0.43	0.59	0.53	0.15	0.07	-0.18	-0.78	0.54	0.73		0.03	0.27	0.86	0.28	0.73	-0.17	-0.32	0.50
Si	0.44	0.08	0.10	-0.02	0.16	0.14	0.15	0.00	0.05	-0.20	0.13	-0.33	-0.29	-0.60	-0.61	0.16	0.25	-0.03	-0.04	0.03		0.63	0.03	0.46	0.45	0.04	-0.46	-0.26
Cu	0.50	-0.02	-0.07	0.07	0.06	-0.03	-0.12	-0.04	-0.25	-0.07	0.05	-0.14	-0.09	-0.56	-0.72	0.39	0.26	-0.29	0.34	0.27	0.63		0.29	0.82	0.69	-0.37	-0.85	0.04
Cr	0.00	0.16	-0.75	0.01	0.02	-0.74	-0.65	0.74	-0.64	0.62	-0.58	0.66	0.57	-0.04	-0.07	-0.43	-0.76	0.62	0.62	0.86	0.03	0.29		0.28	0.70	-0.37	-0.44	0.43
Ni	0.69	0.06	-0.10	0.01	0.09	-0.07	-0.17	-0.03	-0.01	-0.05	-0.07	-0.22	-0.13	-0.69	-0.77	0.34	0.18	-0.33	0.26	0.28	0.46	0.82	0.28		0.76	-0.53	-0.75	0.02
Mo	0.36	0.25	-0.36	0.00	0.16	-0.34	-0.37	0.27	-0.30	0.25	-0.25	0.20	0.19	-0.43	-0.56	0.02	-0.30	0.10	0.53	0.73	0.45	0.69	0.70	0.76		-0.37	-0.70	0.22
V	-0.49	-0.07	0.68	0.06	-0.01	0.69	0.80	-0.47	0.12	-0.60	0.72	-0.36	-0.47	0.29	0.35	0.09	0.10	0.12	-0.10	-0.17	0.04	-0.37	-0.37	-0.53	-0.37		0.58	-0.51
Nb	-0.40	0.05	0.35	-0.08	-0.03	0.29	0.38	-0.18	0.38	-0.24	0.18	-0.16	-0.22	0.52	0.74	-0.22	-0.13	0.17	-0.39	-0.32	-0.46	-0.85	-0.44	-0.75	-0.70	0.58		-0.30
Sn	-0.44	0.11	-0.66	-0.05	-0.05	-0.67	-0.75	0.39	-0.13	0.78	-0.67	0.73	0.82	0.39	0.17	-0.12	-0.46	0.20	0.52	0.50	-0.26	0.04	0.43	0.02	0.22	-0.51	-0.30	

9. References

American Association of State Highway and Transportation Officials (2015). AASHTO LRFD Bridge Design Specifications, Customary U.S. Units, 7th Edition, with 2015 Interim Revisions, American Association of State Highway and Transportation Officials, Washington, D.C.

American Concrete Institute (ACI) Committee 117 (2010), "Specification for Tolerances for Concrete Construction and Materials and Commentary (ACI 117-10)", American Concrete Institute, Farmington Hills, MI.

American Concrete Institute (ACI) Committee 318 (1956), "Building Code Requirement for Reinforced Concrete (ACI 318-56)", American Concrete Institute, Detroit, MI.

American Concrete Institute (ACI) Committee 318 (1971), "Building Code Requirement for Reinforced Concrete (ACI 318-71)", American Concrete Institute, Detroit, MI.

American Concrete Institute (ACI) Committee 318 (2014), "Building Code Requirements for Reinforced Concrete (ACI 318-14)," American Concrete Institute, Farmington Hills, MI.

Aoyama, H., Design of Modern Highrise Reinforced Concrete Structures, Imperial College Press, London, United Kingdom, 2001.

ASTM E8 / E8M-13a, Standard Test Methods for Tension Testing of Metallic Materials, ASTM International, West Conshohocken, PA, 2013, www.astm.org

ASTM A370-14, Standard Test Methods and Definitions for Mechanical Testing of Steel Products, ASTM International, West Conshohocken, PA, 2014, www.astm.org

ASTM A615 / A615M-14, Standard Specification for Deformed and Plain Carbon-Steel Bars for Concrete Reinforcement, ASTM International, West Conshohocken, PA, 2014, www.astm.org

ASTM A706 / A706M-14, Standard Specification for Deformed and Plain Low-Alloy Steel Bars for Concrete Reinforcement, ASTM International, West Conshohocken, PA, 2014, www.astm.org

Bae, S., Mieses, A., and Bayrak, O. (2005). "Inelastic Buckling of Reinforcing Bars." J. Struct. Eng., 131(2), 314–321.

Brown, Jeff, Kunnath, Sashi K. "Low-Cycle Fatigue Failure of Reinforcing Steel Bars." *ACI Materials Journal* 6.110 (2004): 457-65.

Coffin, L. F., Jr., "A Study of the Effect of Cyclic Thermal Stresses on a Ductile Metal," American Society of Mechanical Engineers, V. 76, 1954, 931-950.

Cyril, Nisha, Fatemi, Ali, Cryderman, Bob. "Effects of Sulfur Level and Anisotropy of Sulfide Inclusions on Tensile, Impact, and Fatigue Properties of SAE 4140 Steel." SAE Int. J. Mater. Manf. SAE International Journal of Materials and Manufacturing 1.1 (2008): 218-27.

Deeley, Paul, Kundig, Konrad J.A., Spendelow, Howard R., Jr. "Vanadium." *Ferroalloys & Alloying Additives Online Handbook - Vanadium*. N.p., n.d.

Dodd, L., Restrepo-Posada, J. (1995). ”Model for Predicting Cyclic Behavior of Reinforcing Steel.” J. Struct. Eng., 121(3), 433–445.

Dotreppe, J. C. "Mechanical Properties of Quenched and Self-tempered Reinforcing Steel (at Elevated Temperatures Compared with Recommendations of Eurocode 2 – Part1-2)." *Materials and Structures* 30.7 (1997): 430-38. *Springer Link*. Kluwer Academic Publishers.

Grimaldi A., Rinaldi, Z. “Influence of the Steel Properties on the Ductility of R.C. Structures”. 12WCEE World Conf. on Earthquake Engineering, Auckland New Zealand, January 2000.

Hawileh, R., Rahman, A., Tabatabai, H. "Evaluation of the Low-Cycle Fatigue Life in ASTM A706 and A615 Grade 60 Steel Reinforcing Bars." *Journal of Materials in Civil Engineering* 22.1 (2010): 65-76.

Helgason, Thorsteinn, Hanson, John M., Somes, Norman F., Corley, W. G., Hognestad, Eivind. Fatigue Strength of High-yield Reinforcing Bars. National Cooperative Highway Research Program Report 164. Washington, D.C.: National Research Council, 1976.

Koh, S.K., Stephens, R.I., "Mean Stress Effects on Low Cycle Fatigue for a High Strength Steel," Fatigue & Fracture of Engineering Materials & Structures, 14.4 (1991): 413-28.

Macchi, G., Pinto, P.E., Sanpaolesi, L., "Ductility requirements for reinforcement under Eurocodes," Structural Engineering International, 6.4 (1996): 249-54.

Mander, J. B., Panthaki, F. D., Kasalanati, A. "Low-Cycle Fatigue Behavior of Reinforcing Steel." *Journal of Materials in Civil Engineering* 6.4 (1994): 453-68.

Manson, S. S., “Behavior of Materials Under Conditions of Thermal Stress,” Heat Transfer Symposium, University of Michigan Engineering Research Institute, Ann Arbor, Mich., 1953, 9-75.

Monti, G., Nuti, C. (1992). ”Nonlinear Cyclic Behavior of Reinforcing Bars Including Buckling.” J. Struct. Eng., 118(12), 3268–3284.

NEHRP Consultants Joint Venture, "Use of High-Strength Reinforcement for Earthquake Resistant Concrete Structures," NIST GCR 13-917-30, Applied Technology Council, Redwood City, CA, 2013.

Nikolaou, John, Papadimitriou, George D. "Impact Toughness of Reinforcing Steels Produced by (i) the Tempcore Process and (ii) Microalloying with Vanadium." International Journal of Impact Engineering 31.8 (2005): 1065-80.

Reardon, Arthur C. *Metallurgy for the Non-metallurgist*. 2nd ed. Materials Park, OH: ASM International., 2011.

Restrepo-Posada, J., Dodd, L., Park, R., Cooke, N. (1994). "Variables Affecting Cyclic Behavior of Reinforcing Steel." J. Struct. Eng., 120(11), 3178–3196.

Sokoli, Drit. "Seismic Performance of Concrete Columns Reinforced with High Strength Steel." Thesis. University of Texas at Austin, 2014.

Sokoli, D., Shekarchi, W., Buenrostro, E., Ghannoum, W.M., "Advancing behavioral understanding and damage evaluation of concrete members using high-resolution digital image correlation data," Earthquakes and Structures, V. 7, No. 5, pp. 609-26, November 2014.

Tetelman, A. S., McEvily, A. J., Jr., *Fracture of Structural Materials*. Wiley, 1967.

Tong, X., Wang, D., Xu, H. (1989). "Investigation of cyclic hysteresis energy in fatigue failure process." Int. J. Fatigue, 11(5), 353-359.

Use of High-Strength Reinforcement in Earthquake-Resistant Concrete Structures. Tech. no. NIST GCR 14-917-30. N.p.: National Institute of Standards and Technology, 2014.

Weisman, M. H., "Detail Design and Manufacturing Considerations." *Metal Fatigue: Theory and Design*, ed. A. F. Madayag, Wiley, 1969.